

Properties of small pure and protonated ammonia
clusters from Theoretical Methods

Thesis submitted for the degree of PhD

Paula Estefanía Janeiro-Barral

Cardiff University

September 2010

UMI Number: U585454

All rights reserved

INFORMATION TO ALL USERS

The quality of this reproduction is dependent upon the quality of the copy submitted.

In the unlikely event that the author did not send a complete manuscript and there are missing pages, these will be noted. Also, if material had to be removed, a note will indicate the deletion.



UMI U585454

Published by ProQuest LLC 2013. Copyright in the Dissertation held by the Author.
Microform Edition © ProQuest LLC.

All rights reserved. This work is protected against
unauthorized copying under Title 17, United States Code.



ProQuest LLC
789 East Eisenhower Parkway
P.O. Box 1346
Ann Arbor, MI 48106-1346

Acknowledgements

Massimo Mella, thank you very much for allowing me to be your student for this long. Also *grazie mille* for your teachings, from chemistry to weight-lifting, to NLP, to ska, to mustard turkey... the list is long. I know you've tried, this hollow head has picked up some things, hopefully....

Cardiff University is gratefully acknowledged for the funding of this project.

Thank you Terrie Dumelow for giving us a friendly and efficient hand throughout the duration of this process.

When the going got tough the following people managed to put a smile on my face: Silvia Orenes, Eugene Cheung, Marco Engeler, Xavi Martí, Andy May, Giuseppe Amesbury and the Amesbury-Ursi family, Laura De Francesco, Marta Patrone, Maurizio Muroi and Yuehua Cong, Rhiannon Evans, Gary Coleman, Mike Coogan, Aled Williams and Rosie Lewis, Lucy Taplin, Ian Paul Sharpe and Clare Quinn, Niek Burma, Anabel "Anabelilla" Morte and Verónica "Miss Moneda" González, thank you very much.

Jamie Cross is the root of all kindness. I am much obliged.

Muchas gracias por hacer de cada vez que voy a casa una fiesta de cariño y atenciones, y por las dosis continuas de ánimos y comprensión: Cristina Martínez y Roberto Berdini, Jacobo Pereira y Pilar Flox, Raquel Landeira, Srs. de Cartón, Maruchi, Isabel y Manolo, Cuca, Carmen y Fidel, Morocha y Angel, Manolo, Manola y Marcial, Paco

y a mis abuelos Remigio y María, que se fueron mientras yo estaba aquí.

Muy especialmente a mis padres, Remigio y Pilar, y a mi hermana Adriana. Sé que el esfuerzo es inmenso. Muchas gracias por ser tan generosos conmigo. Os quiero.

The work in this thesis has lead to the following publications:

- Paula E. Janeiro-Barral and Massimo Mella, **“Study of the Structure, Energetics, and Vibrational Properties of Small Ammonia Clusters $(\text{NH}_3)_n$ ($n = 2 - 5$) Using Correlated ab Initio Methods;** *J. Phys. Chem. A*, **2006**, *110*, 11244.
- Paula E. Janeiro-Barral, Massimo Mella and Emanuele Curotto, **Structure and Energetics of Ammonia Clusters $(\text{NH}_3)_n$ ($n = 3 - 20$) Investigated Using a Rigid-Polarizable Model Derived from ab Initio Calculations;** *J. Phys. Chem. A*, **2008**, *112*, 2888.
- Christian Lubombo, Emanuele Curotto, Paula E. Janeiro-Barral and Massimo Mella, **Thermodynamic properties of ammonia clusters $(\text{NH}_3)_n$ ($n = 2 - 11$): Comparing classical and quantum simulation results for hydrogen bonded species;** *J. Chem. Phys.*, **2009**, *131*, 034312.

Abstract

Equilibrium geometries, interaction energies and harmonic frequencies of $(\text{NH}_3)_n$ ($n = 2 - 5$) and $\text{NH}_4^+(\text{NH}_3)_n$ ($n = 2 - 5$) were computed using correlated electronic calculations (MP2) in conjunction with aug-cc-pVXZ (X=D, T, Q) basis sets and the Counterpoise procedure. The zero-point energy (ZPE) on the relative stability of the clusters was estimated using harmonic frequencies. For both pure and protonated ammonia clusters we found that using basis set superposition error (BSSE) corrected forces or freezing the monomer structure to its gas phase geometry had only a weak impact on the energetics and structural properties of the clusters.

For pure ammonia clusters, $(\text{NH}_3)_n$ ($n = 2 - 5$), we found that low lying isomers for $(\text{NH}_3)_4$ and $(\text{NH}_3)_5$ have similar binding energies, perhaps suggesting the presence of a very smooth energy landscape. The harmonic frequencies highlighted the presence of vibrational fingerprints for the presence of double acceptor ammonia molecules. In addition, many-body effects for $n = 2 - 4$ were investigated; we found the 3-body effects to account for 10-15% of the total interaction energy and 4-body effects to be negligible.

Under these premises, a model pair interaction fitted to *ab initio* data for rigid ammonia molecules was developed. It was extended with a description of polarisation effects, introduced by using a noniterative form of the charge-on-spring model, the latter accounting for more than 95% of the dipole induction energy and of the increased molecular dipole. This model was used to optimise putative global minima for $(\text{NH}_3)_n$ ($n = 3 - 20$); the structure and energetics of the clusters with $n = 2 - 5$ were found to be in good agreement with previous *ab initio* results. For larger isomers our model

predicts larger binding energies than previous analytical surfaces, and also predicts a reorganisation of the energy ranking and a different global minimum structure.

For protonated ammonia clusters, we have found two general types of isomeric structures, globular and linear, the former showing larger binding energies. Harmonic frequencies reveal that the signature of these clusters is given mainly by NH_4^+ . In agreement with the literature we also found that higher frequencies for the N-H vibrational modes of the NH_4^+ are seen upon increasing cluster size. Finally, the vaporisation energy computed in this work compares well with previous theoretical and experimental data.

Contents

1	Introduction	2
1.1	Ammonia	2
1.2	Intermolecular interactions	6
1.2.1	Electrostatic forces	7
1.2.2	Dispersion	9
1.2.3	Induction	10
1.2.4	Exchange	11
1.2.5	Hydrogen bond	11
1.2.6	Potential Energy Surface (PES)	12
1.3	Methodology	14
1.3.1	Introduction	14
1.3.2	Møller-Plesset method	21
1.3.3	Basis Set	25
1.3.4	Basis Set Superposition Error	28
1.3.5	Supermolecular approach	31
1.3.6	Many-body effects	32
2	Pure ammonia clusters: $(\text{NH}_3)_n$ ($n = 2 - 5$)	40
2.1	Introduction	40

2.2	Methodology	43
2.3	Results	45
2.3.1	Structural results and binding energies	45
2.3.2	Many body effects and comparison with experiments	55
2.3.3	Harmonic frequencies	58
2.4	Conclusions	63
2.5	Appendix 1	70
2.6	Appendix 2	73
3	Ammonia potential	74
3.1	Introduction	74
3.2	Methodology	76
3.2.1	The potential	79
3.2.2	Polarisation	87
3.2.3	Re-parameterisation	90
3.3	Results	96
3.3.1	Geometry Reproduction of $(\text{NH}_3)_2$	96
3.3.2	Structure and Energetics of $(\text{NH}_3)_n$ ($n = 3 - 20$)	96
3.4	Conclusions	106
3.5	Appendix 1: Routine calling potential	112
3.6	Appendix 2: Potential	113
3.7	Appendix 3: Data file	121
4	Protonated ammonia clusters: $\text{NH}_4^+(\text{NH}_3)_n$ ($n = 1 - 5$)	122
4.1	Introduction	122
4.2	Methodology	126
4.3	Results	126

4.3.1	Structural Results and Binding Energies	126
4.3.2	Many-body Effects: Structural analysis	135
4.3.3	Harmonic Frequencies	147
4.3.4	Comparison with experiments	168
4.4	Conclusions	176
5	Conclusions and further work	183
5.1	Aims and achievements of this work	183
5.2	Further work	184

List of Figures

1.1	1-D potential energy surface along atom-atom distance coordinate, r	12
1.2	Ammonia tetramer for the calculation of many-body effects.	33
2.1	Equilibrium structures for $(\text{NH}_3)_2$ obtained with Counterpoise corrected MP2/aug-cc-pVTZ optimisations. All images in this work have been obtained and visualised using MOLEKEL [26]	47
2.2	Equilibrium structures for $(\text{NH}_3)_3$ obtained with Counterpoise corrected MP2/aug-cc-pVTZ optimisations.	48
2.3	Equilibrium structures for $(\text{NH}_3)_4$ obtained with Counterpoise corrected MP2/aug-cc-pVTZ optimisations.	52
2.4	Equilibrium structures for $(\text{NH}_3)_5$ obtained with MP2/aug-cc-pVTZ optimisations.	54
2.5	N-H stretching frequencies for $(\text{NH}_3)_3$ and $(\text{NH}_3)_4$ obtained using MP2/aug-cc-pVDZ	60
2.6	N-H stretching frequencies for the BB1, BB2, and compact isomers of $(\text{NH}_3)_5$ obtained using MP2/aug-cc-pVDZ	61
2.7	N-H stretching frequencies for the ring, pyramid and tail isomers of $(\text{NH}_3)_5$	62
3.1	Isomer configurations employed to test the model potential.	78

3.2	Reference geometries and coordinates for the two dimensional CP-MP2/aug-cc-pVTZ scans. NN indicates the distance between the hydrogen atoms and A indicates the angle employed in the scans to explore the energy landscape of specific isomerisation proceses.	79
3.3	Performance of model potentials A (black), B (grey) and C (orange) on a rigid scan over the N–N distance in the linear and parallel configurations. . .	82
3.4	Performance of model potentials A (black), B (grey) and C (orange) on a rigid scan over the N–N distance in the mirror and orthogonal configurations.	83
3.5	Performance of model potential C, and <i>ab initio</i> calculations (CP-MP2/aug-cc-pVXZ, X = D, T), on a rigid scan oven the N–N distance in the “linear” and “parallel” configurations	85
3.6	Performance of model potential C, and <i>ab initio</i> calculations (CP-MP2/aug-cc-pVXZ, X = D, T) on a rigid scan over the N–N distance in the “mirror” and “orthogonal” configurations.	86
3.7	Signed energy difference between <i>ab initio</i> and model potential interaction energies. From the top, panel a shows “model C” with parameters and analytical form from reference [12], panel b shows “model C(pol, Q^{frozen})” and panel c shows “model C(pol, Q^{opt})”	94
3.8	Equilibrium geometries for the ammonia dimer obtained using CP-MP2/aug-cc-pVTZ and model C(pol, Q^{opt}), in brackets, distances in Å.	96
3.9	Structure of the putative global minima for $(\text{NH}_3)_n$ ($n = 3 - 11$) optimised using “model C(pol, Q^{opt})”	99
3.10	Structure of the putative global minima for $(\text{NH}_3)_n$, ($n = 12 - 20$) optimised using “model C(pol, Q^{opt})”	101

3.11	Local minimum structures obtained using “model C(pol, Q^{opt})” for some cluster size: (a) “butterfly” isomer for $(\text{NH}_3)_5$; (b) second energy isomer for $(\text{NH}_3)_6$; (c) second energy isomer for $(\text{NH}_3)_8$; (d) second energy isomer for $(\text{NH}_3)_{12}$	101
3.12	Evaporation energy ($E_{vap}(n) = E_n - E_{n-1}$, kcal/mol) for $(\text{NH}_3)_n$ computed using the total energy of putative global minima. Data obtained using “model C(pol, Q^{opt})”; also showing the results provided in references [14, 33]	103
4.1	Isomer 1000 stag (top) 1000 ecli (bottom)	127
4.2	Isomer 1100 stag (top) and 1100 ecli (bottom)	129
4.3	Isomer 1110 stag (top) and 1110 ecli (bottom)	131
4.4	Isomer 2100 stag (top), 2100 ecli (middle) and 2100 ecliecli (bottom).	131
4.5	Isomer 1111 (top left), 2110 (top right), 3100ring (middle left), 2200 (middle right) and 3100 (bottom).	132
4.6	Isomer 2111 (top left), 2111ring (top right), 2210 (second row left), 3110 (second row right), 3200 (third row), 4100 (bottom)	134
4.7	Structural parameters	135
4.8	Vibrational spectra of NH_3 (top) and NH_4^+ calculated for optimised structures at MP2/aug-cc-pVDZ level of theory	149
4.9	Vibrational spectra of NH_4^+NH_3 calculated for optimised structures at MP2/aug-cc-pVDZ level of theory	150
4.10	Vibrational spectra of $\text{NH}_4^+(\text{NH}_3)_2$ calculated for optimised structures at MP2/aug-cc-pVDZ level of theory	151
4.11	Vibrational spectra of $\text{NH}_4^+(\text{NH}_3)_3$ calculated for optimised structures at MP2/aug-cc-pVDZ level of theory	152
4.12	Vibrational spectra of $\text{NH}_4^+(\text{NH}_3)_4$ calculated for optimised structures at MP2/aug-cc-pVDZ level of theory	153

4.13	Vibrational spectrum of $\text{NH}_4^+(\text{NH}_3)_4$ calculated for optimised structure at MP2/aug-cc-pVDZ level of theory	154
4.14	Vibrational spectra of $\text{NH}_4^+(\text{NH}_3)_4$ calculated for optimised structures at MP2/aug-cc-pVDZ level of theory	155
4.15	Vibrational spectra of $\text{NH}_4^+(\text{NH}_3)_4$ calculated for optimised structures at MP2/aug-cc-pVDZ level of theory	156
4.16	Vibrational spectra of $\text{NH}_4^+(\text{NH}_3)_5$ calculated for optimised structures at MP2/aug-cc-pVDZ level of theory	157
4.17	Vibrational spectra of $\text{NH}_4^+(\text{NH}_3)_5$ calculated for optimised structures at MP2/aug-cc-pVDZ level of theory	158
4.18	Vibrational spectra of $\text{NH}_4^+(\text{NH}_3)_5$ calculated for optimised structures at MP2/aug-cc-pVDZ level of theory	159

List of Tables

2.1	Energy values for $(\text{NH}_3)_2$ in kcal/mol.	46
2.2	Energy values for $(\text{NH}_3)_3$ in kcal/mol	49
2.3	Energy values for $(\text{NH}_3)_4$ in kcal/mol.	51
2.4	Energy values for $(\text{NH}_3)_5$ in kcal/mol.	55
2.5	Binding (BE) and vaporisation (ΔE) energies for $(\text{NH}_3)_n$ ($n = 2 - 5$), in kcal/mol.	57
2.6	Many-body contributions to the binding energy of $(\text{NH}_3)_n$ ($n = 2 - 4$), in kcal/mol.	58
2.7	ZPE corrected binding energies computed in this work using Counter- poise corrected electronic energies and ZPE at the MP2/aug-cc-pVXZ (X = D, T) level	73
3.1	Values of the Dipole (μ) and Quadrupole (θ_{zz}) Moments for the Ammo- nia Molecule Computed at the MP2/aug-cc-pVXZ, (X = D, T, Q, 5) Level of Theory ^a	77
3.2	Optmised parameters for the two model potentials, model C(pol, Q^{opt}) and model C(pol, Q^{frozen}) ^a	92
3.3	Total Binding Energy (kcal/mol) for the Putative Global Minima of $(\text{NH}_3)_n$ ($n = 3 - 5$) Computed using “model C(pol, Q^{opt})” and CP- MP2/aug-cc-pVTZ	97

3.4	Total Binding Energy (kcal/mol) for the Putative Global Minima for the three lowest energy isomers of $(\text{NH}_3)_n$ ($n = 6 - 20$) obtained using “model C(pol, Q^{opt})” ^a	102
4.1	Binding Energies for the clusters $\text{NH}_4^+(\text{NH}_3)_n$ $n = 2 - 5$ in kcal/mol. . .	128
4.2	Inter and intramolecular lengths (Å) for optimised protonated ammonia cluster 1000 stag ^a	137
4.3	Inter and intramolecular lengths (Å) for optimised protonated ammonia cluster 1100 stag	137
4.4	Inter and intramolecular lengths (Å) for optimised protonated ammonia cluster 2100 ecli	138
4.5	Intermolecular and intramolecular parameters (Å) for cluster family 1000 → 1100 → 1110 → 1111 → 2111	142
4.6	Intermolecular and intramolecular parameters (Å) for cluster family 2100 → 3100 → 4100	143
4.7	Intermolecular and intramolecular parameters (Å) for cluster 3100ring .	144
4.8	Intermolecular and intramolecular parameters (Å) for cluster family 2100 → 2200 → 3200	145
4.9	Intermolecular and intramolecular parameters (Å) for cluster family 2100 → 2110 → 3110	146
4.10	Intermolecular and intramolecular parameters (Å) for cluster family 2100 → 2110 → 2210	146
4.11	Binding energies for $\text{NH}_4^+(\text{NH}_3)_n$, ($n = 2 - 5$) in kcal/mol ^a	170
4.12	Binding energies (BE) and vaporisation energies (ΔE) for $\text{NH}_4^+(\text{NH}_3)_n$, ($n = 1 - 5$) in kcal/mol, comparison with experiments ^a	173
4.13	Binding energies (BE) and vaporisation energies for $\text{NH}_4^+(\text{NH}_3)_n$, ($n = 1 - 5$) in kcal/mol, comparison with theory ^a	174

Chapter 1

Introduction

1.1 Ammonia

When the ancient city of Thebes became the most important metropolis in Egypt, Amun, the patron of the city [1], knew a fame that surpassed the national frontiers. One of the many constructions erected to the worship of the deity was the Oracle of Siwa, in the oasis of Siwa (Libyan desert) [1, 2]. Both the oasis and the temple were well known by the classic Greeks, who found in Ammon (Greek for Amun) an equivalent of their much respected Zeus [1, 2]. Under the Roman Empire, Jupiter became the deity related to the temple, the oasis became a place of banishment [2] and Latin language coined the eponym “sal ammoniacus” or “sal ammoniac”, literally “salt of Ammon”, to describe the white crystal deposits found in the area of Siwa [3–5]. This accumulation of ammonium chloride crystals comes from burning camel dung as fuel source, and from sun-heating for many years great amounts of camel dung and urine left behind in cesspits by the visitors to the oasis, together with soot and sea salt [3, 5–7].

In full Age of Enlightenment, in 1774, Joseph Priestly isolated “alkaline air” [4, 7, 8] whose composition would be determined to be hydrogen nitride by Claude Louis

Berthollet in 1785 [4, 7, 9]. In between, in 1782, Torbern Olof Bergman is attributed to have devised the name “ammonia” as a bastardisation of the Latin “sal ammoniac” [3, 5, 7, 10]. This novel word would enter the English language, to stay, in less than two decades since its birth [5].

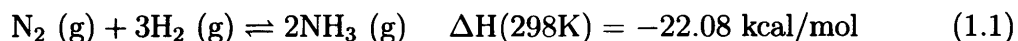
Ammonia may be the most popular name for NH_3 , but is not by any means the only one: azane, hydrogen nitride, spirit of hartshorn, Nitro-Sil or Vaporole have also been used to nominalise this ubiquitous gas of pungent odour [4].

NH_3 is naturally released to the atmosphere from the decomposition of animal and vegetable matter [4]. Nitrogen compounds are a fundamental part of living organisms (e.g. purines, aminoacids, porphyrines). At some point in their metabolic lives they may be broken into ammonium ion or ammonia, both pernicious in the cellular environment. Thus, in animals, an effective mechanism to keep toxic concentrations of ammonium ion at bay is achieved by converting ammonia to urea, that is then excreted through the kidneys. Ammonia is not only directed to excretion, its basicity can be exploited to compensate for severe metabolic acidosis in humans, and is also recycled to anabolise several aminoacids [11]. Interestingly, considering the established role of ammonia in the biochemistry of living organisms, is only recently that the mechanisms for the homoeostasis of NH_3 have started to be understood [12, 13].

In 2004, the tentative detection of ammonia in Mars, triggered the hypothesis of a biological source of the gas in the Red Planet [14]. More radically, NH_3 has been proposed as a molecule from which an alternative biochemistry could stem, therefore substituting water as the “liquid of life” [15, 16]. This idea is mainly based in the existence of ammonia and water analogues (e.g. methylamine and methanol, CH_3NH_2 and CH_3OH) and the likeness of some physico-chemical characteristics (e.g. ability to create hydrogen bonds, solvation properties) [16, 17]. The pitfall of this theory is found within the latter argument, ammonia has a vaporisation heat and surface tension

significantly lower than that of water thus, “ammonia based” organisms could not be structurally kept together in Earth conditions. Notwithstanding, in planets such as Jupiter and Venus, with remarkably different atmospheric conditions and where NH_3 is readily available, metabolism in liquid ammonia could be conceivable [15–17].

At the beginning of the 20th century, the increasing world population put on the rise the demand for the use of fertilisers to feed the crops [18, 19]. At the time, the main source for nitrates was the limited and swiftly vanishing natural resource of the Chile saltpetre (NaNO_3) [4, 18–21]. Fritz Haber and Carl Bosch made possible the synthetic fixation of atmospheric nitrogen to produce ammonia in a large scale around 1913 [18, 21]. Nowadays, the Haber-Bosch process, in equation 1.1 below, is responsible for virtually the entire global manufacture of NH_3 [23].

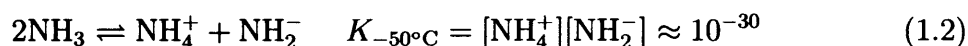


This is a demanding process, taking place at high temperatures (around 500 °C), high pressures (100 - 250 atm) and in the presence of an iron catalyst in order to overcome the inertness of the nitrogen gas and to tilt the equilibrium as much as possible to the formation of NH_3 [21–33].

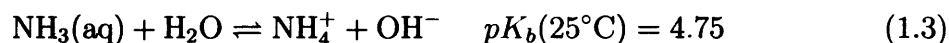
Industrially, ammonia has very diverse uses. It is used as a refrigerant, exploiting its large heat of evaporation. Since is very soluble in water, weak solutions of NH_3 are found as household cleaning products. It is also used in the manufacture of explosives such as NH_4NO_3 and HNO_3 . The textile industry uses ammonia for the manufacture of synthetic fibres like nylon. It is used in the pharmaceutical industry, e.g. urea is used in the production of barbiturates. The rubber industry uses NH_3 to avoid premature coagulation of natural and synthetic latex. In the mining industry metals such as copper, nickel and molybdenum are extracted from their ores using ammonia [19].

Regarding its chemical properties, NH_3 has a trigonal pyramidal shape with a exper-

imental geometry of $r_{NH}=1.0124 \text{ \AA}$, $H\hat{N}H = 106.67^\circ$ [24]. The “valence shell electron pair repulsion theory” (VSEPR) explains that this shape is due to the lone electron pair on the nitrogen atom repelling the N–H bonds and pushing them together, hence deviating the $H\hat{N}H$ angle from that of a regular tetrahedron (the sp^3 hybridisation of the Nitrogen 2p and 2s orbitals would tend to distribute the electron pairs in a tetrahedron). Ammonia is a polar molecule with a dipole moment of 1.42 D, and is able to form hydrogen bonds. The acid-base properties of ammonia result largely from the self-ionisation reaction:



which make ammonia a strong proton-acceptor enabling most potential proton donors to act as an acid [23, 25]; it is also extremely soluble in water [25]:



Ammonia has boiling point of -33.4°C and a melting point of -77.7°C . The liquid form has a large heat of evaporation (1.37 kJ/g at the boiling point) [25]. An interesting property of ammonia is its ability to dissolve alkali metals. The resulting solutions are blue and very good electrical conductors. Moreover, when the solution is very concentrated the conductivity is as good as that of the free metals. It is believed that the metal atoms are ionised in liquid ammonia giving solvated electrons [26].

1.2 Intermolecular interactions

Are intermolecular interactions¹ important? “If the intermolecular interactions were suddenly switched off, the world would disintegrate in about a femtosecond, that is a single period of atomic vibration (the atoms simply would not come back when shifted from their equilibrium positions). Soon after, everything would evaporate and a sphere of gas, the remainder of the earth, would be held by gravitational forces. Isn’t it enough?” [34]

Since the concept of “intermolecular” varies with the system being considered, we would like to point out, even if is obvious, that in this work, “intermolecular” indicates forces between the fragments (i.e. monomers) that constitute a cluster, and “intramolecular” will refer to occurrences within the monomer.

The existence of forces between molecules (intermolecular, also called van der Waals forces) can be deduced from two macroscopic observations. On one hand, the formation of condensed phases indicate the presence of forces between molecules that are strong enough to cause long-term clustering, hence their nature is “attractive”. On the other hand, condensed phases resist further compression, this would mean that intermolecular forces are weak enough to keep the fragments from reacting with one another, preserving the chemical identity of the fragments composing the cluster. This resistance manifests the action of a “repulsive” force [27, 28].

The range of these forces depends on the distance between the fragments, so, intuitively, we can say “long distance” when the fragments are infinitely apart and do not “feel” each other, and “short distance” when the separation of the monomers is at equilibrium. At long distances the contribution to the energy can be divided in three components with robust physical meaning: electrostatic, induction and dispersion ef-

¹I have consulted the following references in the writing of this section[27–32, 34]. I have also used my own work, previously presented in my MSc dissertation.

fects. At very short distances the largest contribution to the energy is repulsive and its component is the exchange effect.

1.2.1 Electrostatic forces

This effect arises from the interaction between the static charges of the interacting monomers. The overall charge distribution of a molecule is represented by its non-zero multipole moments, which are used to describe electrostatic interactions. The outcome of the interaction can lead to attraction or repulsion depending on the orientation and geometry of the molecules.

Multipole moments

Considering a molecule as a spatial distribution of charges, it can then be described in terms of a multipole expansion, a series in which each term is a “moment” of the distribution of charges, the first term being the monopole moment, second term dipole moment, third term is the quadrupole moment, then octupole moment and so on.

The monopole Q , or zeroth moment, is the net charge of the distribution of charges:

$$Q = \sum_i q_i \quad (1.4)$$

where q_i is the charge of atom i , summation is taken over a configuration of point charges. For a charge density distribution ($\rho(x, y, z) = \rho(\vec{r})$), Q is expressed as:

$$Q = \int \rho(\vec{r}) d\vec{r} \quad (1.5)$$

the first moment of the multipole expansion is the dipole ($\vec{\mu}$), which describes the symmetric arrangement of positive and negative charges separated by a vector \vec{r} . This vector is represented as pointing from the negative to the positive charge. For a static

point charge distribution we have:

$$\vec{\mu} = \sum_i q_i \vec{r}_i \quad (1.6)$$

where \vec{r} is the vector position of the i th particle with respect to some origin. For a charge density distribution the dipole becomes:

$$\vec{\mu} = \int \vec{r} \rho(\vec{r}) d\vec{r} \quad (1.7)$$

equation 1.7 indicates that the dipole moment is the average of the position of all charged particles (given by \vec{r}) over the spatial charge distribution $\rho(x, y, z)$.

The simplest representation of a quadrupolar charge distribution is given by four alternating charges of equal magnitude and opposite sign placed at the corners of a square. For a continuous distribution of charge, the quadrupole moment is the set of averages of all pairs of the type x^2 , xy , xz , y^2 , yz and z^2 over the charge distribution ρ .

The presence of multipole moments in a molecule is determined by its own make-up, in terms of composition and geometry, but can be also determined by the presence of a non-uniform electric field such as the one created by the multipole moment of a neighbour molecule. In fact, dipole moments can be divided in two (non-excluding) types: permanent and induced. A permanent dipole moment occurs when a charge separation is always present in a molecule, whereas an induced dipole is a charge separation arising only in the presence of an electric field [29].

In the following sections we introduce dispersion and induction forces. These are also electrostatic in the sense that they derive from the Coulombic interaction of charged particles, but they separate from the notion of “static” because they account for the reordering of the charge distribution when a molecule is exposed to an electric

field.

1.2.2 Dispersion

They are also called London forces, or “induced dipole-induced dipole interactions”, and they are common to all molecules.

Dispersion can be conceptually explained by considering the motion of electrons in the environment of a neutral molecule. The electronic motion causes the charge to be continuously redistributed. This fluctuation can lead to an asymmetric distribution of electron density, creating a transient dipole, which gives rise to transient electric field. The transient field will affect the charge distribution of molecules nearby, resulting in the generation of an induced dipole in the neighbouring molecules.

Electron motion is correlated in such a way that favours lower energy configurations, the induced dipole will be aligned in such a way that it always has a favourable interaction with the first (transient dipole) one. This favourable interaction is always maintained even if molecules move around, because the fluctuations leading to the formation of transient and induced dipoles are very rapid processes compared to the rate at which molecules move due to thermal motion.

Conversely, the orientation of permanent dipoles is ruled by the thermal motion of the molecules, meaning that they are not always aligned in such a way as to have an attractive interaction. In fact, when averaged across the sample the interaction between permanent dipoles is usually much less than the dispersion interaction.

Polar molecules also have instantaneous (or transient) dipoles, so they also interact via dispersion. In this case the time average of each transient dipole does not vanish, but corresponds to the permanent dipole. Hence, polar molecules interact through their permanent dipoles and the instantaneous fluctuations in them [32].

1.2.3 Induction

The ease with which the electron distribution can be distorted from its normal shape by an electric field is called polarisability (α). This susceptibility to respond to an external electric field determines the strength of the dispersion interaction. The more polarisable a molecule is, the bigger is the separation of charges (hence, its induced dipole), and the stronger is the dispersion interaction.

The dipole induced on an atom ($\vec{\mu}_{ind}$) by a uniform, infinitesimal electric field (\vec{E}) can be written as:

$$\vec{\mu}_{ind} = \alpha \vec{E} \quad (1.8)$$

equation 1.8 shows a linear relationship between $\vec{\mu}_{ind}$ and \vec{E} , this is the case for small (infinitesimal) fields. For large fields, $\vec{\mu}_{ind}$ may depend on higher powers of \vec{E} ($\vec{\mu}_{i,ind} = \alpha \vec{E} + \alpha_2 \vec{E}^2 + \alpha_3 \vec{E}^3 + \dots$) [29], when expanded as a series, the term hyperpolarisability must be applied. In addition, $\vec{\mu}_{ind}$ and \vec{E} do not have to point in the same direction, a more general representation of the induced dipole would be:

$$\vec{\mu}_{i,ind} = \sum_{j=1}^3 \alpha_{ij} \vec{E}_j \quad (i, j = x, y, z) \quad (1.9)$$

equation 1.9 indicates how the components of the dipole moment are affected by the direction of the electric field, introducing the concept of polarisability as a tensor. The polarisability is the induced dipole moment per unit of applied electric field [29]; it can also be expressed as polarisability volume (α'), where ϵ_0 is the vacuum permittivity:

$$\alpha' = \frac{\alpha}{4\pi\epsilon_0} \quad (1.10)$$

1.2.4 Exchange

Exchange is a purely quantum effect, however, a physical picture of the exchange phenomenon can be given considering the situation in which molecules come close together. In this situation, the space available for electron motion is extended to both molecules, and when two electrons of the same spin attempt to occupy the same region of the space, Pauli exclusion principle forces a redistribution of the charge. The exchange effect controls the steepness of the repulsion interaction.

1.2.5 Hydrogen bond

When the hydrogen atom bonds an electronegative atom, a polarised bond is created in which the latter has partial negative charge and the hydrogen has a partial positive charge. This allows the hydrogen to interact with another electronegative atom (to which is not “formally” bonded) to create the hydrogen bond.

The strength of the hydrogen bond covers a wide and continuous energy scale from around 0.5 kcal/mol to nearly 40 kcal/mol [37]. It contains energy contributions from electrostatic, induction and dispersion interactions, as well as some degree of covalent interaction [38].

For maximum stability the hydrogen donor pair and the acceptor tend to form a linear structure in species like (H_2O) and $(\text{HF})_2$. However, this is not observed in ammonia, where after some debate, is now accepted that a deviation from linearity is preferred.

1.2.6 Potential Energy Surface (PES)

Graphically, the combination of attractive and repulsive interactions between two atoms or molecules as a function of the distance separating them, has the following form:

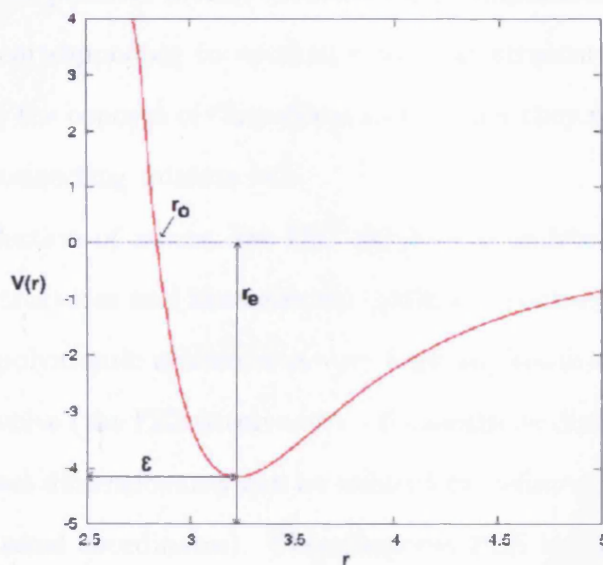


Figure 1.1: 1-D potential energy surface along atom-atom distance coordinate, r .

The range of the interaction is defined by the dependence of the potential energy, $V(r)$, on the separation r . Moreover, the span of the interaction of an n -pole with an m -pole can be predicted by [27, 32]:

$$V(r) \propto \frac{1}{r^{n+m-1}} \quad (1.11)$$

where $V(r)$ is the potential energy in terms of the distance and n and m are the order of the multipole moments on which the interaction operates ($n = 1$ for monopole, $n = 2$ for dipole, $n = 3$ for quadrupole and so on). Thus, for example, dipole-dipole interaction falls off as r^{-3} , dipole-quadrupole as r^{-4} and quadrupole-quadrupole as r^{-5} . From this sequence it can be seen that the interaction energy falls more rapidly

the higher the order of the multipole. We will also mention that dispersion interaction decays as r^{-6} , but we will not go into the details of the calculation.

Figure 1.1 is a one dimensional representation of a Potential Energy Surface (PES). More accurately, the PES is a hypersurface defined by the potential energy of a collection of atoms over all possible atomic arrangements. Important points in the surface are local minima, corresponding to optimal molecular structures; and saddle points, which are related to the concept of “transition state” since they represent lowest energy barriers on paths connecting minima [40].

For a given collection of atoms, the PES provides complete information about all possible chemical structures and isomerisation pathways connecting them. However, a complete PES for polyatomic molecules is very hard to visualise because of the many dimensions they involve (the PES involves $3N - 6$ coordinate dimensions, where $N \geq 3$; for practical purposes dimensionality can be reduced by defining the degrees of freedom with respect to internal coordinates). Therefore, the PES is normally presented as a “slice” involving a single coordinate (e.g. atom-atom distance, r , as in figure 1.1) or two [40].

A typical model to describe the empirical intermolecular potential (e.g. figure 1.1) is that by Lennard-Jones:

$$V_{LJ}(r) = 4\epsilon \left[\left(\frac{r_0}{r} \right)^{12} - \left(\frac{r_0}{r} \right)^6 \right] \quad (1.12)$$

where ϵ is the well depth and r_0 is the distance at which $V_{LJ}(r) = 0$. The minimum interaction energy occurs at $r_e = 2^{1/6}r_0$, r_e being the equilibrium intermolecular distance. The first term in brackets in equation 1.12 accounts for the repulsive term of the intermolecular forces (left hand side of the minimum in figure 1.1), and the second term accounts for the attractive forces (right hand side of the minimum in figure 1.1). The 6^{th} power was adopted following London’s work on dispersion forces, while

the 12th power was thought to be mathematically convenient for describing the speed of the repulsive potential. It is now known that an exponential function (i.e. $e^{-\alpha r}$) is closer to the description of the exponential decay of atomic wavefunctions at large distances, and hence to the overlap that is responsible for repulsion [32].

1.3 Methodology

1.3.1 Introduction

The Schrödinger equation

In order to determine the electron structure of atoms and molecules, one has to solve the Schrödinger equation. We will be concerned with its time-independent form only²:

$$\hat{H}\Psi = E\Psi \quad (1.13)$$

E is the energy of the atomic or molecular system being investigated. Ψ is the wavefunction containing the full description of the system, this is, all the properties of the system that are open to experimental determination (observables). \hat{H} is the Hamiltonian operator corresponding to the total energy of the system, which in turn is the sum of a kinetic energy and a potential energy operators acting on all the particles of the system. For a single particle (e.g. electron) of mass m , with a position vector $\vec{r} = x\vec{i} + y\vec{j} + z\vec{k}$, under the influence of a field V (e.g. the electrostatic potential due to the nuclei of a molecule)[40], we can write:

$$\left\{-\frac{\hbar^2}{2m}\nabla^2 + V\right\}\Psi(r) = E\Psi(r) \quad (1.14)$$

²To write this section I have consulted references[38, 40 42, 50]. The following sections contain my own work, previously presented in my MSc dissertation: “Practical considerations”, “Basis Set Superposition Error”, “Supermolecular approach” and “Many-body effects”.

In equation 1.14, \hbar is Plank's constant divided by 2π and ∇^2 is the Laplacian operator. V is the potential energy operating on the system.

In order to solve Schrödinger's equation values of E and Ψ have to be found such that when the energy Hamiltonian operates on the wavefunction it returns the wavefunction multiplied by the energy [40]. Exact solutions for the Schrödinger equation cannot be obtained for any molecular systems: hence, for N -particle systems, such as the clusters in this work, approximation techniques are needed.

The interpretation of Ψ

The relationship between the wavefunction and the particle location it describes is probabilistic in nature[41]. Born suggested that the probability that a particle will be found in the volume element $d\tau$ ($d\tau = dxdydz$) at the point r is proportional to $|\Psi|^2$.

$$|\Psi|^2 = \Psi\Psi^* \quad (1.15)$$

where Ψ^* is the complex conjugate of Ψ . Born's interpretation means that $|\Psi|^2$ is a probability density, and also implies normalisation. It is said that a wavefunction is normalised if:

$$\int |\Psi|^2 d\tau = 1 \quad (1.16)$$

In other words, given that if we multiply Ψ by a constant in both sides of equation 1.13 the equality would still be obeyed, we would like to find a constant that ensures that the probability of finding the electron in the space volume is 1.

The variational principle

One approach to the solution of Schrödinger's equation for a many-body system of a known Hamiltonian, is to build an approximation to the problem wavefunction, Ψ_{approx} . This will return an approximate value of the energy of the system, E_{approx} . The variational principle applies the Rayleigh ratio (equation 1.17) to the evaluation of E_{approx} .

$$E_{\text{approx}} = \frac{\langle \Psi_{\text{approx}} | \hat{H} | \Psi_{\text{approx}} \rangle}{\langle \Psi_{\text{approx}} | \Psi_{\text{approx}} \rangle} \quad (1.17)$$

The variational principle states that the energy calculated from an approximation to the true wavefunction, E_{approx} , will always be greater than the true energy, E_{exact} [40].

$$E_{\text{approx}} \geq E_{\text{exact}} \quad (1.18)$$

The significance of this principle is that the optimum wavefunction will be the one for which the energy of the Rayleigh ratio is a minimum, because it will be the closest we can get to the true energy of the system. Ψ_{approx} is typically expressed in terms of one or more adjustable parameters that are varied until equation 1.17 is minimised [42].

Born-Oppenheimer approximation

For a system of N nuclei and n electrons we can write the Hamiltonian as:

$$\hat{H} = -\frac{\hbar^2}{2m_e} \sum_i^n \nabla_i^2 - \frac{\hbar^2}{2M_N} \sum_A^N \nabla_A^2 - \sum_i^n \sum_A^N \frac{Z_A e^2}{4\pi\epsilon_o r_{iA}} + \frac{1}{2} \sum_i^n \sum_{j>i}^n \frac{e^2}{4\pi\epsilon_o r_{ij}} + \sum_A^N \sum_{B>A}^N \frac{Z_A Z_B}{4\pi\epsilon_o R_{AB}} \quad (1.19)$$

where m_e and M_A are the electron and nuclear masses respectively and e and Z are the electron and nuclear charges, respectively. The first term is the kinetic energy operator for the electrons; the second term is the kinetic energy operator for the nuclei; the third term is the electron-nucleus Coulombic attraction; the fourth term is the electron-electron repulsive interaction and the fifth term is the nucleus-nucleus repulsive interaction.

The rationale behind the Born-Oppenheimer approximation is the great difference in masses between the nuclei and the electrons (the resting mass of the lightest nucleus, the proton, is 1836 times heavier than the resting mass of the electron [40]). This difference implies that the electrons can respond almost instantaneously to any changes in the positions of the nuclei [40, 42]. Therefore, the motion of nuclei and electrons can be decoupled, meaning that the nuclei can be considered fixed (or clamped) in their positions in a particular instant, giving rise to a static electric potential “felt” by the electrons. In this situation, the Hamiltonian can be simplified to:

$$\hat{H}_{\text{elec}}(R) = -\frac{\hbar^2}{2m_e} \sum_i^n \nabla_i^2 - \sum_i^n \sum_A^N \frac{Z_A e^2}{4\pi\epsilon_o r_{iA}} + \frac{1}{2} \sum_i^n \sum_{j>i}^n \frac{e^2}{4\pi\epsilon_o r_{ij}} + \sum_A^N \sum_{B>A}^N \frac{Z_A Z_B}{4\pi\epsilon_o R_{AB}} \quad (1.20)$$

$\hat{H}_{\text{elec}}(R)$, is the electronic Hamiltonian that depends on all the nuclear positions, R , at once. Now, the problem at hand is to solve a Schrödinger equation that involves only the electronic degrees of freedom (R denoting the dependence on the particular configuration of the nuclei):

$$\hat{H}_{\text{elec}}(R)\Psi_{\text{elec}}(R) = \hat{H}_{\text{elec}}(R)E_{\text{elec}}(R) \quad (1.21)$$

When approximate solutions to equation 1.21 are computed without the use of empirical parameters the calculation is known as “*ab initio*”, meaning “from the be-

ginning”. Once equation 1.21 has been solved, the Hamiltonian for the nuclei, \hat{H}_N , can be written by adding the nuclear kinetic energy (left out from equation 1.20) to the electronic energy, $E_{\text{elec}}(R)$:

$$\hat{H}_N = -\frac{\hbar^2}{2M_N} \sum_A^N \nabla_A^2 + E_{\text{elec}}(R) \quad (1.22)$$

Hence, the Schrödinger equation for the complete system, which would return the energy including contributions from the electrons and the nuclei would be:

$$\hat{H}_N \Psi_N = E \Psi_N \quad (1.23)$$

In this thesis we will be concerned with electronic energy calculations, hence with equation 1.21, from here onwards we will drop the subscripts.

Molecular Orbital approximation

Even with the Born-Oppenheimer approximation, Schrödinger’s equation remains very difficult to solve for an N -particle system. The evaluation of the electron-electron potential energy is particularly difficult because it depends on all possible and simultaneous pairwise interactions between electrons (fourth term in equation 1.19). To avoid dealing with this, it is further assumed that any one electron moves in an average potential due to the other electrons and the nuclei, (which is to say that electrons behave independently from each other, hence, electron correlation is neglected). The electronic Hamiltonian is rewritten as a sum of the one electron operators:

$$\hat{H} \approx \sum_i^n \hat{h}_i \quad (1.24)$$

where \hat{h}_i is known as “core Hamiltonian”:

$$\hat{h}_i = -\frac{\hbar^2}{2m_e} \nabla_i^2 - \sum_A^N \frac{Z_A e^2}{4\pi\epsilon_o r_{iA}} \quad (1.25)$$

Equally, the wavefunction Ψ is then taken to be a product of one-electron wavefunctions:

$$\Psi(r_1, r_2 \dots r_n) = \psi_1(r_1)\psi_2(r_2) \dots \psi_n(r_n) = \prod_{i=1}^n \psi_i(r_i) \quad (1.26)$$

equation 1.26, also called “Hartree product”, does neither fulfil the Pauli principle nor take into consideration the antisymmetry of the electronic wavefunction. Fock suggested that, in order to satisfy both of these requirements, equation 1.26 should be re-written as a Slater determinant:

$$\Psi = \frac{1}{\sqrt{n!}} \begin{vmatrix} \psi_1(r_1) & \overline{\psi_1(r_1)} & \psi_2(r_1) \cdots & \overline{\psi_{n/2}(r_1)} \\ \psi_1(r_2) & \overline{\psi_1(r_2)} & \psi_2(r_2) \cdots & \overline{\psi_{n/2}(r_2)} \\ \vdots & \vdots & & \vdots \\ \psi_1(r_n) & \overline{\psi_1(r_n)} & \psi_2(r_n) \cdots & \overline{\psi_{n/2}(r_n)} \end{vmatrix} \quad (1.27)$$

where $\frac{1}{\sqrt{n!}}$ ensures normalisation of the wavefunction, $n!$ being the number of terms in the determinant; $\psi_1(r_1)^3$ is electron 1 in orbital ψ_1 with α spin, while $\overline{\psi_1(r_1)}$, is electron 1 in orbital ψ_1 with β spin. The columns in a Slater determinant are the single-electron wave-functions (orbitals) and along the rows are the electron coordinates.

Hartree-Fock method

From now on we will assume a closed-shell system, this is a system with all electrons spin paired (e.g. NH_3), the method is then called “Restricted Hartree-Fock” (RHF). In the HF method the Rayleigh ratio (equation 1.17) is minimised respect to ψ in order

³To introduce the electron spin, the one electron wavefunctions (ψ) are multiplied by spin orbital functions (α or β). Thus, $\psi(r) \times \alpha = \psi(r)$ and $\psi(r) \times \beta = \overline{\psi(r)}$

to find a set of one-electron wave functions that obeys the expression:

$$\hat{f}\psi_i = \epsilon_i\psi_i \quad (1.28)$$

where \hat{f} is the Fock operator for a closed-shell system with n electrons in $n/2$ orbitals:

$$\hat{f} = \hat{h}_i + \sum_{j=1}^{n/2} 2\hat{J}_j - \hat{K}_j \quad (1.29)$$

the first term is the “core Hamiltonian”, seen in equation 1.25. The second term, J_j , is the “Coulomb operator”, representing the Coulombic interaction of an electron in orbital i with an electron in orbital j . The third term is the “exchange operator”, which takes into account the spin effects, but has no physical meaning.

If equation 1.28 is solved for each electron in turn, a set of orbital energies is obtained:

$$\epsilon_i = h_{ii} + \sum_{j=1}^{n/2} 2J_{ij} - K_{ij} \quad (1.30)$$

Note that for any solution found for one electron, the solutions of the other electrons in the system will be affected. Hence, the strategy to solve these equations is to set a trial of one-electron wavefunctions by using the variation method. These are used to calculate the Coulomb and exchange operators. Then the HF equations are solved giving a second set of solutions which are used again in the same fashion. This is the Self Consistent Method (SCF) that gradually refines the one-electron solutions. Energies lower with each iteration. The process is repeated until the results for all the electrons are unchanged (or the change is an acceptably small quantity), when they are said to be “self-consistent”.

In order to solve the HF equations for molecules, Roothaan and Hall, independently,

suggested using a linear combination of known basis functions with which to expand the one-electron orbitals. In this way the HF equations are reduced to a matrix problem and facilitate its solution:

$$\psi_i = \sum_{v=1}^K c_{vi} \phi_v \quad (1.31)$$

where ψ_i represents a molecular orbital, and ϕ_v represent an atomic orbital with an associated coefficient c_{vi} . The coefficients represent the contribution of different atomic orbitals (ϕ) to the molecular orbital (ψ). The use of a linear combination like that in equation 1.31 in the HF equations leads to the expression:

$$FC = SC\epsilon \quad (1.32)$$

where F is a $K \times K$ squared matrix called the Fock matrix, C is a $K \times K$ matrix containing the coefficients c_{vi} , ϵ is a diagonal matrix containing the orbital energies and S is the overlap (between different basis ϕ) matrix. The solution of equation 1.32 is also an iterative process. The total energy for the ground state is given by:

$$E = \sum_{i=1}^n \epsilon_i - \sum_{i=1}^{n/2} \sum_{j=1}^{n/2} (2J_{ij} - K_{ij}) \quad (1.33)$$

1.3.2 Møller-Plesset method

The method that Møller and Plesset proposed to address the problem of electron correlation is based in the Rayleigh-Schrödinger perturbation theory. In this theory, the true or exact Hamiltonian, \hat{H} , is considered a small perturbation of a “zeroth order” Hamiltonian, $\hat{H}^{(0)}$ for which a set of molecular orbitals can be obtained [40].

$$\hat{H} = \hat{H}^{(0)} + \lambda V \quad (1.34)$$

where λ is a parameter that can vary between 0 and 1, when $\lambda = 0$ there is no perturbation and the exact Hamiltonian, \hat{H} , equals the zeroth-order Hamiltonian, $\hat{H}^{(0)}$; and when $\lambda = 1$, the perturbation is “on” and \hat{H} equals its true value.

In the same way, the wavefunctions, Ψ_i , and energies, E_i , of the true Hamiltonian \hat{H} can be expanded as a power series in λ :

$$\Psi_i = \Psi_i^{(0)} + \lambda \Psi_i^{(1)} + \lambda^2 \Psi_i^{(2)} + \dots \quad (1.35)$$

$$E_i = E_i^{(0)} + \lambda E_i^{(1)} + \lambda^2 E_i^{(2)} + \dots \quad (1.36)$$

where $\Psi_i^{(0)}$ is the wavefunction of $\hat{H}^{(0)}$ with energy $E_i^{(0)}$. The ground state wavefunction is then $\Psi_0^{(0)}$ and its energy is $E_0^{(0)}$. $E_i^{(1)}$ is the first-order correction to the energy, $E_i^{(2)}$ is the second-order correction to the energy and so on. The series of equations 1.35 and 1.36 are substituted in $\hat{H}\Psi_i = E_i\Psi_i$, and then terms of the same order are collected together:

$$E_i^{(0)} = \langle \Psi_i^{(0)} | \hat{H}^{(0)} | \Psi_i^{(0)} \rangle \quad (1.37)$$

$$E_i^{(1)} = \langle \Psi_i^{(0)} | V | \Psi_i^{(0)} \rangle \quad (1.38)$$

$$E_i^{(2)} = \langle \Psi_i^{(0)} | V | \Psi_i^{(1)} \rangle \quad (1.39)$$

$$E_i^{(3)} = \langle \Psi_i^{(0)} | V | \Psi_i^{(2)} \rangle \quad (1.40)$$

In the MP method the unperturbed Hamiltonian $\hat{H}^{(0)}$ is the sum of the one-electron Fock Hamiltonians over the total number of electrons n :

$$\hat{H}^{(0)} = \sum_i^n \hat{f}_i \quad (1.41)$$

The Hartree-Fock (ground state) wavefunction $\Psi_0^{(0)}$ is a function of the HF (zeroth-order, unperturbed) Hamiltonian, $\hat{H}^{(0)}$, with an energy value of $E_0^{(0)}$ given by the sum of the orbital energies of all the occupied one electron orbitals. This means that the sum of $E_0^{(0)}$ (equation 1.31) and $E_0^{(1)}$ (equation 1.32) corresponds to the HF energy:

$$\begin{aligned} E_0^{(0)} + E_0^{(1)} &= \langle \Psi_0^{(0)} | \hat{H}^{(0)} | \Psi_0^{(0)} \rangle + \langle \Psi_0^{(0)} | V | \Psi_0^{(0)} \rangle \\ &= \langle \Psi_0^{(0)} | \hat{H} | \Psi_0^{(0)} \rangle \end{aligned} \quad (1.42)$$

Therefore, the first correction to the Hartree-Fock energy is given by the second order perturbation theory. This level of theory is called MP2 and involves equation 1.33. The higher order wavefunction $\Psi_0^{(1)}$ is expanded as a linear combination of solutions to the zeroth-order Hamiltonian, to give:

$$\Psi_0^{(1)} = \sum_j c_j^{(0)} \Psi_j^{(0)} \quad (1.43)$$

$$E_0^{(2)} = \sum_{j \neq 0} \frac{|\langle \Psi_0^{(0)} | V | \Psi_j^{(0)} \rangle|^2}{E_0^{(0)} - E_j^{(0)}} \quad (1.44)$$

where $\Psi_j^{(0)}$ includes excitations obtained by promoting electrons into virtual orbitals obtained from HF calculation. Also, $\Psi_j^{(0)}$ is a function of $\hat{H}^{(0)}$ with corresponding energy $E_j^{(0)}$.

The advantage of MBPT is that is size-consistent, even when a truncated expansion is used, such as MP2. However, is not a variational theory, meaning that it can sometimes give energies lower than the “true” energy [40].

Practical Considerations

The level of theory used throughout this work is second order Møller-Plesset Perturbation Theory (MP2). The reasoning behind this choice is that ammonia dimer is held together partly by dispersion forces, and since this is a correlation effect [36, 38] a post-Hartree-Fock evaluation is mandatory. MP2 is also a popular way of accounting for electron correlation [40] and it has been shown to be successful when applied to many weakly bound and hydrogen bond complexes. For this particular case of ammonia, it was found in references [39, 43] that MP2 provides quantitative results for both equilibrium structure and interaction energies when compared with MP4, suggesting that higher order dispersion components contribute only weakly. This means that MP2 gives a good compromise between accuracy and performance with no real shortcomings over a more expensive MP approach.

Full Configuration Interaction (CI) is too expensive a method for evaluating ammonia clusters. In addition, the application of CI would lead to a non size-consistent treatment of the systems we are involved with, which is incompatible with the “super-molecular approach” also used in this work.

In the 2003 study by Boese *et al.* [43], a broad representation of Density Functional Theory (DFT) functionals were evaluated, and it was concluded that none of the density functionals tested in their work contains information to accurately describe the structure, or the relative energies, particularly dispersion forces, of the ammonia dimer. With “structure” they referred to the bent, i.e. non-linear, hydrogen bond displayed by the pair of fluxional putative minima dimers, a feature that an *ab initio* method can reproduce.

1.3.3 Basis Set

The basis set is a set of known mathematical functions from which the wavefunction is constructed. When molecular calculations are performed, molecular orbitals are expressed as linear combinations of atomic functions (equation 1.45, again below), whose coefficients are determined by the iterative solution of the HF equations.

$$\psi_i = \sum_{v=1}^K c_{vi} \phi_v \quad (1.45)$$

The basis (atomic) functions first used were the Slater Type Orbitals (STO), but it was found that in HF theory they gave rise to integrals that were very difficult to evaluate. This problem was bypassed by Boys' suggestion of replacing STOs by Gaussian type orbitals (GTOs), which are easier to handle. However, this is not a one-to-one replacement, since this leads to significant errors due to the different properties of STOs and GTOs. Roughly, three times as many GTOs are needed to achieve a certain accuracy compared with STOs [50], hence, STOs are modelled as linear combinations of GTOs. This is to say that each atomic orbital (ϕ from equation 1.45) is represented as a linear combination of GTOs.

$$\phi_v = \sum_{k=1}^L d_{km} \phi_k(\alpha_{km}) \quad (1.46)$$

where d_{km} is the coefficient of the “primitive”⁴ Gaussian function ϕ_k , which has an exponent α_{km} and L is the number of functions in the expansion.

The best representation of a molecular orbital would be given by the use of an infinite number of basis sets, the complete basis set (CBS), which when applied to the HF method would provide the energy associated to the HF limit. This would mean

⁴each of the individual Gaussian functions from which the expansion is built. Also, when a basis function is defined as a linear combination of GTOs it is said to be “contracted”

that the difference between the HF energy E_{HF} and the true energy of the system E is the electron correlation E_{corr} [38]:

$$E_{corr} = E - E_{HF} \quad (1.47)$$

The use of a complete basis set is impractical; hence, in practice, the aim is for a finite number of basis sets to approach the HF limit efficiently. Basis sets can be constructed using an optimisation procedure in which the coefficients and the exponents in equation 1.46 are varied to give the lowest atomic energies. The approach chosen to this construction leads to the different “families” of basis sets (e.g. Pople, Dunning).

Practical considerations

Within the framework of this thesis, the choice of basis set is of importance for two specific reasons. First, it defines the accuracy of the computed energies required to calculate binding energies. Second, the accurate calculation of multipole moments is important to us given our interest in decomposing the many-body effect for ammonia clusters and the construction of a potential energy surface.

The choice of basis set dealing with small ammonia clusters has been tested in the literature [39, 49] and by us in a project prior to this thesis. Dunning’s and Pople’s basis set families were tested and compared⁵. The initial test between the two families of basis sets focused on the calculations of monomer properties known to play a role in intermolecular interactions (dipole moment, quadrupole moment and polarisability, etc.), and we compared this with available experimental data afterwards. This comparison was extended to the study of the structures and energetics of the

⁵The performance of the cheaper Pople’s triple- ζ basis set family 6-311++G with increasing polarisation functions (2d,2p), (3d,3p) and (3df,3pd) were first tested in the small structures $(\text{NH}_3)_2$ and $(\text{NH}_3)_3$ hoping that they could provide a less costly alternative when computing the ammonia PES, and so we could extrapolate roughly the MP2 interaction energies

$(\text{NH}_3)_2$ and $(\text{NH}_3)_3$ structures. As a result, we concluded that Dunning’s family of basis set provides the best choice of functions for exploring ammonia clusters at the MP2 level of theory, as they give a more balanced performance with increasing basis set size. Hence, that was our choice to describe the $(\text{NH}_3)_4$ and $(\text{NH}_3)_5$ structures in our study. The notation for the basis set and level of theory will be the following:

$$\text{MP2/aug-cc-pVXZ} \quad (X = D, T, Q, 5)$$

Dunning’s basis set can be double (D), triple (T), quadruple zeta (Q), etc. depending on how many basis functions define the valence (V) orbitals (two, three or four, respectively). The core is described by six contracted Gaussian primitives. Large basis set are used in an attempt to obtain total energies and energy differences close to the basis set limit (CBS) [49]. Correlation consistency or “cc” means that regardless the function type (s,p,d,f...) the ones that contribute the same amount of correlation energy are added to the basis set at the same stage [50]. The addition of diffuse functions is referred to as “augmentation”, or “aug”, and polarisation functions are represented by a “p”. For contraction scheme see reference [50], for polarisation functions included in each basis set see “Gaussian98 User Reference 2nd Edition” [46].

Both references [39, 49] and us have concluded that MP2/aug-cc-pVTZ gives the best compromise between cost and accuracy for ammonia dimers, and we have used the same method for bigger clusters $((\text{NH}_3)_n, n = 4, 5)$.

In this work, the inclusion of diffuse functions is mandatory. On the one hand, because they help to define the “tail” of the wavefunction. This “tail” is, in principle, of secondary importance to the total energy [36, 50]; however, it carries useful information in describing the multipole values and polarisabilities of molecules, which

are both relevant for a faithful estimation of the interaction energy, of particular importance in this work. On the other hand, different studies [39, 51, 52] point out the necessity of using diffuse functions due to the flat bottom of the ammonia PES dimer. Since putative minima structures are separated by small energy differences, not adding diffuse functions to the basis set during the optimisation process leads to missing the “isolation” of one of them, as one isomer “falls down” into the other [39, 51].

Finally, polarisation functions are necessary in the calculations for monomers and clusters to describe electron correlation and the distortion of the atomic orbitals when a bond is made or an interaction occurs.

1.3.4 Basis Set Superposition Error

This work has chosen the Boys and Bernardi [44] Counterpoise Correction (CP) approach to tackle Basis Set Superposition Error (BSSE). It is established that for closed-shell interactions BSSE can be corrected by applying this method [35], and this procedure is also available in the Gaussian98 [46] and Gaussian03 [47] suites of codes which have been used to run all calculations in this work.

The aspects of CP correction are neatly summarised in the work by Ponti and Mella [48], the diagrams and equations shown below are based in their paper.

There are two factors to be considered when tackling BSSE: the basis set of choice, and the geometry of the monomers constituting the aggregate.

To illustrate these two points let us consider two free monomers A and B, that when interacting change (or “deform”) their geometry to A^d and B^d , in order to form a dimer, $A^d B^d$.

$$A, B \xrightarrow{\Delta E_{def}} A^d + B^d \xrightarrow{\Delta E_{A^d B^d}} A^d B^d \quad (1.48)$$

In the scheme above ΔE_{def} , of positive value, is the energy required to bring monomers A and B to the dimer geometry is what we will call “deformation energy”, ΔE_{def} .

$$A \xrightarrow{\Delta E_{defA}} A^d \quad \Delta E_{defA} = E_{A^d} - E_A \quad (1.49)$$

$$B \xrightarrow{\Delta E_{defB}} B^d \quad \Delta E_{defB} = E_{B^d} - E_B \quad (1.50)$$

$$\Delta E_{def} = (E_{A^d} - E_A) + (E_{B^d} - E_B) \quad (1.51)$$

$\Delta E_{A^dB^d}$, in equation 1.48, generally of negative value, is the formation energy of the dimer. A first approach to $\Delta E_{A^dB^d}$ according to the “supermolecular approach” adopted in this work and introduced in the following section, is given by:

$$\Delta E_{A^dB^d} = E_{A^dB^d} - E_A - E_B \quad (1.52)$$

All values at the right hand side of equation 1.52 can be computed. However, since the use of complete basis sets is impractical, the interacting monomers of a cluster will use each other’s basis set in order to complete their own basis set and improve their own energy. This results in an artificial lowering of the total energy of the complex, or overbinding effect. Hence, the formation energy calculated with equation 1.52 carries an error, the BSSE, because the complex has been effectively computed with a bigger basis than the monomers. In fact, BSSE can be defined as the difference in energy between the monomers in the complex geometry structure (i.e. “deformed”) computed with the cluster basis set (i.e full basis) and with just their own basis set.

$$BSSE = (E_{A^d}^{fullbasis} - E_A^{A^dbasis}) + (E_{B^d}^{fullbasis} - E_B^{Bdbasis}) \quad (1.53)$$

Let us note that BSSE vanishes at the Complete Basis Set limit (CBS). Boys and Bernardi [44] recipe is to calculate the formation energy of the cluster as follows:

$$\Delta E_{A^dB^d}^{BB} = E_{A^dB^d} - E_{A^d}^{fullbasis} - E_{B^d}^{fullbasis} \quad (1.54)$$

This means that we subtract from the complex energy the energy of the monomers in their cluster geometry calculated with the full basis set. Equation 1.54 does not account for deformation energy, ΔE_{def} (equations 1.49-1.51), so it has to be added. This, however, includes another difficulty, since for the energies to be comparable one would have to calculate the non-interacting monomers at the non-deformed geometry with the full basis as well. More specifically, the problem appears when defining the centring of monomer's B functions for the computation of monomer A at full basis, and vice versa, because the choice of location of monomer's B basis set functions becomes arbitrary. Thus, the deformation energy cannot be unambiguously computed with the full basis set. In this situation the Counterpoise corrected formation energy will be written as:

$$\Delta E_{A^dB^d}^{CP} = E_{A^dB^d}^{BB} + E_{defA} + E_{defB} \quad (1.55)$$

which expanded gives:

$$\underbrace{\Delta E_{A^dB^d}^{CP} = E_{A^dB^d} - E_{A^d}^{fullbasis} - E_{B^d}^{fullbasis}} + [(E_{A^d}^{A^dbasis} - E_A) + (E_{B^d}^{Bdbasis} - E_B)] \quad (1.56)$$

Gaussian suit of codes 98 [46] and 03 [47] provide the Counterpoise corrected energy,

E_{gauss}^{CP} , considering the elements underbraced in equation 1.56. Hence, for calculating the interaction energy in this work we use:

$$\Delta E_{A^dB^d} = E_{gauss}^{CP} - E_A - E_B \quad (1.57)$$

1.3.5 Supermolecular approach

The interaction energies throughout our work have been calculated by means of the “supermolecular approach”. This method considers that the interaction energy of a molecular aggregate is defined as the energy difference between the supermolecule (the aggregate or cluster) and the free fragments that constitute its whole. Thus, for a dimer constituted by fragments A and B the interaction energy would have the following form:

$$\Delta E = E_{AB} - E_A - E_B \quad (1.58)$$

In the expression above E_{AB} represents the interaction energy of the dimer AB, while E_A and E_B represent the energy of the fragments A and B, respectively.

A faithful description of the supermolecule interaction depends on how reliably we can compute the energies of the aggregate and the monomers. The reliability of the numerical values comprises three demands [35], two related to the method of choice and one to the basis set. First, our method of choice must provide energies of similar accuracy for the cluster and its individual fragments; this implies the election of a size-consistent method. Secondly, our method of choice should be able to reproduce non-additive effects (e.g. many-body). Finally, it is known that the evaluation of the energy of a system is very sensitive to the choice of basis set. Fragments and aggregate should be evaluated using the same basis set (basis set consistency) and the BSSE, discussed previously, should be taken into account.

1.3.6 Many-body effects

Let us consider an assembly of N molecules. A first approximation to the calculation of the total energy of the system (E) would be to take the molecules in pairs:

$$E = \sum_i^n E_i + \sum_{j>i=1}^n E_{ij} \quad (1.59)$$

In equation 1.59, $\sum_i^n E_i$ indicates the summation of the monomer energies, and $\sum_{j>i=1}^n E_{ij}$ accounts for the energy of each pair of molecules. This is the pairwise additivity assumption, in which the energies of each pair are calculated as if the other molecules were not present. However, they are, and do affect the stability of the pair considered. This means that when we consider the binding energy of a cluster, there is a many-body correction to be accumulatively added: three-body for a trimer, four-body for a tetramer and so on. That said, the many-body correction is usually small in magnitude, continuously decreasing upon increasing cluster size.

In this work, we have decomposed the interaction energies into their n -body contributions for the pure ammonia clusters up to the tetramer in an attempt to improve our understanding of the molecular interactions. The computational strategy for the many-body decomposition can be summarised using $(\text{NH}_3)_4$ as an example, and with the help of the energy decomposition described by the following equation:

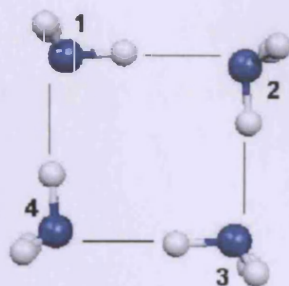


Figure 1.2: Ammonia tetramer for the calculation of many-body effects.

This is one of the isomeric structures we have isolated for $(\text{NH}_3)_4$. It can be structurally decomposed by considering that it contains six dimers (12,13,14,23,24,34) contributing the 2-body interaction energy and three sets of trimers (123,134,234) contributing the 3-body interaction energy. The 4-body contribution to the interaction energy (1234) is obtained as a complement to the total energy value. Image obtained with MOLEKEL [45]

$$E(x_1, x_2, x_3, x_4) = \sum_{i=1}^4 E^1(x_i) + \sum_{i<j=1}^4 E^2(x_i x_j) + \sum_{i<j<k=1}^4 E^3(x_i x_j x_k) + \sum_{i<j<k<l=1}^4 E^4(x_i x_j x_k x_l) \quad (1.60)$$

where $E(x_1, x_2, x_3, x_4)$ is the $(\text{NH}_3)_4$ interaction energy, x_i is the position of all the atoms in the i th molecule, $E^1(x_i)$ is the energy required to distort NH_3 from its gas-phase structure to the one in the complex, $E^2(x_i x_j)$ is the 2-body interaction between two molecules i and j , and so on. Given an optimised isomer, (either fully relaxed or with the intramolecular structure kept frozen to the experimental gas-phase geometry), single point calculations were performed on the single monomers, pairwise and threewise fashion to evaluate the 1-body, 2-body and 3-body distortion effects. The 4-body effect is obtained as the complement to the total interaction energy value.

Bibliography

- [1] "*Amun*", <http://en.wikipedia.org/wiki/Amun>, last accessed: 2010, September 27.
- [2] "*Siwa Oasis*", http://en.wikipedia.org/wiki/Siwa_Oasis, last accessed: 2010, September 27.
- [3] "*Eponyms*", <http://www.bbc.co.uk/dna/h2g2/alabaster/A632990>, last accessed: 2010, September 27.
- [4] "*Ammonia*", <http://en.wikipedia.org/wiki/Ammonia>, last accessed: 2010, September 27.
- [5] "*The Merriam Webster New Book of Word Histories*" (on-line preview), http://books.google.co.uk/books?id=IrcZEZ1b0JsC&pg=PA13&lpg=PA13&dq=merriam+webster+New+book+of+word+histories+ammonia&source=web&ots=7Putpd4C0l&sig=XroQg2BRA8mhvpN74ij44zsX0cI&hl=en&sa=X&oi=book_result&resnum=3&ct=result#PPA13,M1, last accessed: 2010, September 27.
- [6] "*Siwa. Resort of Kings*", <http://www.saudiaramcoworld.com/issue/197904/siwa-resort.of.kings.htm>, last accessed: 2010, September 27.
- [7] Sebastian, A. "*A Dictionary of the History of Science*" (on-line preview),

- <http://books.google.co.uk/books?id=gTXFN-8v95MC&pg=PA204&dq=Anton+Sebastian+ammonia&sig=ACfU3U3pujb77uRtmTxNQdxmBZqkHARwIQ#PPA17,M1>, last accessed: 2010, September 27.
- [8] “*Joseph Priestly*”, http://en.wikipedia.org/wiki/Joseph_Priestley, last accessed: 2010, September 27.
- [9] “*Claude Louis Berthollet*”, http://en.wikipedia.org/wiki/Claude_Louis_Berthollet, last accessed: 2010, September 27.
- [10] Shawcross, D. L.; Olde Damnik, S. W. M.; Butterworth, R. F.; Jalan, R. *Metabolic Brain Disease*, **2005**, *20*, 169.
- [11] McGilvery, R. W.; Goldstein, G. W. *BIOCHEMISTRY: A Functional Approach*, W. B. Saunders Company, Japan, **1983**.
- [12] Khademi, S.; O’Connell III, J.; Remis, J.; Robles-Colmenares, Y.; Miercke, L.J.W; Stroud, R.M. *Science*, **2004**, *305*, 1587.
- [13] Yoshino, R.; Morio, T.; Yamada, Y.; Kuwayama, H.; Sameshima, M.; Tanaka, Y; Sesaki, H.; Iijima, M. *Eukaryotic Cell*, **2007**, *6*, 2419.
- [14] “*Ammonia on Mars could mean life*”, <http://news.bbc.co.uk/1/hi/sci/tech/3896335.stm>, last accessed: 2010, September 27.
- [15] “*Science: Liquid of Life*”, <http://www.time.com/time/magazine/article/0,9171,872899,00.html?iid=chix-sphere>, last accessed: 2010, September 27.
- [16] “*Ammonia-based life*”, <http://www.daviddarling.info/encyclopedia/A/ammonialife.html>, last accessed: 2010, September 27.
- [17] Benner, A.; Ricardo, A.; Carrigan, M. A. *Current Opinion in Chemical Biology*, **2004**, *8*, 672.

- [18] Zmaczynski, R. “*The effect of the Haber process on fertilisers*”, <http://www.princeton.edu/~hos/mike/texts/readmach/zmaczynski.htm>, last accessed: 2010, September 27.
- [19] Modak, J. M. “*Haber process for ammonia synthesis*”, <http://www.ias.ac.in/resonance/Sept2002/pdf/Sept2002p69-77.pdf>, last accessed: 2010, September 27.
- [20] “*Sodium Nitrate*”, http://en.wikipedia.org/wiki/Sodium_nitrate, last accessed: 2010, September 27.
- [21] “*The Nobel Prize in Chemistry 1918. Fritz Haber*”, http://nobelprize.org/nobel_prizes/chemistry/laureates/1918/press.html, last accessed: 2010, September 27.
- [22] “*Haber process*”, http://en.wikipedia.org/wiki/Haber_process#cite_note-4, last accessed: 2010, September 27.
- [23] Bailar, J. C.; Emeléus, H. J.; Nyholm, R.; Trotman-Dickenson, A. F. *Comprehensive Inorganic Chemistry*, **1973**, Pergamon Press.
- [24] Benedict, W.S.; Gailar, N.; Plyler, E.K. *Can. J. Phys.*, **1957**, 35, 1235.
- [25] Cotton, F. A.; Wilkinson, G.; Gars, P. L. *Basic Inorganic Chemistry*, **1995**, 3rd Edition, John Wiley & Sons.
- [26] Butler, I.; Harrod, J. *Inorganic Chemistry*, **1989**, The Benjamin Cummins Publishing Company.
- [27] Stone, A. J. *The Theory of Intermolecular Forces*, **1996**, Oxford Univeristy Press.
- [28] Berry, R. S.; Rice S. A.; Ross, J. *Physical Chemistry*, **2000**, Oxford Univeristy Press.

-
- [29] Dill, K; Broomberg, S. *Molecular Driving Forces*, **2003**, Garland Science.
- [30] Keeler, J.; Wothers, P. *Chemical Structure and Reactivity*, **2008**, Oxford University Press.
- [31] Alberti, R. A.; Silbey, R. J. *Physical Chemistry*, **1995**, John Wiley & Sons.
- [32] Atkins, P.; de Paula, J. *Physical Chemistry*, **2006**, 8th Edition, Oxford University Press.
- [33] Shriver, D. F.; Atkins, P. W. *Inorganic Chemistry*, **1999** Oxford University Press.
- [34] Piela, L. *Ideas of Quantum Chemistry*, **2007**, Elsevier.
- [35] Scheiner, S *Molecular Interactions: From van der Waals to Strongly Bound Complexes*, **1997**, John Wiley & Sons, Ltd.
- [36] Chalasiński, G.; Szcześniak, M. *Chem. Rev.*, **1994**, *94*, 1723.
- [37] Desiraju, G. R.; Steiner, T. *The Weak Hydrogen Bond*, **1999**, Oxford University Press.
- [38] Cramer, C.J. *Essentials of Computational Chemistry*, **1995**, John Wiley & Sons., Inc.
- [39] Lee, J.S.; Park, S.Y. *J. Chem. Phys.*, **2000**, *112*, 230.
- [40] Leach, A.R., *Molecular Modelling Principles and Applications*, **2001**, Pearson Education Limited.
- [41] Green, N. J. B.; *Quantum Mechanics I: Foundations*, **2001**, Oxford Science Publications.

- [42] Atkins, P.; Friedman, R. *Molecular Quantum Mechanics*, **2005**, 4th Edition, Oxford Univeristy Press.
- [43] Boese, A.D.; Chandra, A; Martin, J.M.L.; Marx, D *J. Chem. Phys.*, **2003**, *119*, 5965.
- [44] Boys, S.F.; Bernardi, F. *Mol. Phys.*, **1970**, *19*, 553.
- [45] Flükiger, P.; Lüthi, H. P.; Portmann, S.; Weber, J. MOLEKEL 4.3, Swiss National Supercomputing Centre: Manno (Switzerland).
- [46] M. J. Frisch, G. W. Trucks, H. B. Schlegel, G. E. Scuseria, M. A. Robb, J. R. Cheeseman, V. G. Zakrzewski, J. A. Montgomery, Jr., R. E. Stratmann, J. C. Burant, S. Dapprich, J. M. Millam, A. D. Daniels, K. N. Kudin, M. C. Strain, O. Farkas, J. Tomasi, V. Barone, M. Cossi, R. Cammi, B. Mennucci, C. Pomelli, C. Adamo, S. Clifford, J. Ochterski, G. A. Petersson, P. Y. Ayala, Q. Cui, K. Morokuma, P. Salvador, J. J. Dannenberg, D. K. Malick, A. D. Rabuck, K. Raghavachari, J. B. Foresman, J. Cioslowski, J. V. Ortiz, A. G. Baboul, B. B. Stefanov, G. Liu, A. Liashenko, P. Piskorz, I. Komaromi, R. Gomperts, R. L. Martin, D. J. Fox, T. Keith, M. A. Al-Laham, C. Y. Peng, A. Nanayakkara, M. Challacombe, P. M. W. Gill, B. Johnson, W. Chen, M. W. Wong, J. L. Andres, C. Gonzalez, M. Head-Gordon, E. S. Replogle, and J. A. Pople. Gaussian 98, Revision, A.11.1, Gaussian, Inc., Pittsburgh, PA, **2001**.
- [47] M. J. Frisch and G. W. Trucks and H. B. Schlegel and G. E. Scuseria and M. A. Robb and J. R. Cheeseman and Montgomery, Jr., J. A. and T. Vreven and K. N. Kudin and J. C. Burant and J. M. Millam and S. S. Iyengar and J. Tomasi and V. Barone and B. Mennucci and M. Cossi and G. Scalmani and N. Rega and G. A. Petersson and H. Nakatsuji and M. Hada and M. Ehara and K. Toyota and R.

Fukuda and J. Hasegawa and M. Ishida and T. Nakajima and Y. Honda and O. Kitao and H. Nakai and M. Klene and X. Li and J. E. Knox and H. P. Hratchian and J. B. Cross and V. Bakken and C. Adamo and J. Jaramillo and R. Gomperts and R. E. Stratmann and O. Yazyev and A. J. Austin and R. Cammi and C. Pomelli and J. W. Ochterski and P. Y. Ayala and K. Morokuma and G. A. Voth and P. Salvador and J. J. Dannenberg and V. G. Zakrzewski and S. Dapprich and A. D. Daniels and M. C. Strain and O. Farkas and D. K. Malick and A. D. Rabuck and K. Raghavachari and J. B. Foresman and J. V. Ortiz and Q. Cui and A. G. Baboul and S. Clifford and J. Cioslowski and B. B. Stefanov and G. Liu and A. Liashenko and P. Piskorz and I. Komaromi and R. L. Martin and D. J. Fox and T. Keith and M. A. Al-Laham and C. Y. Peng and A. Nanayakkara and M. Challacombe and P. M. W. Gill and B. Johnson and W. Chen and M. W. Wong and C. Gonzalez and J. A. Pople Gaussian 03, Revision B.05, Gaussian, Inc., Pittsburgh, PA, **2003**.

- [48] Ponti, A.; Mella, M. *J. Phys. Chem. A*, **2003**, *99*, 5976.
- [49] Stårling, J.; Schütz, M.; Lindh, R.; Karlström, G.; Widmark, P.O. *Mol. Phys.*, **2002**, *100*, 3389.
- [50] Jensen, F. *Introduction to Computational Chemistry*, **1999**, John Wiley & Sons Ltd.
- [51] Hasset, D.M.; Marsden, C.J.; Smith, B.J. *J. Chem. Phys. Lett.*, **1991**, *183*, 449.
- [52] Tao, F.M.; Klemperer, W.J. *J. Chem. Phys.*, **1993**, *99*, 5976.

Chapter 2

Pure ammonia clusters: $(\text{NH}_3)_n$

$(n = 2 - 5)$

2.1 Introduction

Among ammonia clusters, the dimer is the most studied structure both theoretically and experimentally. Up to the publication of the microwave study for $(\text{NH}_3)_2$ by Klemperer and co-workers [1] in 1985, it was assumed that such a structure would feature a classical (i.e. linear) hydrogen bonded structure, just as $(\text{H}_2\text{O})_n$ and $(\text{HF})_n$ clusters. The idea of “non-linearity” was also supported by the investigation of the Fourier Transform Infrared (FTIR) spectra of ammonia in noble gas matrices [2]. It was further suggested, based on isotope substitution microwave experiments [3], that the ammonia dimer structure would also be quite rigid near the equilibrium structure, a finding that was contradicted by the infrared predissociation spectra of reference [4] and other subsequent IR experiments [5–8] in which a “floppy” ammonia dimer was predicted.

In parallel to the experiments, several theoretical investigations involving *ab initio*

and model potentials were carried out. Hirao *et al.* [9] computed the binding energy of the ammonia clusters up to the pentamer using Hartree-Fock (HF) and the 6-31G* basis set. In contrast with the experimental suggestions, a linear H-bond was found. More accurate calculations revised this result [10–16], proposing the existence of two stationary points for the ammonia dimer. On one hand, the minimum energy structure having C_s symmetry and a H-bond less linear than that predicted by HF calculations. On the other hand, a “centrosymmetric” cyclic structure with C_{2h} symmetry, which would be the transition state in the hydrogen bond donor-acceptor interchange. The barrier high for this process was predicted to be very low (roughly 3.5 cm^{-1} [14] or 5.9 cm^{-1} [16]). The model potential by Olthof *et al.* [13], in which a model surface was fitted to the $(\text{NH}_3)_2$ infrared spectra [7], supported these ideas and could also explain the existing experimental IR data. In conclusion, all modern evidence suggests that $(\text{NH}_3)_2$ is a hydrogen bonded complex with a non-linear H-bond structure with the tendency to interchange the donor/acceptor nature of the two molecules easily. In this respect, a very recent study by Curotto and Mella [44] performing different quantum Monte Carlo simulations on ammonia clusters, has indicated that the “donor-acceptor” configuration is visited with the same likelihood as the “acceptor-donor” configuration for the ammonia dimer.

Regarding clusters up to the hexamer, the experimental data from references [4–6, 17, 38], indicate that these structures would have a very small electric dipole moment, suggesting a cyclic or ring-like arrangement. However, the presence of a broad IR absorption band in the spectrum of the pentamer [5] was interpreted as an indication of a less rigid structure than the tetramer and trimer, perhaps suggesting that $(\text{NH}_3)_5$ may have a fluxional nature, making structural assignments more difficult. Larger species than the hexamer ($n = 18, 745, 1040$) were studied by Buck *et al.* [18] but direct structural information was not extracted from the experiment data.

The *ab initio* geometry optimisation for $(\text{NH}_3)_n$ ($n = 3 - 5$) by Hirao *et al* [9] predicted a ring like geometry for the global minima of these isomers, albeit largely overestimating their binding energies, most likely due to the lack of BSSE corrections. The model potential with polarisable terms of Dykstra and Andrews [33] found that the trimer and tetramer are symmetric, cyclic structures. Using a nonpolarisable model potential calibrated against Coupled Pair Functional (CPF) results [31], Greer *et al.* [32] found, as before, that the trimer and tetramer arranged in cycles, but that the pentamer, hexamer and heptamer preferred 3D structures for their global minima. In particular, the pentamer was found to display a distorted pyramid conformation. The investigation of clusters up to $n = 18$ by Beu and Buck [25] using a nonpolarisable model potential parameterised to the crystal sublimation energy of ammonia by Impey and Klein [34], provided the same result, that pentamer and higher isomers tend to form 3D isomeric structures that are very close in energy.

As far as we know, three correlated *ab initio* methods have also been used to investigate clusters larger than the dimer. The work of Slipchenko *et al.* [38] recently studied, both experimentally and using MP2 calculations, clusters up to the tetramer, once again predicting cyclic arrangements for the trimer and tetramer global minima structures. Kulkarni and Pathak [30] computed interaction energies and equilibrium geometries for $(\text{NH}_3)_n$ ($n = 3 - 6$). They presented and compared cyclic and linear arrangements for the clusters, concluding that linear species have smaller binding energies than cyclic ones, as found for neutral and protonated water clusters [19, 20]. Finally, Szcześniak *et al.* [21] focused on addressing the decomposition of $(\text{NH}_3)_3$ interaction energy in different components employing symmetry adapted perturbation theory (SAPT).

It seems to us that high level calculations on ammonia clusters larger than the dimer are scarce, particularly indicated by the lack of consensus on the structure of a

relatively small isomer like the pentamer. Hence, this chapter presents an MP2 study of the structure, intermolecular binding energies and harmonic frequencies of $(\text{NH}_3)_n$ ($n = 2 - 5$). Several isomers for each cluster were optimised, and their interaction energy decomposed in 2-, 3- and 4-body contributions. Harmonic frequencies were computed and used to correct for the nuclear zero-point motion.

2.2 Methodology

As advanced in the introduction of this thesis, all of the electronic structure calculations on $(\text{NH}_3)_n$ ($n = 2 - 5$) were performed using the Gaussian 98 [27] and 03 [28] *ab initio* suits of codes using second-order Møller-Plesset perturbation theory (MP2) with frozen core. Also, for the initial optimisation steps for clusters $n = 3$ and 4, for structural aspects only, we found useful the use of the Hartree-Fock (HF) level of theory. BSSE was accounted for by means of the Counterpoise (CP) correction procedure [22–24] on the optimised structures.

We think it is worth mentioning the optimisation strategy followed throughout this work. The first step was to encode each geometrical structure in a Z-Matrix that could be used as an input for the geometry optimisation. Possible putative minima structures were obtained from previous published results, obtained mostly using model interaction potentials [25]; and also from considering molecular arrangements likely to have relatively strong hydrogen bonds.

Basis sets were used hierarchically, meaning that the output of an optimisation was then used as an input for the following, larger basis set optimisation calculation. We used two routes for the optimisation of the $(\text{NH}_3)_n$ $n = 2 - 4$ structures: on one hand, we allowed the whole structure to relax; on the other hand, we kept the intramolecular structure of the monomers frozen to the experimental values of gas-phase ammonia

($r_{\text{NH}} = 1.0124 \text{ \AA}$, $\text{H}\hat{\text{N}}\text{H} = 106.67^\circ$) [29]. The reason for this is, given our goal of developing an *ab initio* based interaction potential between rigid ammonia molecules, to see whether for a given isomer the relaxation of the intramolecular geometry has any impact on the energetics and structure of the cluster. It can be advanced that the adoption of the frozen intramolecular approximation produces negligible changes from the results of the “fully relaxed” approach for both energy and structure (for comparison Appendix 1 can be seen, it contains BSSE energies for $(\text{NH}_3)_n$, $n = 2 - 5$ keeping intramolecular parameters frozen to the experimental value).

After each optimisation with a different basis set, we performed a single point BSSE corrected calculation. If we consider two PES's, one not accounting for BSSE and a second one BSSE corrected, performing a single point correction on the first one is equivalent to obtain the “vertical” corrected energy. In addition, a further optimisation was performed on the optimised geometry (a “re-optimisation”) including BSSE correction. In other words, we allow our “vertical” point energy to find the minimum in the BSSE corrected PES.

Also, to improve our understanding of the intermolecular interaction, we proceeded to decompose the interaction energies into their n -body contributions for the clusters up to the tetramer. The computational strategy for the many-body decomposition was explained in the introduction of this thesis using $(\text{NH}_3)_4$ as an example.

Finally, harmonic frequencies were computed on the fully relaxed clusters as a way to introduce zero-point energy (ZPE) correction and to study the effects of vibrational motion on their relative stability. We also investigated possible patterns in the N-H frequency shifts of the ammonia aggregates that could be used as a spectroscopic signature of some structural feature.

2.3 Results

2.3.1 Structural results and binding energies

Figures 2.1 to 2.4 show the optimised structures for $(\text{NH}_3)_n$ $n = 2 - 5$ obtained at the CP corrected MP2/aug-cc-pVTZ level of theory. Tables 2.1 to 2.4 show the energetic data, in kcal/mol, for all the isomeric species obtained in this work together with previously published *ab initio* and model potential data. For all tables 2.1 to 2.4 “BE” is the BSSE uncorrected binding energy for an optimised cluster (i.e. binding energy computed using the energy of fully relaxed local minima); “ZPE” is its harmonic zero point energy; “BE^{CP}” gives its single point CP-corrected (i.e. BSSE corrected) binding energy, and “Opt^{CP}” gives the BSSE corrected binding energy after structural relaxation on the counterpoise corrected surface.

Dimer

All basis set results support the asymmetric isomer (asym, I) as the most stable one, with the cyclic species (II) being a transition state (TS). The relative energy difference between these two isomers represents the hydrogen donor-acceptor exchange barrier [14], it amounts to roughly 3 cm^{-1} at the CP-corrected MP2/aug-cc-pVQZ level of theory. These results are in good agreement with the work by Lee and Park [14]. As expected, introducing single point Counterpoise (i.e. vertical) correction on the optimised isomeric geometries reduces the binding energy, but no substantial changes are seen in the relative energy of the two isomers. In the same way, only slight changes are observed after the structural relaxation on the CP-corrected PES.

Looking at table 2.1, we also notice that energy results at the MP2/aug-cc-pVTZ level are in very good agreement with those obtained at MP2/aug-cc-pVQZ level of theory. Let us stress that MP2 has already been reported to compare well with the

Table 2.1: Energy values for $(\text{NH}_3)_2$ in kcal/mol.

	MaDZ ^j			MaTZ ^j			MaQZ ^j			Other
$(\text{NH}_3)_2$	BE(ZPE)	BE ^{CP}	Opt ^{CP}	BE(ZPE)	BE ^{CP}	Opt ^{CP}	BE	BE ^{CP}	Opt ^{CP}	
asym ^a	3.624(44.647)	2.735	2.771	3.287(44.777)	3.001	3.011	3.220	3.089	3.090	4.03 ^h
TS ^a	3.403	2.735	2.756	3.239	2.999	2.999	3.197	3.082	3.082	
asym ^b	3.623	2.737		3.286	3.000		3.219	3.088		3.138 ^c
TS ^b	3.404	2.729		3.239	2.995		3.196	3.081		3.130 ^c
asym										2.923 ^d
asym										3.090 ^e
dimer										2.934 ^f
asym										2.784 ^g

^a This work; ^b Ref. [14], MP2/aug-cc-pVXZ, X= D, T; ^c Ref. [16], W2 result; ^d Ref. [15], LMP2/aug-cc-pVTZ; ^e Ref. [31, 32], coupled pair functional (CPF); ^f Ref. [33], model potential; ^g Ref. [25], model potential; ^h Ref. [30], MP2/6-31++G(d,p) result; ^j MaXZ (X=D, T, Q) is a shorthand notation for MP2/aug-cc-pVXZ. BE are the BSSE uncorrected values for an optimised cluster (i.e. binding energy computed using the energy of fully relaxed local minima); “ZPE” is the calculated zero point correction; “BE^{CP}” gives its single point CP-corrected (i.e. BSSE corrected) binding energy, and “Opt^{CP}” gives the BSSE corrected binding energy after structural relaxation on the counterpoise corrected surface. The “Other” column collects literature values obtained using both *ab initio* calculations and model potentials.

more expensive MP4 and Coupled Cluster methods [14] for several atomic basis. The good agreement between basis sets in our calculations suggests that the MP2/aug-cc-pVTZ level may provide an accurate representation for the energetics of the ammonia clusters.

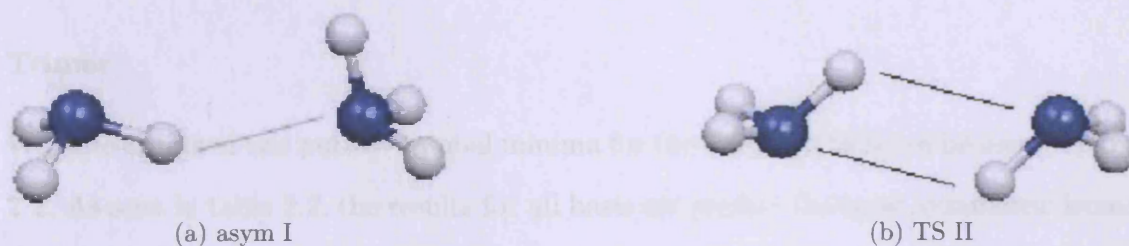


Figure 2.1: Equilibrium structures for $(\text{NH}_3)_2$ obtained with Counterpoise corrected MP2/aug-cc-pVTZ optimisations. All images in this work have been obtained and visualised using MOLEKEL [26]

Also, our best value for the asymmetric dimer (asym, I) agrees very well with the coupled pair functional results reported by Sagarik *et al.* [31, 32] which is the most accurate *ab initio* data available. Good agreement is also seen with the results of the W2 method by Boese *et al.* [16], the relative energy difference between the asymmetric and cyclic dimers is predicted to be roughly 3 cm^{-1} as in this work. In addition, good agreement is also seen, particularly at the MP2/aug-cc-pVTZ level of theory, between this work and the local-MP2/aug-cc-pVTZ data of Stålring *et al.* [15]. On the other hand, the BE for the asymmetric dimer (asym, I) obtained by Beu and Buck [25] using the Impey and Klein [34] potential is 2.784 kcal/mol . This represents an underestimation of roughly 0.3 kcal/mol respect to the MP2 values, although we found that the optimised structure is in good agreement with all of the *ab initio* results. In opposition to this, the equilibrium structure presented by Dykstra and Andrews model potential [33] in as the minimum energy structure for the dimer does not match any of the stationary points reported in the literature or by this work. This fact has already been discussed in the literature [35, 36] and it is thought to be due to the difficulty

at the time of parameterising properly the nonelectric part of the potential model. Nonetheless, the interaction energy for this “odd” isomer is 2.934 kcal/mol [33], only slightly lower than the *ab initio* values, perhaps suggesting that induction may play an important part in defining the interaction energy.

Trimer

We have obtained two putative global minima for the trimer, which can be seen in figure 2.2. As seen in table 2.2, the results for all basis set predict the most symmetric isomer (“equi”) as the most stable structure, with isomer II (asym) lying 3.4-3.7 kcal/mol above isomer “equi” on the BSSE corrected surface. This energy difference is the largest to be seen between the BEs of two local minima among all of the cluster sizes. It is due to the inverted ammonia in the “asym” ring, which also induces a large dipole moment in the structure (3.04 D versus 0 D for “equi”). Kulkarni and Pathak [30] provide the only other correlated *ab initio* result for the most stable isomer “equi” using MP2/6-31++G(d,p). Their result is roughly 2.7 kcal/mol more binding than our best results, due to the lack of BSSE correction in their calculations.

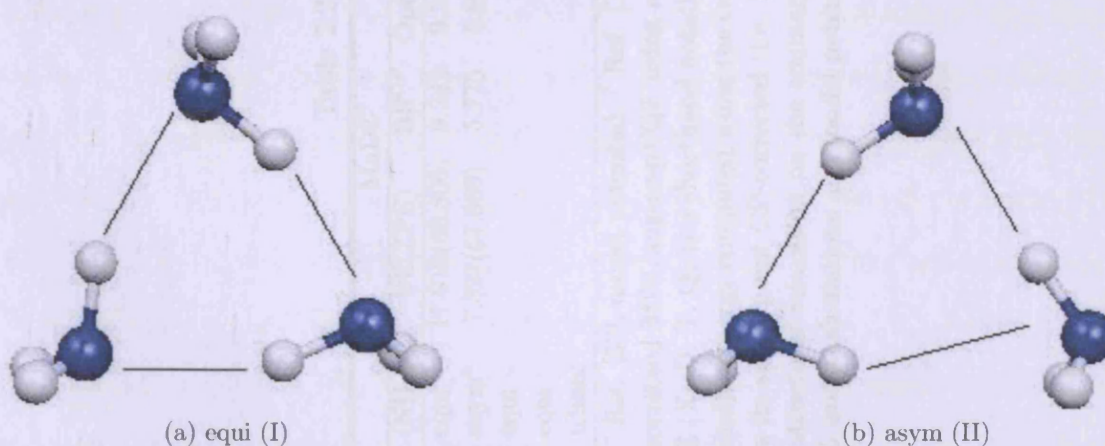


Figure 2.2: Equilibrium structures for $(\text{NH}_3)_3$ obtained with Counterpoise corrected MP2/aug-cc-pVTZ optimisations.

Table 2.2: Energy values for $(\text{NH}_3)_3$ in kcal/mol

	MaDZ ^j			MaTZ ^j			MaQZ ^j			Other
$(\text{NH}_3)_3$	BE(ZPE)	BE ^{CP}	Opt ^{CP}	BE(ZPE)	BE ^{CP}	Opt ^{CP}	BE	BE ^{CP}	Opt ^{CP}	
equi ^a	11.919(68.806)	9.242	9.326	10.974(69.001)	10.067	10.074	10.747	10.334	10.329 ⁱ	13.02 ^h
asym ^a	7.827(67.886)	5.775	5.886	7.182(68.155)	6.439	6.453	6.961	6.633	6.633 ⁱ	
equi										8.263 ^g
equi										8.439 ^e
trimer										9.392 ^f

^a This work; ^e Ref. [32], model potential; ^f Ref. [33], model potential; ^g Ref. [25], model potential; ^h Ref. [30], MP2/6-31++G(d,p) result; ⁱ CP-corrected MP2/aug-cc-pVQZ using a geometry obtained with a CP-corrected optimization at the MP2/aug-cc-pVTZ level; ^j MaXZ (X=D, T, Q) is a shorthand notation for MP2/aug-cc-pVXZ. BE are the BSSE uncorrected values for an optimised cluster (i.e. binding energy computed using the energy of fully relaxed local minima); “ZPE” is the calculated zero point correction; “BE^{CP}” gives its single point CP-corrected (i.e. BSSE corrected) binding energy, and “Opt^{CP}” gives the BSSE corrected binding energy after structural relaxation on the counterpoise corrected surface. The “Other” column collects literature values obtained using both *ab initio* calculations and model potentials.

Also, table 2.2 shows the model potential results by references [25, 32, 33]. Two structures, also labelled “equi” obtained by Beu and Buck [25] and Greer *et al.* [32] are almost identical to our lowest energy isomer. Their resulting interaction energies agree well between themselves, data obtained using rigid body pairwise additive potentials. However, these values underestimate by roughly 2 kcal/mol our CP-corrected MP2/aug-cc-pVQZ value, suggesting that the lack of many-body effects in the model potentials may undermine the accuracy to reproduce larger clusters energy landscapes. Regarding the data by Dykstra and Andrews [33], similarly to the dimer case, the geometry of their trimer shows a cycle of three ammonia molecules that are rotated by 60° around their C_3 axis with respect to our *ab initio* “equi” structure [35, 36]. Even in this case, the energy difference in binding energy when compared to our CP-corrected MP2/aug-cc-pVQZ is only 1 kcal/mol.

Tetramer

We obtained three stationary structures for $(\text{NH}_3)_4$ (figure 2.3). The two most stable isomers (I “boat” and II “planar”) are almost degenerate at the CP-corrected MP2/aug-cc-pVTZ level. The estimated binding energy at the aforementioned level of theory is roughly 15.5 kcal/mol, the sign and magnitude of the small energy differences between the isomers depending on the level of the calculations. Structurally, “boat” and “planar” isomers have as a main structural difference the value of the torsional angle formed by the four nitrogen atoms, in isomer II (“planar”) they are constrained to lie in the same plane. Depending on the calculation level, isomer II “planar”, is either a transition state (at MP2/aug-cc-pVDZ) connecting two equivalent “boat” isomers through a puckering (rocking or pseudorotation) motion; or a minimum (at MP2/aug-cc-pVTZ). Looking at table 2.3 it can be seen that the results by Kulkarni and Pathak [30], which do not account for BSSE, predict a larger binding energy for the “boat”

Table 2.3: Energy values for $(\text{NH}_3)_4$ in kcal/mol.

$(\text{NH}_3)_4$	MaDZ ^j			MaTZ ^j			Other
	BE(ZPE)	BE ^{CP}	Opt ^{CP}	BE	BE ^{CP}	Opt ^{CP}	
boat ^a	18.523(92.244)	14.304	14.427	17.002	15.515	15.527	20.12 ^h
planar ^a	18.52	14.298	14.426	17.009	15.514	15.535	
tail ^a	15.128(91.442)	11.503	11.640	13.786	12.552	12.569	
boat							12.632 ^g
planar							12.613 ^g
boat							13.098 ^e
boat							14.119 ^f

^a This work; ^e Ref. [32], model potential; ^f Ref. [33], model potential; ^g Ref. [25], model potential; ^h Ref. [30], MP2/6-31++G(d,p) result. ^j MaXZ (X=D, T, Q) is a shorthand notation for MP2/aug-cc-pVXZ. BE are the BSSE uncorrected values for an optimised cluster (i.e. binding energy computed using the energy of fully relaxed local minima); “ZPE” is the calculated zero point correction; “BE^{CP}” gives its single point CP-corrected (i.e. BSSE corrected) binding energy, and “Opt^{CP}” gives the BSSE corrected binding energy after structural relaxation on the counterpoise corrected surface. The “Other” column collects literature values obtained using both *ab initio* calculations and model potentials.

structure than our results. In addition, model potential results from references [25] and [32] underestimate our *ab initio* binding energies by 2.9 and 2.4 kcal/mol, respectively. This represents a worsening of the model potentials with respect to the $(\text{NH}_3)_3$ case, in the previous subsection. The model used by Dykstra and Andrews [33] performs better, the discrepancy with our *ab initio* data being only 1.4 kcal/mol.

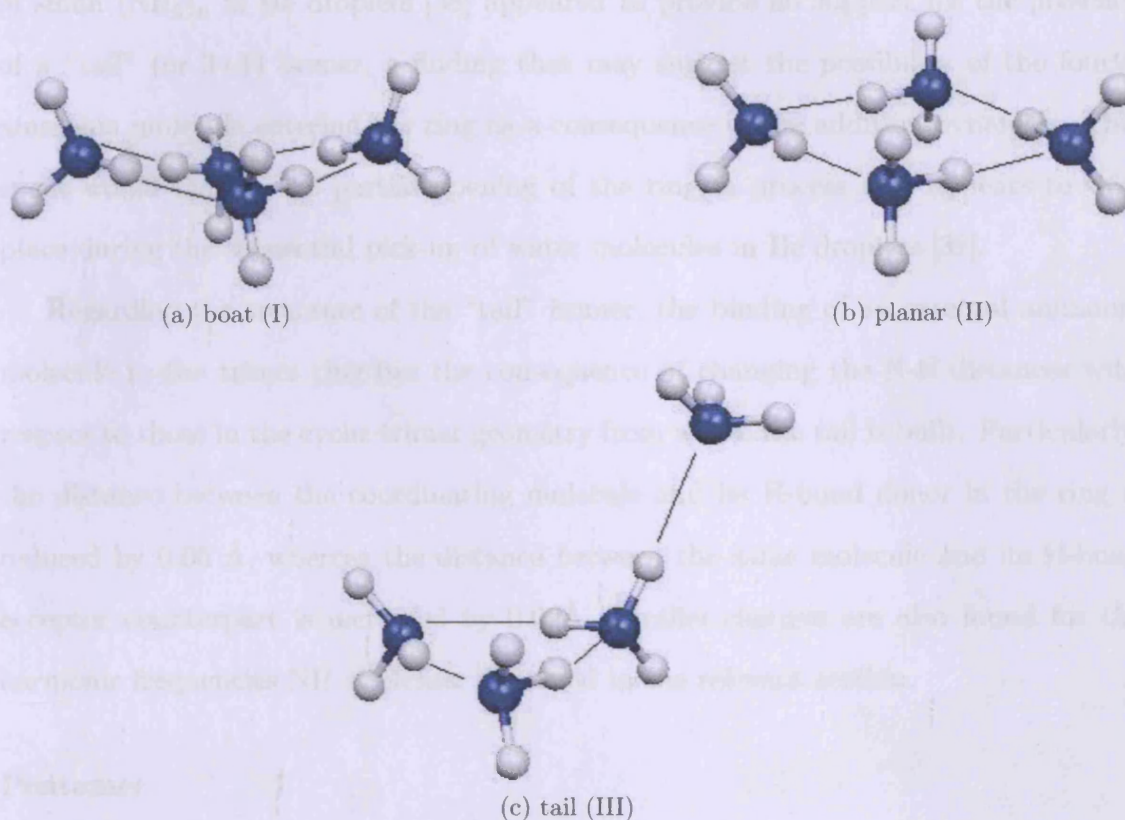


Figure 2.3: Equilibrium structures for $(\text{NH}_3)_4$ obtained with Counterpoise corrected MP2/aug-cc-pVTZ optimisations.

The third isomer (III, “tail”), lies roughly 3 kcal/mol above isomer I (“boat”) and is the first time that it is reported, while isomers “boat” and “planar” already have equivalents in the literature [25, 32, 33]. The “tail” isomer was built by adding an external ammonia molecule to the “equi” trimer. This optimisation strategy was used as a way to explore the possibility of an ammonia molecule remaining trapped outside the ring. This would be a feasible scenario during the formation of $(\text{NH}_3)_4$ by sequential pick up of ammonia molecules in a dissipating cold environment (i.e. He droplets [37]); facilitated by the fact that during the pick up process the cyclic trimer might form before the fourth ammonia is added to the droplet and by the compact nature and lack of dipole moment of the cyclic trimer. However, recent IR spectra

of small $(\text{NH}_3)_n$ in He droplets [38] appeared to provide no support for the presence of a “tail” (or 3+1) isomer, a finding that may suggest the possibility of the fourth ammonia molecule entering the ring as a consequence of the addition dynamics. This event would require the partial opening of the ring, a process that appears to take place during the sequential pick-up of water molecules in He droplets [39].

Regarding the structure of the “tail” isomer, the binding of an external ammonia molecule to the trimer ring has the consequence of changing the N-N distances with respect to those in the cyclic trimer geometry from where the tail is built. Particularly, the distance between the coordinating molecule and its H-bond donor in the ring is reduced by 0.06 Å, whereas the distance between the same molecule and its H-bond acceptor counterpart is increased by 0.09 Å. Parallel changes are also found for the harmonic frequencies NH stretches, discussed in the relevant section.

Pentamer

All the putative local minimum we found for $(\text{NH}_3)_5$ are shown in figure 2.4. From table 2.4 we can see that the pentamer “tail” isomer is the least stable species, lying roughly 2 kcal/mol above all the others, due to the lower number of H-bond contacts. On the other hand, we can also see that the energy ranking for the remaining pentamer isomers is quite compressed and strongly sensitive to the level of treatment. In this respect, uncorrected results using both MP2/aug-cc-pVDZ and MP2/aug-cc-pVTZ favour compact species as the most stable, while CP-corrected values predict the “ring” as the most stable one, although marginally. This reversal in energy ranking is due to a different magnitude of BSSE correction, which is in turn related to the number of H-bond contacts.

As far as we know, only a few structures have been proposed as stationary species using model potentials. The binding energies of the two 3D structures described by Beu

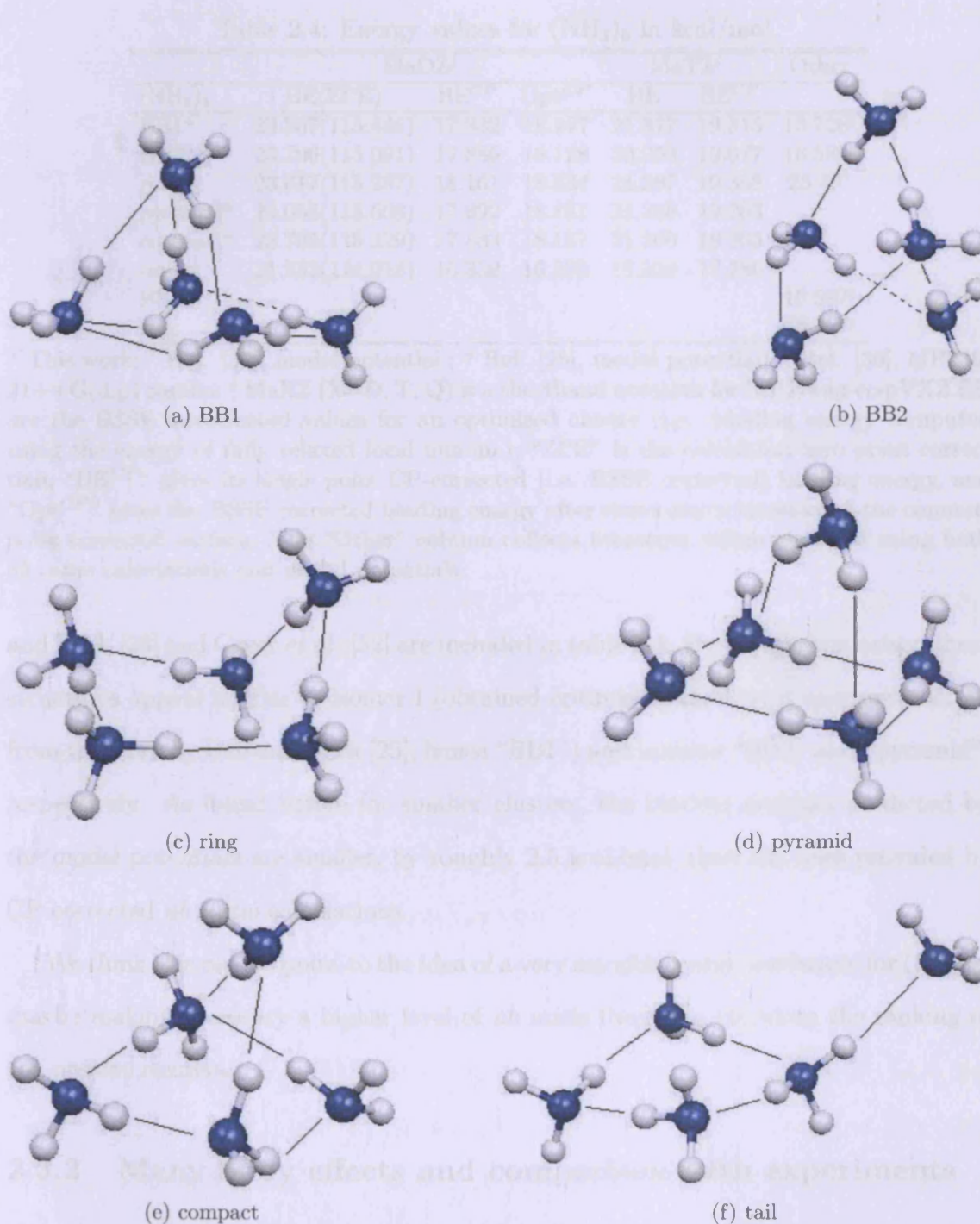


Figure 2.4: Equilibrium structures for $(\text{NH}_3)_5$ obtained with MP2/aug-cc-pVTZ optimisations.

Table 2.4: Energy values for $(\text{NH}_3)_5$ in kcal/mol.

$(\text{NH}_3)_4$	MaDZ ^j			MaTZ ^j		Other
	BE(ZPE)	BE ^{CP}	Opt ^{CP}	BE	BE ^{CP}	
BB1 ^a	23.867(115.445)	17.932	18.177	21.377	19.315	16.728 ^g
BB2 ^a	23.706(115.091)	17.886	18.128	20.958	19.077	16.589 ^g
ring ^a	23.617(115.287)	18.161	18.334	21.287	19.358	25.48 ^h
pyramid ^a	24.053(115.608)	17.892	18.181	21.388	19.263	
compact ^a	23.705(115.329)	17.883	18.127	21.260	19.203	
tail ^a	21.532(114.918)	16.359	16.533	18.930	17.286	
BB3						16.587 ^g
ring						16.927 ^e

^a This work; ^e Ref. [32], model potential.; ^g Ref. [25], model potential; ^h Ref. [30], MP2/6-31++G(d,p) results; ^j MaXZ (X=D, T, Q) is a shorthand notation for MP2/aug-cc-pVXZ. BE are the BSSE uncorrected values for an optimised cluster (i.e. binding energy computed using the energy of fully relaxed local minima); “ZPE” is the calculated zero point correction; “BE^{CP}” gives its single point CP-corrected (i.e. BSSE corrected) binding energy, and “Opt^{CP}” gives the BSSE corrected binding energy after structural relaxation on the counterpoise corrected surface. The “Other” column collects literature values obtained using both *ab initio* calculations and model potentials.

and Buck [25] and Greer *et al.* [32] are included in table 2.4. By visual comparison these structures appear similar to isomer I (obtained optimising the lowest energy structure from the work by Beu and Buck [25], hence “BB1”) and isomers “BB2” and “pyramid”, respectively. As found before for smaller clusters, the binding energies predicted by the model potentials are smaller, by roughly 2.5 kcal/mol, than the ones provided by CP-corrected *ab initio* calculations.

We think this results point to the idea of a very smooth energy landscape for $(\text{NH}_3)_5$, maybe making necessary a higher level of *ab initio* theory to elucidate the ranking of the present isomers.

2.3.2 Many body effects and comparison with experiments

We have used the results presented in tables 2.1 to 2.4 to predict molecular evaporation energies in order to compare them with other results from the literature, both theoretical and experimental. The results can be seen in 2.5. All of the incremen-

tal energy data from this work have been computed using zero point energies at the MP2/aug-cc-pVXZ ($X = \text{D}$ for $(\text{NH}_3)_4$ and $(\text{NH}_3)_5$; $X = \text{T}$ for $(\text{NH}_3)_2$ and $(\text{NH}_3)_3$) and CP-corrected results for the electronic energies obtained using the largest affordable basis set and CP corrected optimisation when possible. For each cluster size we list only the BE for the isomer with the lowest total energy.

Aside from our data, table 2.5 also presents the thermochemical data for the formation of $(\text{NH}_3)_n$ from $(\text{NH}_3)_{n-1}$ [40], data derived from photodissociation of $(\text{NH}_3)_n$ into $(\text{NH}_3)_{n-1}$ [6], photoionisation studies [41] and we also list the evaporation energies predicted by reference [32], which are calculated from binding energies that are not ZPE corrected.

From table 2.5 we can see that ZPE accounts for a 35%-45% reduction in the BE for all cluster sizes. No significant changes were found in the relative energy ranking upon introduction of the ZPE correction for all clusters (see Appendix 2 for a more detailed account of BE computed with ZPE corrections for all clusters), the only result to mention being the increase in stability of the “ring” and “BB2” pentamers. Looking at table 2.5 it can also be seen that less energy is required to evaporate an ammonia molecule from the pentamer than from the trimer and tetramer, a result supported by the less compact structure of the larger size clusters.

We see a reasonable agreement between the experimental ΔE data and the theoretical values in table 2.5, especially taking into account the small magnitude of the measured quantity and the difficulties measuring it. All the values from this work fall in the energy range obtained by the photodissociation experiments from reference [6]. There is, however, a relatively large discrepancy between theory and experiment in the case of $(\text{NH}_3)_4$ and $(\text{NH}_3)_5$. In particular, the experiments in references [40] and [41] provide substantially higher evaporation energies than the theory, this result was explained by Greer *et al.* [32] with the suggestion that the concentration of small clus-

Table 2.5: Binding (BE) and vaporisation (ΔE) energies for $(\text{NH}_3)_n$ ($n = 2 - 5$), in kcal/mol.

n	BE ^a	ΔE^a	ΔE^b	ΔE^c	ΔE^d	ΔE^e
2	3.011(1.651)	1.651	3.090	4.6(5)	≤ 2.85	2.8
3	10.074(6.197)	4.546	5.637	3.9(5)	$2.85 \leq \Delta E \leq 5.72$	3.5
4	15.537(10.125)	3.928	4.659	5.5(5)	$2.85 \leq \Delta E \leq 5.72$	5.1
5	19.358(12.612)	2.487	3.828	3.9(5)		5.1

^a This work; ^b Ref. [32], model potential; ^c Ref. [40], thermochemical measurements; ^d Ref. [6], photodissociation experiments; ^e Ref. [41], ionisation threshold measurements. The first column shows adiabatic and ZPE corrected (between brackets) binding energies computed in this work using Counterpoise corrected energies and ZPE at the MP2/aug-cc-pVXZ ($X = D$ for $(\text{NH}_3)_4$ and $(\text{NH}_3)_5$; $X = T$ for $(\text{NH}_3)_2$ and $(\text{NH}_3)_3$) level. ΔE values from this work are computed including ZPE corrections.

ters was overestimated during the thermochemical experiments due to the variation in ionisation probability with cluster size.

Table 2.6 presents the many-body decomposition (equation 55, chapter 1) of the binding energies for clusters up to the tetramer. They were calculated at the CP-corrected optimisation MP2/aug-cc-pVTZ level of theory. In order to have values of many-body effects that are directly comparable across different cluster sizes, the different contributions (i.e. 2-, 3-, and 4-bodies) have been divided by the number of possible sub-clusters contained in a particular cluster size (i.e. the total 2-body contribution in a tetramer has been divided by 6, the number of different dimers it contains).

From table 2.6 we can see that the 4-body effect appears to be negligible, whilst 2- and 3-body effects are mandatory for an accurate decomposition of the total binding energy for any given cluster. This finding is of importance for the task of building a model potential for ammonia, suggesting that one may concentrate only on low order many-body effects. In addition, looking at the normalised 2-body effects in table 2.6 one can see that they decrease with increasing cluster size, the principal reason for

Table 2.6: Many-body contributions to the binding energy of $(\text{NH}_3)_n$ ($n = 2 - 4$), in kcal/mol.

System	2-body	3 body	4 body
n=2, asym	3.011	3.011	
n=2, sym	2.999	2.999	
n=3, equi	9.053	3.018	1.142
n=3, asym	6.206	2.069	0.369
n=4, boat	12.984	2.164	2.632
n=4, plane	13.171	2.195	2.441
n=4, tail	11.561	1.927	1.150

For each n-body contribution, the first column presents the total value; the second column shows the total contribution divided by the number of n-body moieties in the cluster.

this trend being the longer distance on average, between pairs of ammonia molecules in large clusters. Finally, let us add that in view of the small magnitude of 4-body effects in the tetramer, we did not calculate higher many-body contributions for the pentamers.

2.3.3 Harmonic frequencies

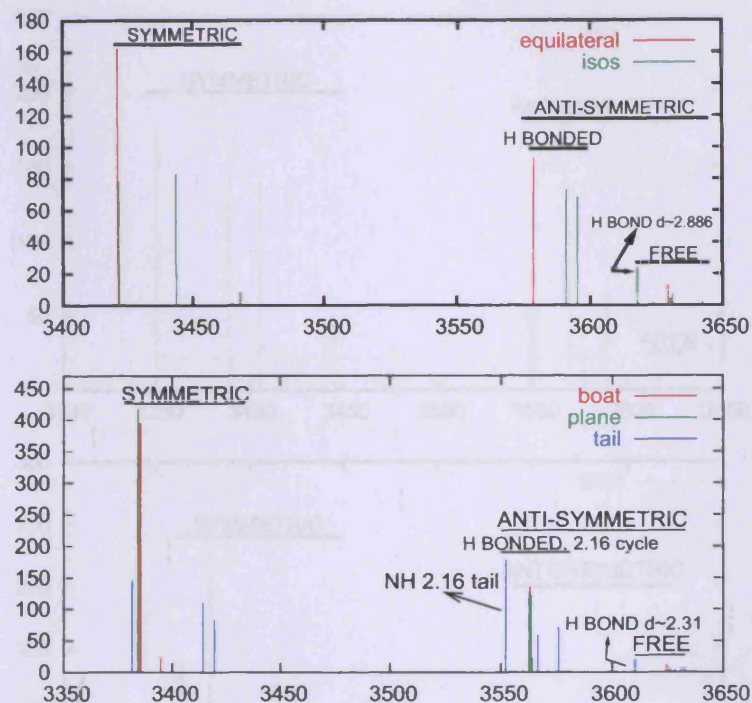
Ab initio harmonic frequencies were calculated for ammonia clusters on the fully optimised structures at the MP2/aug-cc-pVDZ level. These were analysed in order to extract information on the frequency shift for the N–H stretching modes, in an attempt to associate a particular geometrical feature to a range of frequencies [42]. The results of our frequency calculations for the N–H stretches are shown in figures 2.5, 2.6 and 2.7 for the trimers, tetramers, and pentamers, respectively.

Firstly, we observe that all NH stretch frequencies are seen to decrease upon increasing cluster size, a common feature present in several H-bonded clusters [42]. Although somewhat difficult to quantify due to the complicated dependency on the aggregate geometry, we notice that the average frequency of antisymmetric stretches decreases

by roughly 20 cm^{-1} going from the trimers to the tetramers, and by roughly $5 - 10 \text{ cm}^{-1}$ from tetramers to pentamers. In the case of symmetric stretches, the frequency shifts are found to be larger: roughly 50 cm^{-1} going from the trimer to tetramers and roughly $10 - 20 \text{ cm}^{-1}$ from tetramers to pentamers.

Our analysis also highlighted the presence of two additional overlapping trends, one of which is the common occurrence of a lower frequency (roughly $100 - 200 \text{ cm}^{-1}$) for the symmetric stretches when compared to the asymmetric ones. Moreover, free H atoms are always found to participate only in antisymmetric stretches, vibrating at higher frequencies (roughly $40 - 50 \text{ cm}^{-1}$) than H-bonded ones. In the case of antisymmetric H-bonded NH stretches, we also found a clear dependency of the frequency on the H-bond length (i.e. the N-H...N distance), with the NH involved in long H-bonds (above 2.24 \AA) showing a higher frequency ($20 - 40 \text{ cm}^{-1}$) than short H-bonded ones. According to our optimised structures, these long H-bonds are present when an ammonia molecule acts as a double donor, or double acceptor, a feature shown only by our cage-like and “tail” structures. Thus, the presence of the vibrational signature for these long H-bonds could be used as an indication of the transition from a planar ring-like structure to a 3D one, or for the presence of “docked” ammonia molecules outside a cycle arrangement.

An energetic ordering similar to the one found for antisymmetric stretches is also found for the symmetric vibrations. Once again, low-frequency values are associated with atoms involved in short N-H...N bonds, whereas high values are representative of symmetric stretches involving atoms implicated in long N-H...N bonds for any particular isomer.

Figure 2.5: N-H stretching frequencies for $(\text{NH}_3)_3$ and $(\text{NH}_3)_4$ obtained using MP2/aug-cc-pVDZ

The labels in the pictures have the following meaning: "H BOND d 2.886" indicates a NH bond involved in a H-bond with the two nitrogens at a distance of roughly 3.833 Å; "NH 2.16 tail" indicates the stretching of the NH bond of the ammonia in the ring donating an H-bond to the external NH_3 with an N-H distance of 2.16 Å; "H BOND d 2.31" indicate the stretching of an NH involved in a long H-bond (roughly 2.31 Å long).

Figure 2.6: N-H stretching frequencies for the BB1, BB2, and compact isomers of $(\text{NH}_3)_5$ obtained using MP2/aug-cc-pVDZ

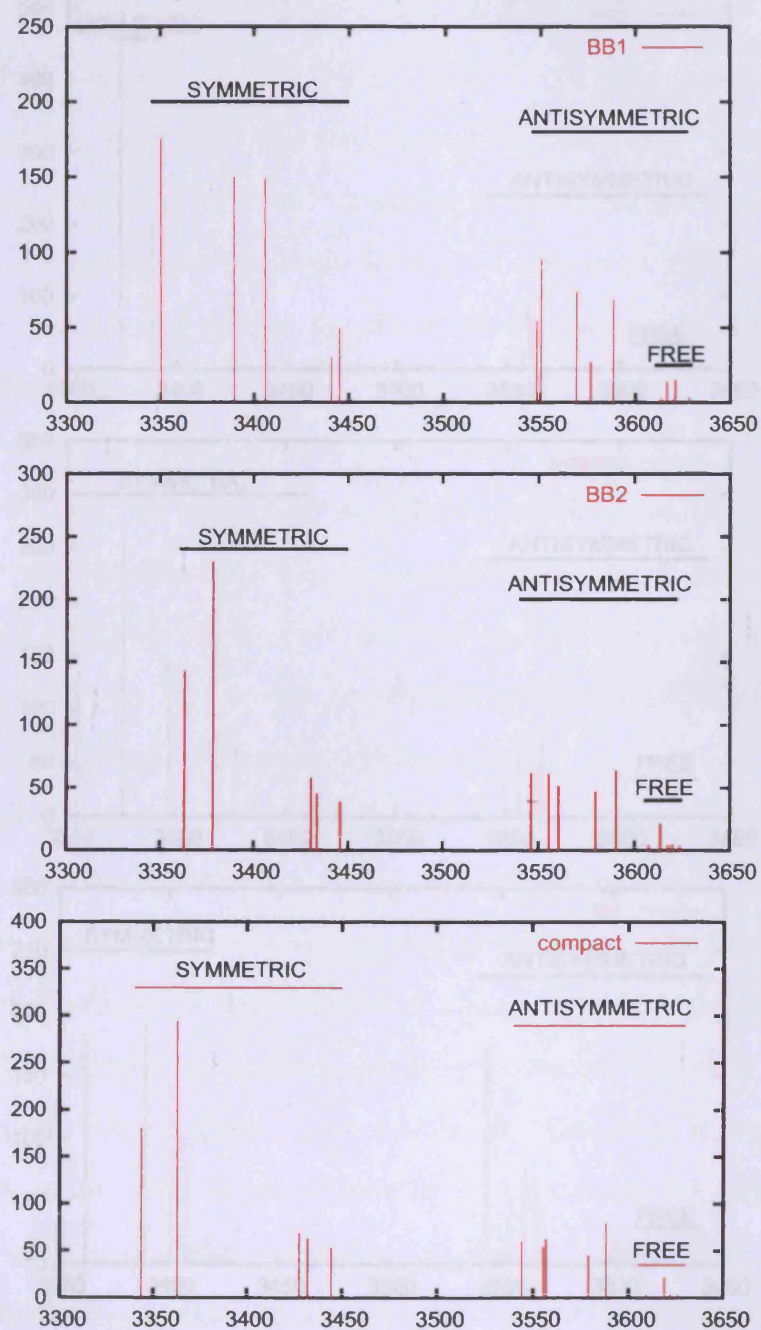
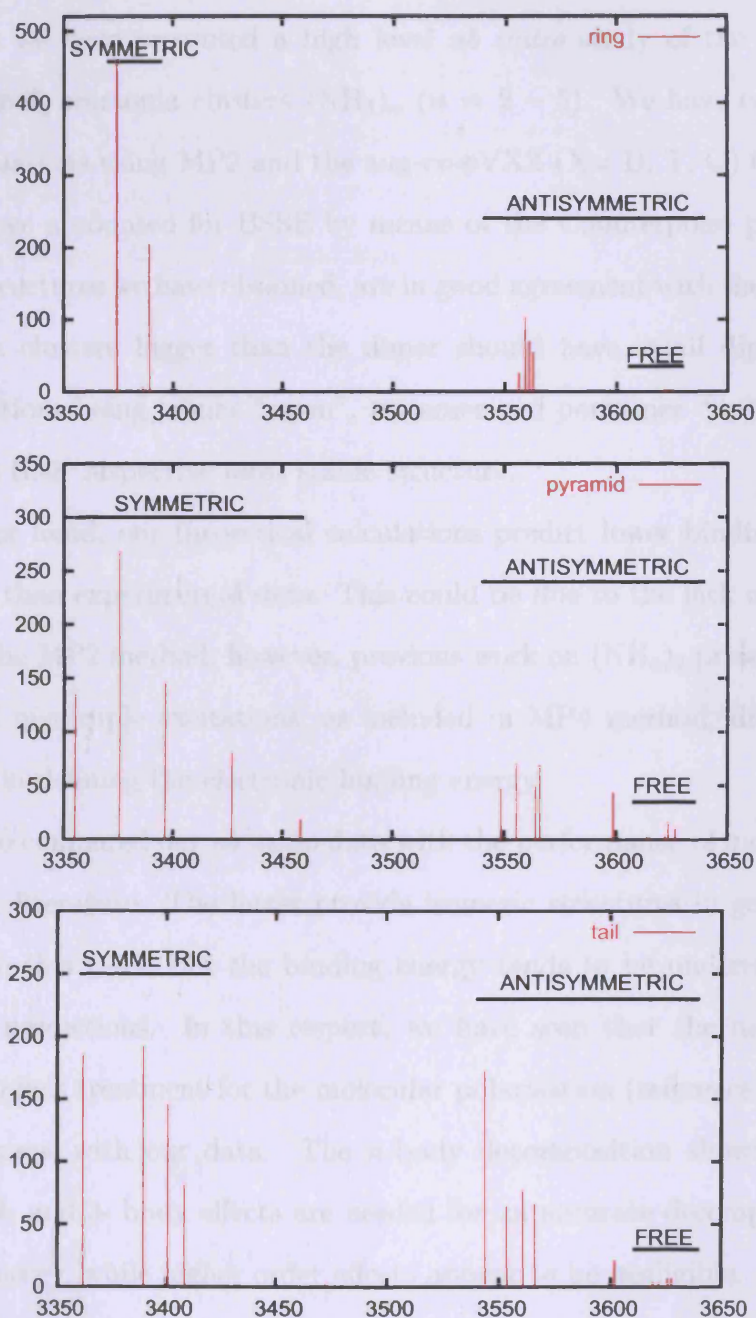


Figure 2.7: N-H stretching frequencies for the ring, pyramid and tail isomers of $(\text{NH}_3)_5$ 

2.4 Conclusions

In this chapter we have presented a high level *ab initio* study of the structure and energetics of small ammonia clusters $(\text{NH}_3)_n$ ($n = 2 - 5$). We have carried out the electronic calculations using MP2 and the aug-cc-pVXZ ($X = \text{D, T, Q}$) family of basis sets, and we have accounted for BSSE by means of the Counterpoise procedure [22]. The isomeric structures we have obtained, are in good agreement with the experimental conclusion that clusters bigger than the dimer should have small dipole moments. The only exceptions being trimer “asym”, tetramer and pentamer “tail”, lying 3 – 4 kcal/mol above their respective most stable structure.

On the other hand, our theoretical calculations predict lower binding and evaporation energies than experimental data. This could be due to the lack of higher order excitations in the MP2 method; however, previous work on $(\text{NH}_3)_2$ presented evidence that triple and quadruple excitations, as included in MP4 method, did not play an important role in defining the electronic binding energy.

We have also compared our *ab initio* data with the performance of model potentials available in the literature. The latter provide isomeric structures in good agreement with those from this work, but the binding energy tends to be underestimated with respect to our predictions. In this respect, we have seen that the model potential including an explicit treatment for the molecular polarisation (reference [33]) provides a better agreement with our data. The n -body decomposition shown in table 2.6 indicates that 2- and 3- body effects are needed for an accurate decomposition of the total binding energy, while higher order effects appear to be negligible.

Our calculations suggest that the tetramer and the pentamer have several, almost degenerate, isomers. This points at the possibility of a smooth energy landscape, and also at the occurrence of fast interconversion between the most stable, same size isomers. This compact energy ranking is not significantly altered upon introduction of

harmonic ZPE correction, which, as seen in neutral water clusters, may not be enough for an adequate treatment of quantum motion effects in “floppy” clusters. In fact, recent investigations led by Curotto and Mella [43, 44] using Monte Carlo simulations, have established that the quantum effects on the binding energy per ammonia molecule are large: 42% of the total binding energy of the dimer, 38% of the trimer and 35% of the total binding energy for the tetramer and pentamer.

Bibliography

- [1] Nelson, D. D. Jr.; Fraser, G. T.; Klemperer, W., *J. Chem. Phys.*, **1985**, *83*, 6201.
- [2] Süzer, S.; Andrews, L. *J. Chem. Phys.*, **1987**, *87*, 5131.
- [3] Nelson, D. D. Jr.; Klemperer, W.; Fraser, G. T.; Lovas, F. J.; Suenram, R. D., *J. Chem. Phys.*, **1987**, *87*, 6364.
- [4] Snels, M.; Fantoni, R.; Sanders, R.; Meerts, W. L., *Chem. Phys.*, **1987**, *115*, 79.
- [5] Huiskens, F.; Pertsch, T. *Chem. Phys.*, **1988**, *126*, 213.
- [6] Heijmen, B.; Bizarri, A.; Stolte, S.; Reuss, J. *Chem. Phys.*, **1988**, *126*, 201.
- [7] Loeser, J. G.; Schmuttenmaer, C. A.; Cohen, R. C.; Elrod, M. J.; Steyert, D. W.; Saykally, R. J.; Bumgarner, R. E.; Blake, G. A., *J. Chem. Phys.*, **1992**, *97*, 4727.
- [8] Havenith, M.; Linnartz, H.; Zwart, E.; Kips, A.; ter Meulen, J. J.; Meerts, W. L.; *Chem. Phys. Lett.*, **1992**, *193*, 261.
- [9] Hirao, K.; Fujikawa, T.; Konishi, H.; Yamabe, S., *Chem. Phys. Lett.*, **1984**, *104*, 184.
- [10] Hasset, D. M.; Marsden, C. J.; Smith, B. J., *Chem. Phys. Lett.*, **1991**, *183*, 449.
- [11] Cybulski, S. M., *Chem. Phys. Lett.*, **1994**, *228*, 451.

-
- [12] Tao, F.-M.; Klemperer, W., *J. Chem. Phys.*, **1993**, *99*, 5976.
- [13] Olthof, E. H. T.; van der Avoird, A.; Wormer, P. E. S., *J. Chem. Phys.*, **1994**, *101*, 8430.
- [14] Lee, J. S.; Park, S. Y., *J. Chem. Phys.*, **2000**, *112*, 230.
- [15] Stålring, J.; Schütz, M.; Lindh, R. Karlstrom, G.; Widmark, P-O., *Mol. Phys.*, **2002**, *100*, 3389.
- [16] Boese, A. D.; Chandra, A.; J. M. L. Martin, J. M. L.; Marx, D., *J. Chem. Phys.*, **2003**, *119*, 5965.
- [17] Odutola, J. A.; Dyke, T. R.; Howard, B. J.; Muentner, J. S., *J. Chem. Phys.*, **1979**, *70*, 4884.
- [18] Buck, U.; Krohne, R.; Schütte, S., *J. Chem. Phys.*, **1997**, *106*, 109.
- [19] Gregory, J. K.; Clary, D. C., *J. Phys. Chem.*, **1996**, *100*, 18014.
- [20] Mella, M.; Clary, D. C.; Kuo, J.-L.; Klein, M. L., *Phys. Chem. Chem. Phys.*, **2005**, *7*, 2324.
- [21] Szczeniak, M. M.; Kendal, R. A.; Chalasiński, G., *J. Chem. Phys.*, **1991**, *95*, 5169.
- [22] Boys, S. F.; Bernardi, F. *Mol. Phys.*, **1970**, *19*, 553.
- [23] Xanteas, S. S. *J. Chem. Phys.*, **1996**, *104*, 8821.
- [24] Salvador, P.; Duran, M.; Dannenberg, J. J. *J. Phys. Chem. A*, **2002**, *106*, 6883.
- [25] Beu, T.; Buck, U. *J. Chem. Phys.*, **2001**, *114*, 7848.

- [26] Flükiger, P.; Lüthi, H. P.; Portmann, S.; Weber, J. MOLEKEL 4.3, Swiss National Supercomputing Centre: Manno (Switzerland).
- [27] M. J. Frisch, G. W. Trucks, H. B. Schlegel, G. E. Scuseria, M. A. Robb, J. R. Cheeseman, V. G. Zakrzewski, J. A. Montgomery, Jr., R. E. Stratmann, J. C. Burant, S. Dapprich, J. M. Millam, A. D. Daniels, K. N. Kudin, M. C. Strain, O. Farkas, J. Tomasi, V. Barone, M. Cossi, R. Cammi, B. Mennucci, C. Pomelli, C. Adamo, S. Clifford, J. Ochterski, G. A. Petersson, P. Y. Ayala, Q. Cui, K. Morokuma, P. Salvador, J. J. Dannenberg, D. K. Malick, A. D. Rabuck, K. Raghavachari, J. B. Foresman, J. Cioslowski, J. V. Ortiz, A. G. Baboul, B. B. Stefanov, G. Liu, A. Liashenko, P. Piskorz, I. Komaromi, R. Gomperts, R. L. Martin, D. J. Fox, T. Keith, M. A. Al-Laham, C. Y. Peng, A. Nanayakkara, M. Challacombe, P. M. W. Gill, B. Johnson, W. Chen, M. W. Wong, J. L. Andres, C. Gonzalez, M. Head-Gordon, E. S. Replogle, and J. A. Pople. Gaussian 98, Revision A.11.1 Gaussian, Inc., Pittsburgh, PA, **2001**.
- [28] M. J. Frisch and G. W. Trucks and H. B. Schlegel and G. E. Scuseria and M. A. Robb and J. R. Cheeseman and Montgomery, Jr., J. A. and T. Vreven and K. N. Kudin and J. C. Burant and J. M. Millam and S. S. Iyengar and J. Tomasi and V. Barone and B. Mennucci and M. Cossi and G. Scalmani and N. Rega and G. A. Petersson and H. Nakatsuji and M. Hada and M. Ehara and K. Toyota and R. Fukuda and J. Hasegawa and M. Ishida and T. Nakajima and Y. Honda and O. Kitao and H. Nakai and M. Klene and X. Li and J. E. Knox and H. P. Hratchian and J. B. Cross and V. Bakken and C. Adamo and J. Jaramillo and R. Gomperts and R. E. Stratmann and O. Yazyev and A. J. Austin and R. Cammi and C. Pomelli and J. W. Ochterski and P. Y. Ayala and K. Morokuma and G. A. Voth and P. Salvador and J. J. Dannenberg and V. G. Zakrzewski and S. Dapprich

and A. D. Daniels and M. C. Strain and O. Farkas and D. K. Malick and A. D. Rabuck and K. Raghavachari and J. B. Foresman and J. V. Ortiz and Q. Cui and A. G. Baboul and S. Clifford and J. Cioslowski and B. B. Stefanov and G. Liu and A. Liashenko and P. Piskorz and I. Komaromi and R. L. Martin and D. J. Fox and T. Keith and M. A. Al-Laham and C. Y. Peng and A. Nanayakkara and M. Challacombe and P. M. W. Gill and B. Johnson and W. Chen and M. W. Wong and C. Gonzalez and J. A. Pople Gaussian 03, Revision B.05, Gaussian, Inc., Pittsburgh, PA, **2003**.

- [29] Benedict, W. S.; Gailar, N.; Plyler, E. K. *Can. J. Phys.*, **1957**, 35, 1235.
- [30] Kulkarni, S. A.; Pathak, R. K., *Chem. Phys. Lett.*, **2001**, 336, 278. **2002**, 100, 3389.
- [31] Sagarik, K. P.; Ahlrichs, R.; Brode, S., *Mol. Phys.*, **1986**, 57, 1247.
- [32] Greer, J. C.; Ahlrichs, R.; Hertel, I. V., *Chem. Phys. Lett.*, **1989**, 133, 191.
- [33] Dykstra, C. E.; Andrews, L., *J. Chem. Phys.*, **1990**, 92, 6043.
- [34] Impey, R. W.; Klein, M. L., *Chem. Phys. Lett.*, **1984**, 104, 579.
- [35] Greer, J. C.; Ahlrichs, R.; Hertel, I. V., *J. Chem. Phys.*, **1991**, 95, 3861.
- [36] Dykstra, C. E.; Augspurger, J. D. *J. Chem. Phys.*, **1991**, 95, 3863.
- [37] Nauta, K.; Miller, R. E. *Science*, **1999**, 283, 1895.
- [38] Slipchenko, M. N.; Sartakov, B. G.; Vilesov, A. F.; Xantheas, S. S. *J. Phys. Chem. A*, **2007**, 111, 7460.
- [39] Burnham, C. J.; Xantheas, S. S.; Miller, M. A.; Applegate, B. E.; Miller, R. E. *J. Chem. Phys.*, **2002**, 117, 1109.

- [40] Cook, K. D.; Taylor, J. W.; *Int. J. Mass Spectrom. Ion Phys.*, **1979**, *30*, 345.
- [41] Kamke, V.; Herrmann, R.; Wang, Z.; Hertel, I. V. *Z. Phys. D*, **1988**, *10*, 491.
- [42] Buch, V; Devlin, J *J. Chem. Phys.*, **1991**, *94*,4091.
- [43] Lubombo, C.; Curotto, E; Janeiro-Barral, P. E.; Mella, M. *J. Chem. Phys.*, **2009**, *131*, 034312.
- [44] “*Quantum Monte Carlo simulations of selected ammonia clusters ($n = 2 \rightarrow 5$): Isotope effects on the ground state of typical hydrogen bonded systems*”, submitted to *J. Chem. Phys.*, September **2010**.

2.5 Appendix 1

BSSE energies for $(\text{NH}_3)_n$ $n = 2 - 5$ keeping intramolecular structure frozen to the experimental values of gas-phase ammonia ($r_{\text{NH}} = 1.0124 \text{ \AA}$, $\text{H}\hat{\text{N}}\text{H} = 106.67^\circ$)[29]

DIMER: aug-cc-pVQZ OPT(CP)

ASYM

Counterpoise: corrected energy = -112.960470820965

Counterpoise: BSSE energy = 0.000206290483

TS

Counterpoise: corrected energy = -112.960457737844

Counterpoise: BSSE energy = 0.000183566942

TRIMER: aug-cc-pVTZ(OPT(CP))//aug-cc-pVQZ

EQUI

Counterpoise: corrected energy = -169.449780047474

Counterpoise: BSSE energy = 0.000641702363

ISOS

Counterpoise: corrected energy = -169.443889581016

Counterpoise: BSSE energy = 0.000500604192

TETRAMER: aug-cc-pVTZ OPT(CP)

BOAT

Counterpoise: corrected energy = -225.866920349343

Counterpoise: BSSE energy = 0.002300909277

PLANAR

Counterpoise: corrected energy = -225.866918379990

Counterpoise: BSSE energy = 0.002313794820

TAIL

Counterpoise: corrected energy = -225.862191870340

Counterpoise: BSSE energy = 0.001908038378

PENTAMER: aug-cc-pVDZ OPT(CP)

BB1

Counterpoise: corrected energy = -282.053416100966

Counterpoise: BSSE energy = 0.008667270387

BB2

Counterpoise: corrected energy = -282.053337240919

Counterpoise: BSSE energy = 0.008494293937

RING

Counterpoise: corrected energy = -282.053666340281

Counterpoise: BSSE energy = 0.008137552514

PYRAMID

Counterpoise: corrected energy = -282.053421910139

Counterpoise: BSSE energy = 0.008876060350

COMPACT

Counterpoise: corrected energy = -282.053336718090

Counterpoise: BSSE energy = 0.008494678588

TAIL

Counterpoise: corrected energy = -282.050796341986

Counterpoise: BSSE energy = 0.007665106411

Table 2.7: ZPE corrected binding energies computed in this work using Counterpoise corrected electronic energies and ZPE at the MP2/aug-cc-pVXZ (X = D, T) level

$(\text{NH}_3)_2$	MaDZ	MaTZ
asym	1.279	1.651
$(\text{NH}_3)_3$		
equi	5.252	6.197
asym	2.732	3.422
$(\text{NH}_3)_4$		
boat	8.493	10.125
tail	6.507	7.960
$(\text{NH}_3)_5$		
BB1	10.619	12.412
BB2	10.923	12.527
ring	10.934	12.612
pyramid	10.460	12.196
compact	10.686	12.416
tail	9.502	10.909

2.6 Appendix 2

Chapter 3

Ammonia potential

3.1 Introduction

Analytical representations for the intermolecular forces between two rigid ammonia molecules have been derived from the experimental [1–5] and theoretical [6–9] studies on the $(\text{NH}_3)_2$. The parameterisation of these model potentials have been carried out by adjusting atom-atom potential coefficients to microwave data [10], to second virial coefficient and lattice energy of the solid [11] or by fitting theoretical results [12, 13].

In chapter 2, we compared our *ab initio* data to the analytical models of references [14] and [27]. We found that these potentials are generally in agreement with the structures of global minima (except for the pentamer), but they invariably underestimate the binding energies for ammonia clusters respect to the *ab initio* data. Motivated by the performance of the model potentials available at the time, and by the goal of this group of simulating the process of evaporation/condensation of medium size $(\text{NH}_3)_n$ we saw necessary the construction of a more accurate model potential. This would improve the description for the relative energetics of medium sized $(\text{NH}_3)_n$, which in turn would provide a higher accuracy for the dissociation rates. Also, it could be used to

increase the scarce pool of data [15–18] attempting to accurately reproduce ammonia condensed-phase.

In the work by Szczęśniak *et al.* [19] the relative contribution from several components of the total interaction energy in $(\text{NH}_3)_3$ was investigated employing a Symmetry-Adapted Perturbation Theory (SAPT) based analysis. This was useful in highlighting the relative importance of the several ingredients that would provide a quantitative description of ammonia-ammonia interactions: induction forces account for at least 70% of the three-body contribution (roughly 10% of the total two-body component). Also, the Heitler-London term was highlighted, but it was found only to be important for unusual conformations of the trimer. This led us to think that the underestimation in binding energy seen for $(\text{NH}_3)_n$ ($n = 3 - 5$) may be due to the lack of an explicit treatment of induction forces. This idea is also supported by the improvement in accuracy provided by the polarisable model built by Dykstra and co-workers [20].

We think that the construction of a more accurate model potential for $(\text{NH}_3)_n$ should be based on *ab initio* energy results. Also, as we have mentioned in the introduction and chapter 2, we think MP2 level of theory with aug-cc-pVXZ ($X = \text{D, T, Q, 5}$) basis set and Counterpoise correction for the BSSE provides a good compromise between cost and accuracy for the study of ammonia clusters. In addition, we believe the model potential should contain the explicit treatment for the many-body induction component of the interaction forces. Therefore, high level *ab initio* calculations have been performed to generate an extensive set of interaction energies for $(\text{NH}_3)_2$. This set of data has been subsequently employed to optimise the parameters of a sensible analytical form of the model potential, this being the model potential “C” developed by Hinchliffe *et al.* [12], which was then supplemented with an explicit description of induction forces based on the idea of polarisable point dipoles.

Employing the new model potential, minimum energy structures for $(\text{NH}_3)_n$ ($n =$

6 – 20) have been optimised in this work and used in the search of putative global minima. Also, we compare the model PES results and electronic structure theory results for $(\text{NH}_3)_n$ ($n = 3 - 5$).

As supplementary information for this chapter, we show in appendixes 1, 2 and 3 the codes used for the calculation of the intermolecular forces and an example of a dimer geometry data file.

3.2 Methodology

All *ab initio* calculations on the ammonia monomer and dimer were carried out using the Gaussian 98 [29] and 03 [30] suit of codes at the MP2/aug-cc-pVXZ ($X = \text{D, T, Q, 5}$) with frozen-core level of theory. As before, interaction energies were corrected for BSSE using the Counterpoise (CP) procedure proposed by Boys and Bernardi [28]. The internal structure of ammonia was kept rigid at the experimental geometry ($r_{\text{NH}} = 1.0124 \text{ \AA}$, $\text{H}\hat{\text{N}}\text{H} = 106.67^\circ$) [31].

The long range behaviour of the intermolecular potential is dominated by the electrostatic properties of the monomers, particularly dipole-dipole and dipole-quadrupole interactions, decaying as $1/r^3$ and $1/r^4$, respectively. In order to test the performance of our level of theory, we evaluated the rate of convergence of electrostatic properties by running single point calculations on the ammonia monomer with increasingly larger basis sets. The results obtained for the dipole and quadrupole moments using the series MP2/aug-cc-pVXZ ($X = \text{D, T, Q, 5}$) are presented in table 3.1

Table 3.1: Values of the Dipole (μ) and Quadrupole (θ_{zz}) Moments for the Ammonia Molecule Computed at the MP2/aug-cc-pVXZ, (X = D, T, Q, 5) Level of Theory^a

X	μ (au)	θ_{zz}
D	1.5355	-2.12
T	1.5238	-2.09
Q	1.5297	-2.10
5	1.5323	-2.10

From table 3.1 it can be seen that both the dipole μ and θ_{zz} have converged to at least 99% of their Complete Basis Set (CBS) values at the MP2/aug-cc-pVTZ level. When compared with the experimental values (+1.47 au and -2.12 au, respectively), the *ab initio* results appear to overestimate μ and underestimate θ_{zz} only slightly, indicating the adequacy of the MP2 level with Dunning basis set to estimate the electrostatic properties of the ammonia molecule. These findings are also in good agreement with the results obtained by Quack and co-workers, who obtained a six dimensional representation for the dipole moment as a function of the molecular geometry [32].

We have produced 1D scans along the N-N distance, using CP-corrected MP2/aug-cc-pVXZ X=D,T level of theory. In choosing the geometries to be explored, we started from the four orientations employed by Hinchliffe *et al.* [12], named “linear” (σ_v), “parallel” (C_{3v}), “mirror” (D_{3h}) and “orthogonal” shown in figure 3.1. The relative orientations were reproduced in MOLDEN [24], using the Z-Matrix application. Images of the isomers obtained with MOLEKEL [25].

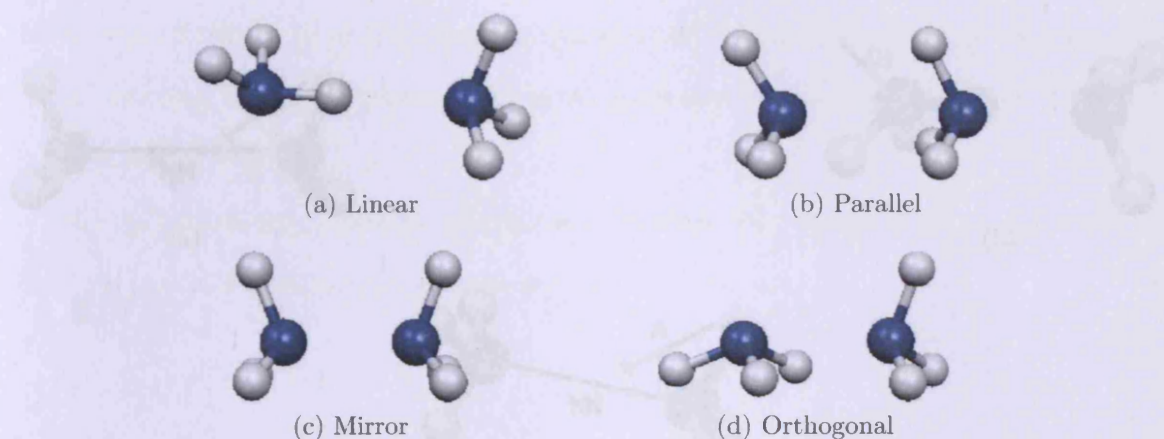


Figure 3.1: Isomer configurations employed to test the model potential.

Also, we have used CP-corrected MP2/aug-cc-pVTZ calculations to generate two dimensional cuts of the PES for $(\text{NH}_3)_2$ as a function of the relative molecular orientation. In order to do this, the 1D scans along the N-N distance were supplemented with a torsional angle to obtain high quality information on the energy barrier for the acceptor-donor exchange, the internal rotation of a single monomer and the global anisotropy of the interaction energy. Four different scan strategies were tested, they are shown in figure 3.2:

3.2.1 The potential

A routine that calculates the potential between a pair of ammonia molecules (a position 1, 2 angle) was built based on the work by Hinchliffe et al. [12]. Their working hypothesis was to combine atom-wise potentials and point charges located on or about the nuclei of two rigid ammonia molecules. The charge distribution being defined by parameters Z and Q . Q (0.62 au) is placed at the site of each hydrogen nucleus, and a negative charge of three times $(Z-3Q)$ is placed on the N_1 axis at a

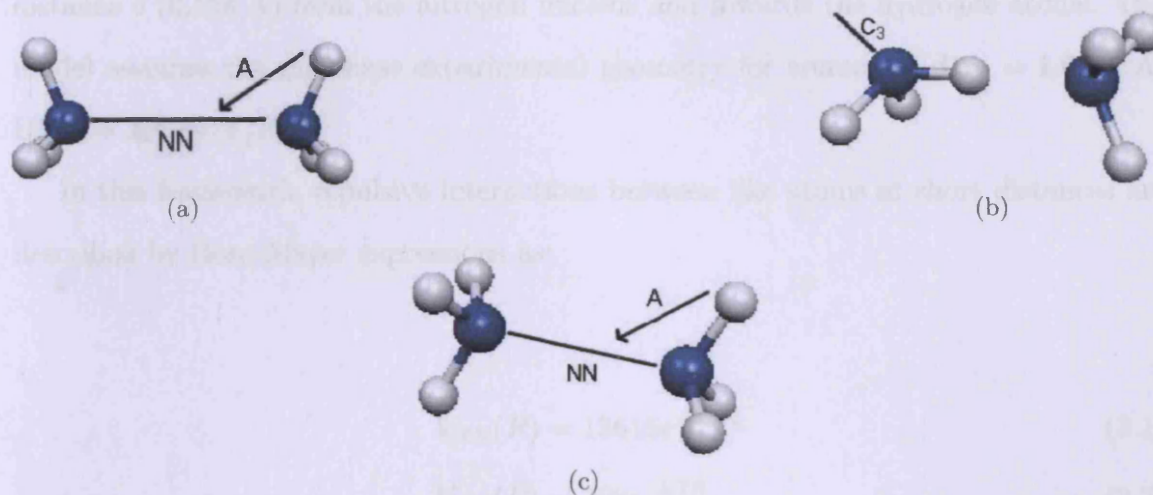


Figure 3.2: Reference geometries and coordinates for the two dimensional CP-MP2/aug-cc-pVTZ scans. NN indicates the distance between the hydrogen atoms and A indicates the angle employed in the scans to explore the energy landscape of specific isomerisation processes.

We employed the angle formed by the two nitrogen atoms and one of the hydrogen atoms on the plane of the paper, in panel a. Also from panel a, we employed the dihedral angle formed by the two nitrogen atoms and the two hydrogen atoms on the plane of the paper. From panel b, we employed the rotation around the C_3 axis of the hydrogen donor ammonia molecule. Finally, we employed the angle formed by the C_3 axis of one of the ammonia molecules with the N-N direction (panel c).

3.2.1 The potential

A routine that calculates the potential between a pair of ammonia molecules (appendixes 1, 2 and 3) was built based on the work by Hinchliffe *et al.* [12]. Their working hypothesis was to combine atom-atom potentials and point charges located on or about the atoms of two rigid ammonia molecules; the charge distribution being defined by parameters δ and Q . Q (0.462 au) is placed at the site of each hydrogen nucleus, and a negative charge of three times Q ($-3Q$) is placed on the C_3 axis at a

distance δ (0.156 Å) from the nitrogen nucleus and towards the hydrogen atoms. The model assumes the gas-phase experimental geometry for ammonia ($d_{NH} = 1.0124$ Å, $\hat{H}\hat{N}\hat{H} = 106.67^\circ$) [36].

In this framework, repulsive interactions between like atoms at short distances are described by Born-Mayer expressions as:

$$V_{NN}(R) = 13615e^{-2.7R} \quad (3.1)$$

$$V_{HH}(R) = 700e^{-3.7R} \quad (3.2)$$

The parameters in equations 3.1 and 3.2 were reported to have been obtained by fitting to the lattice energy and zero wave vector lattice vibrational frequencies of solid ammonia. The units are kcal/mol and Å.

Intending to describe the hydrogen bond contribution to the dimer energy, the short range attractive interaction between nitrogen and hydrogen atoms was assumed to follow a Morse potential:

$$V_{NH}(R) = 0.4e^{(-4.6(R-2.5))} - 0.8e^{(-2.3(R-2.5))} \quad (3.3)$$

with the values of the parameters of the expression 3.3 above being obtained by fitting SCF dimer calculations. The units are kcal/mol and Å.

A SCF approach will neglect correlation, hence dispersion interaction, and possibly BSSE; although since an extended basis set is used, Hinchliffe *et al.* [12] feel confident that this error is likely to be small and make no attempt to eliminate it on the basis of the considerable computational effort needed at the time. Dispersion is accounted for by adding to the nitrogen-nitrogen atom potential an inverse power series that at small distances is corrected by a damping function of the following form:

$$V_{disp}(R) = f(R) \left(\frac{d_6}{R^6} + \frac{d_8}{R^8} + \frac{d_{10}}{R^{10}} \right) \quad (3.4)$$

$$f(R) = \begin{cases} 1 & , R \geq R^* \\ e^{\left(\frac{(R-R^*)^2}{R^2}\right)} & , R \leq R^* \\ \text{with } R^* = 4.7 \end{cases}$$

$$d_6 = 1230, d_8 = 6500, d_{10} = 42100$$

The dispersion parameters d_6 , d_8 and d_{10} used above have been use by Hinchliffe *et al.* in previous works [11, 12, 17, 21] and have been obtained by means of *ab initio* calculations [37]. The units are kcal/mol and Å.

Through combining equations 3.1 to 3.4, together with different choices of δ and Q , Hinchliffe *et al.* propose three different model potentials namely “model A”, “model B” and “model C”.

“Model A” includes the short range atom-atom potentials of equations 3.1, 3.2 and 3.3, with point charges fitted to SCF values of μ (1.85 D) and θ (-2.43 DÅ), its two main drawbacks being the lack of dispersion correction and the fact that SCF polar moments are much higher than the experimental values. “Model B” includes the short range atom-atom potentials of equations 3.1 to 3.3, plus the dispersion description of equation 3.4. Point charges still fitted to SCF values of μ and θ . Finally, “model C” includes the short range atom-atom potentials as above (equations 3.1 to 3.3) and dispersion (equation 3.4), plus point charges fitted to experimental values of μ (1.47 D) and θ (-2.12 DÅ).

As a first step we reproduced and compared the aforementioned models for each of the configurations reported (figure 3.1). The results, in agreement with reference [12],

can be seen below.

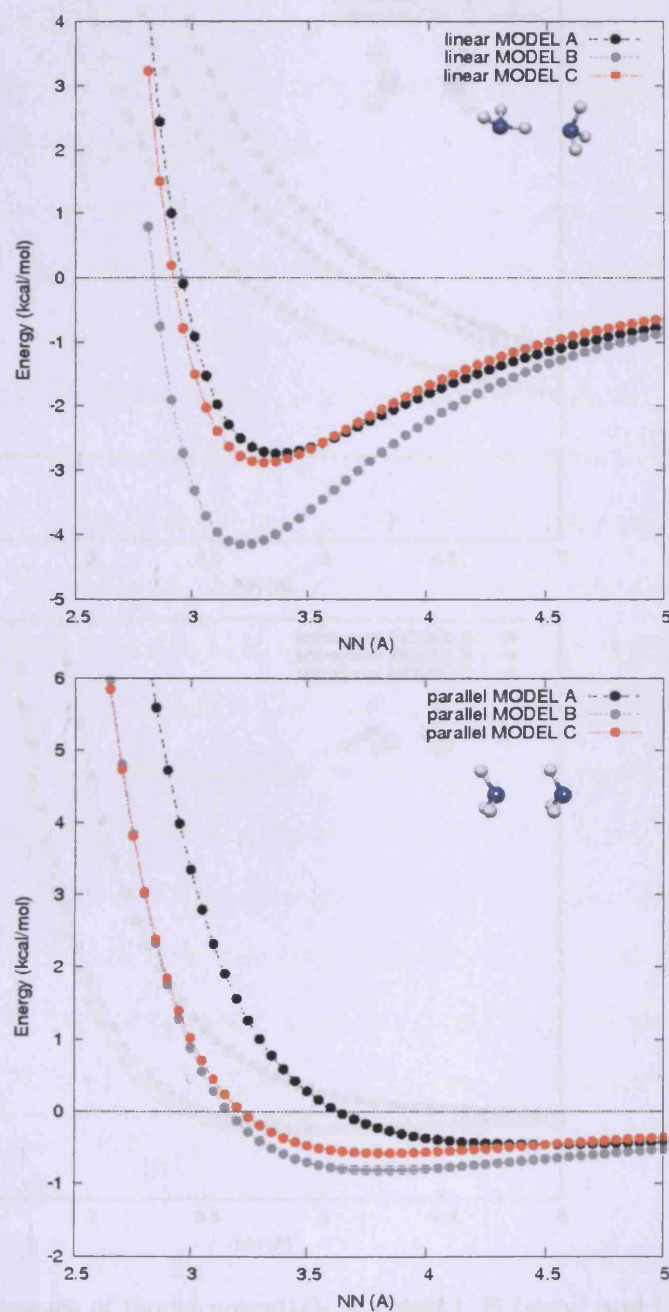


Figure 3.3: Performance of model potentials A (black), B (grey) and C (orange) on a rigid scan over the N-N distance in the linear and parallel configurations.

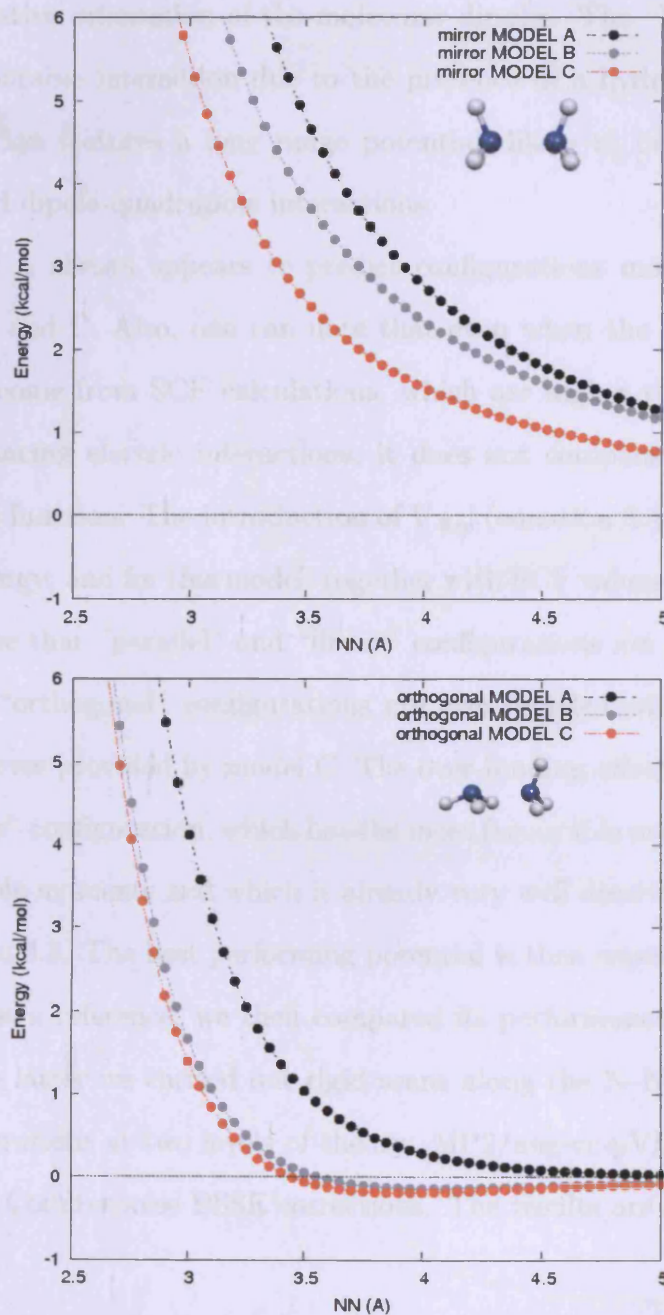


Figure 3.4: Performance of model potentials A (black), B (grey) and C (orange) on a rigid scan over the N-N distance in the mirror and orthogonal configurations.

As it can be seen from figures 3.3 and 3.4 the $(\text{NH}_3)_2$ model potential is strongly anisotropic. The “mirror” geometry presents a repulsive potential energy curve due

to the relative orientation of the molecular dipoles. The “linear” geometry shows the most favourable interaction due to the presence of a hydrogen bond. The “parallel” configuration features a long range potential, likely to be due to favourable dipole-dipole and dipole-quadrupole interactions.

Model A always appears to predict configurations more weakly interacting than models B and C. Also, one can note that even when the electrical moments used in model A come from SCF calculations, which are higher than the experimental ones, thus enhancing electric interactions, it does not compensate for the absence of the dispersion function. The introduction of V_{disp} (equation 3.4) in model B lowers the potential energy; and for this model, together with SCF values for the electrical moments, one can see that “parallel” and “linear” configurations are over-bound, whereas “mirror” and “orthogonal” configurations are over-repelled with respect to the potential energy curves provided by model C. The over-binding effect is particularly obvious for the “linear” configuration, which has the most favourable orientation for the interaction of multipole moments and which is already very well described by the Morse potential of equation 3.3. The best performing potential is then expected to be model C. Taking model C as a reference, we then compared its performance with *ab initio* values. To obtain the latter we carried out rigid scans along the N–N distance (2.5Å to 5Å) for all configurations at two levels of theory: MP2/aug-cc-pVDZ and MP2/aug-cc-pVTZ both with Counterpoise BSSE corrections. The results are shown below.

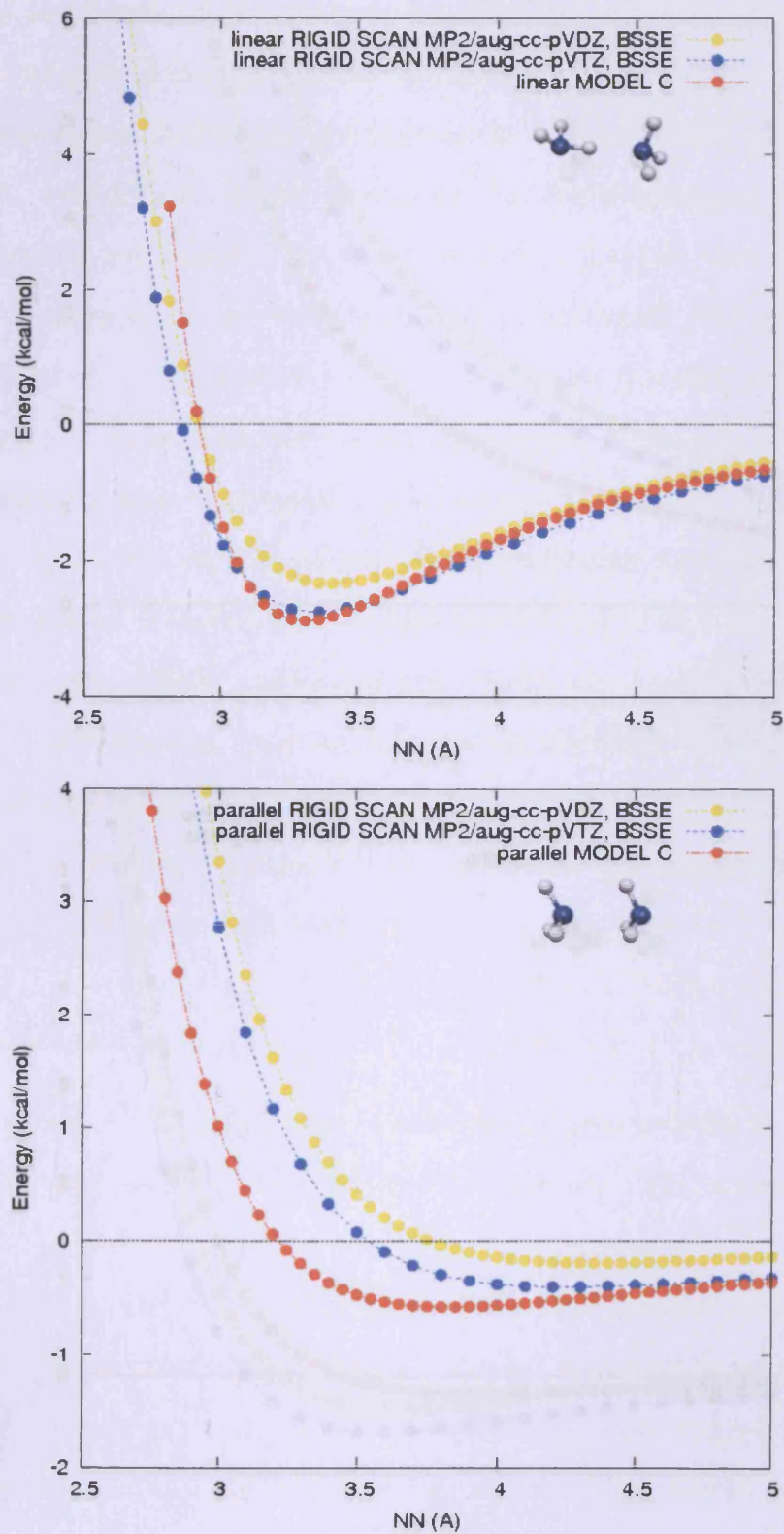


Figure 3.5: Performance of model potential C, and *ab initio* calculations (CP-MP2/aug-cc-pVXZ, X = D, T), on a rigid scan over the N-N distance in the “linear” and “parallel” configurations

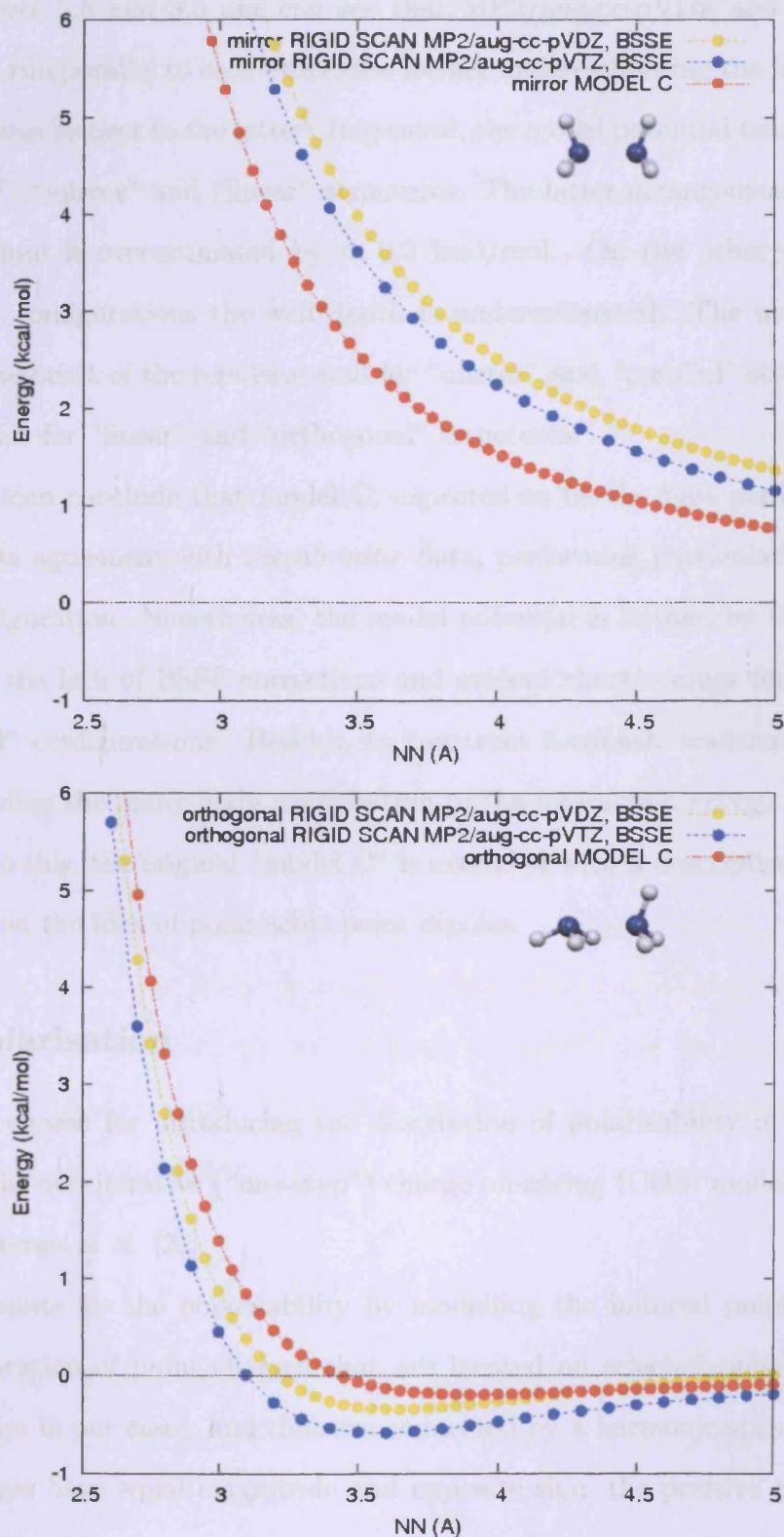


Figure 3.6: Performance of model potential C, and *ab initio* calculations (CP-MP2/aug-cc-pVXZ, X = D, T) on a rigid scan over the N-N distance in the "mirror" and "orthogonal" configurations.

From figures 3.5 and 3.6 one can see that MP2/aug-cc-pVDZ and MP2/aug-cc-pVTZ curves run parallel to each other, the former underestimating the binding energy for all structures respect to the latter. In general, the model potential tends to overbind the “parallel”, “mirror” and “linear” structures. The latter arrangement, close to the global minimum is overestimated by ≈ 0.2 kcal/mol. On the other hand, for the “orthogonal” configurations the well depth is underestimated. The model potential also delays the onset of the repulsive wall for “mirror” and “parallel” structures, while it accelerates it for “linear” and “orthogonal” structures.

Thus, we can conclude that model C, expected to be the best performing model potential, is in agreement with the *ab initio* data, performing particularly well for the “linear” configuration. Nonetheless, the model potential is limited by the use of SCF calculations, the lack of BSSE corrections and evident shortcomings for the “mirror” and “parallel” configurations. Besides, to construct a robust, transferable model, a scheme including the many-body contribution to the interaction energy is mandatory. In order to do this, the original “model C” is extended with a description of induction forces based on the idea of polarisable point dipoles.

3.2.2 Polarisation

The method chosen for introducing the description of polarisability in the ammonia potential is the non-iterative (“one-step”) charge-on-spring (COS) model as developed by van Gunsteren *et al.* [22].

COS accounts for the polarisability by modelling the induced point dipoles as a variable separation of point charges that are located on selected polarisable centres (nitrogen atom in our case), and that are connected by a harmonic spring.

The charges have equal magnitude and opposite sign, the positive charge is fixed at the nucleus while the negative charge is allowed to move under the presence of

a field. An external electric field proportionally displaces the negative point charge (“polarisation charge”, q_{pol}) from its equilibrium position.

The “one-step” approach to the polarisability is based on the approximation that the contribution from the permanent charges will dominate the total electric field. Then, the effect of other induced dipoles should be weak and it can be added to the electric field due to permanent charges as a perturbation. This is to say, that the induced dipoles are not themselves polarisable, although they interact with each other. Also, the “one-step” method is supported by the fact that more than 95% of the point dipole induction energy in water aggregates is obtained after the first iteration [23]

To avoid the complex algebra involved in the evaluation of dipole-dipole forces, and to be able to treat them as pointlike dipole interactions, one has to further assume that the separation of the polarised charges will be small. This assumption requires the use of a large value for the polarisation charge (see equation 3.8 below); while $q_{pol} = 8 e$ was used in reference [22], in this work we have opted for the higher value $q_{pol} = 16 e$.

An expression for the induction energy of non-converged dipoles was derived by Palmo and Krim [23], which, on the basis of what is explained above, was applied to the ammonia potential and added as another contribution to the total potential energy.

As a support to our strategy, the mathematics involved in the description of the polarisability is explained next. If the induced dipoles $\vec{\mu}_i$ of a molecular system with polarisable sites i are obtained iteratively one can write

$$\vec{\mu}_i = \vec{\mu}_i^{(0)} + \vec{\mu}_i^{(1)} + \vec{\mu}_i^{(2)} + \dots \quad (3.5)$$

The fully induced dipole at site i ($\vec{\mu}_i$) is proportional to the polarisability of the polarisable centre and to the electric field at the position \vec{r}_i of the point dipole:

$$\vec{\mu}_i = \alpha_i (\vec{E}_i^{(0)} + \vec{E}_i^{(ind)}) \quad (3.6)$$

where $\vec{E}_i^{(0)}$ is the electric field resulting from the permanent atomic charges, and $\vec{E}_i^{(ind)}$ is the field resulting from the induced dipoles.

The total electric field is given by

$$\vec{E}_i = (\vec{E}_i^{(0)} + \vec{E}_i^{(ind)}) \quad (3.7)$$

The electric field at polarisable centres is evaluated for a given molecular arrangement to estimate the polarisable charge displacement, as given by

$$\vec{r}_i' = \vec{r}_i + \frac{\alpha_i}{q_{pol}} \vec{E}_i^{(0)} \quad (3.8)$$

The new dipole field $\vec{E}_i^{(ind)}$ is computed as a contribution over all induced dipole, each written as

$$\vec{E}_i^{(ind)} = \sum_i \pm \frac{q_{pol}}{R^2} \hat{u}_R \quad (3.9)$$

being R the distance between the induced dipoles and \hat{u}_R the unitary vector determining the direction of $\vec{E}_i^{(ind)}$.

The induction energy for the “one-step” approach may be estimated by:

$$V_{ind} = -\frac{1}{2} \vec{\mu}_i^{(0)} \vec{E}_i^{(0)} - \frac{1}{2} \vec{\mu}_i^{(0)} \vec{E}_i^{(1)} \quad (3.10)$$

where $\vec{E}_i^{(0)}$ is the initial external field experienced by the i th molecule resulting from the fixed point charges of other molecules; $\vec{\mu}_i^{(0)}$ is the dipole induced in the i th molecule as obtained substituting $\vec{E}_i^{(0)}$ in equation 3.8, and $\vec{E}_i^{(1)}$ is the field experienced by the i th molecule due to the induced component of the dipole in other molecules.

Preliminary Monte Carlo simulations revealed that with decreasing distances between atoms of different molecules (less than one bohr), V_{ind} , at first repulsive, even-

tually becomes large and negative, causing walkers to remain trapped in unphysical configurations. This situation persists even when a large number of iterations is performed. Therefore, a multiplicative switching function is used to turn off V_{ind} smoothly:

$$S(r) = \frac{1}{2}\{1 + \tanh[10(r - 1)]\}$$

where r is the distance between any atom in molecule i and the nitrogen atom in molecule j .

3.2.3 Re-parameterisation

The optimisation, or re-parameterisation, has been carried out for all free parameters of the analytical form with exception of the coefficients in the dispersion energy expression d_6 , d_8 and d_{10} in equation 3.4. Also, for the sake of clarity, it can be advanced that the parameters describing the interaction between hydrogen atoms were kept identical to those in reference [12], since their optimisation did not provide any significant improvement into the description of the interaction. In addition, the Morse potential function (equation 3.3), meant to improve the description of the H-bond interaction in the original “model C”, was eliminated once it was noticed that the parameter optimisation was making its contribution negligible.

To find the array of parameters providing the lowest error, an optimisation was carried out using the Powell method [26], starting from several sets of initial values. Initially, this was achieved by minimising the weighted square difference, $\Delta(p)$, between the model potential values and the *ab initio* values and multiplying it by a weight factor w_i , as:

$$\Delta(p) = \sum_i \left(V_{MP2}(R_i) - V_{pot}(R_{i,p}) \right)^2 w_i \quad (3.11)$$

where $V_{MP2}(R_i)$ is the *ab initio* energy, and $V_{pot}(R_i)$ is the energy from the model potential. The weight factor, w_i , allows for different contributions to the total error from different regions from the potential. The closer w_i is to 0, the less contribution a particular configuration has towards the total error. The weight factor has been chosen as $w = 1$ for energy values between -1 and -3 kcal/mol, (this range of energy embraces the minimum region of the potential energy surface), $w = 0.25$ for values from -1 to 0 kcal/mol, $w = 0.1$ for energy values between 0 and +4 kcal/mol, and $w = 0$ for energies bigger than +4 kcal/mol. So one can see that the regions where less error is allowed, the ones with a higher value of w_i , are those most populated and close to the lowest energy region. Values above +4 kcal/mol, correspond to dimeric arrangements with very small nitrogen-nitrogen distances, dominated by repulsion forces, that are not well described by the model potential and that have been observed to affect the quality of the fitting in more significant regions of the PES; hence, the low value of w_i .

Since the error in the fitting is defined as the difference between the *ab initio* and the model potential binding energies (as seen in brackets in equation 3.11); a negative error value means that the model potential energy curve would lie higher than the theory calculation curve, so our model PES underestimates the dimer interaction. Conversely, an error with a positive value means that our model potential overestimates the energy respect to *ab initio* data.

Table 3.2 shows the values of three sets of parameters. The first set corresponds to the values used by Hinchliffe *et al.* [12]. The set labelled as model C(pol, Q^{pt}) includes as an optimisable variable the charge magnitude located in the hydrogen atoms Q . A priori, one would think that this could have a negative effect on the long-range interaction description, but as we will see below (panels C and D, vide infra) optimising Q will have a favourable impact in the model potential performance. Finally, the set called model C(pol, Q^{frozen}) keeps Q identical as in reference [12].

Table 3.2: Optimised parameters for the two model potentials, model C(pol,Q^{opt}) and model C(pol,Q^{frozen})^a

parameters	model C[12]	model C(pol,Q ^{opt})	model C(pol,Q ^{frozen})
a_{NN}	13165	9162.98329	6903.06545
b_{NN}	-2.7	2.63500285	2.35033248
a_{NH}	0.4	0.427713623	0.247394716
b_{NH}	2.3	3.60109836	3.66458152
r_{NH}^*	2.5	2.606558	2.73514533
a_{HH}	700	700	700
b_{HH}	3.7	3.7	3.7
r^*	4.7	4.7	4.7
Q	0.462	0.526420468	0.462
d	0.156	0.156	0.156
d_6	1230	1230	1230
d_8	6500	6500	6500
d_{10}	42100	42100	42100

^a Also shown are the parameters for the original analytical form, model C[12], where the analytical form $V_{ij}(r_{ij}) = a_{ij}[\exp(-b_{ij}(r_{ij} - r_{ij}^*)) - 1]^2 - a_{ij}$ was used to describe the interaction between N and H atoms in different molecules. Several significant figures are reported for the optimised parameters to guarantee an accurate reproduction of the new model potentials. Units are: kcal/mol for a_{ij} ; Å for r_{ij}^* , δ and r^* ; au for Q . The units of the dispersion parameters d_6, d_8 and d_{10} are respectively kcal/(mol Å⁶), kcal/(mol Å⁸), kcal/(mol Å¹⁰)

The following three pictures, figure 3.7, show the 2-D surfaces representing the error between the re-fitted “model C” from reference [12], in different parameterised forms, and the *ab initio* values obtained at the CP-MP2/aug-cc-pVTZ level of theory. The initial coordinate used in the plots can be seen in figure 3.2 (c). Angle A scans over 180° in steps of 5°, starting from 0. R_{NN} scanned from 2.5 Å to 5 Å in steps of 0.25 Å. In this way, the region around $\theta \approx 0^\circ$ represents the “N to N” approach of the two molecules. Also, this scan sweeps through two meaningful configurations from figure 3.1, the so called “parallel” (when $\theta \approx 180^\circ$) where the scan ends, and most importantly the “linear” arrangement ($\theta \approx 80^\circ$), corresponding to the minimum region of the potential energy surface.

Figure 3.7a, shows the error between “model C” potential before fitting and the *ab initio* potential energy surface. This error surface shows a considerable error, especially

at small nitrogen-nitrogen distances. This is true for all configurations but specially for the “parallel” and the starting configurations where the model potential overbinds by more than 1 kcal/mol. This contrasts with the acceptable description around the minimum. One can also notice, that as the distance along R_{NN} increases the error value becomes negative, suggesting that “model C” underestimates the dispersion interaction with respect to the *ab initio* potential.

Figure 3.7b, differs from figure 3.7a, in that now the model potential includes a polarisation description (i.e. “model C(pol, Q^{frozen})”). In this situation, the error surface seems to increase its value at all N-N distances for the initial configuration with respect to figure 3.7a. The region describing the barrier between the initial scan configuration and the linear H-bond arrangement is seemingly underestimated with respect to the *ab initio* potential. The linear H-bond configuration itself is fairly well described, with a slight decrease of the error respect to figure 3.7a around R_{NN} of 3.4 Å, getting a poorer performance upon increasing the distance between the nitrogen atoms. No major changes are seen with respect to figure 3.7a for the “parallel” structure.

Panel 3.7c shows the difference between *ab initio* interaction energies and our model potential with polarisation correction and optimisation of the set parameters including the charge magnitude Q (i.e. “model C(pol, Q^{opt})”).

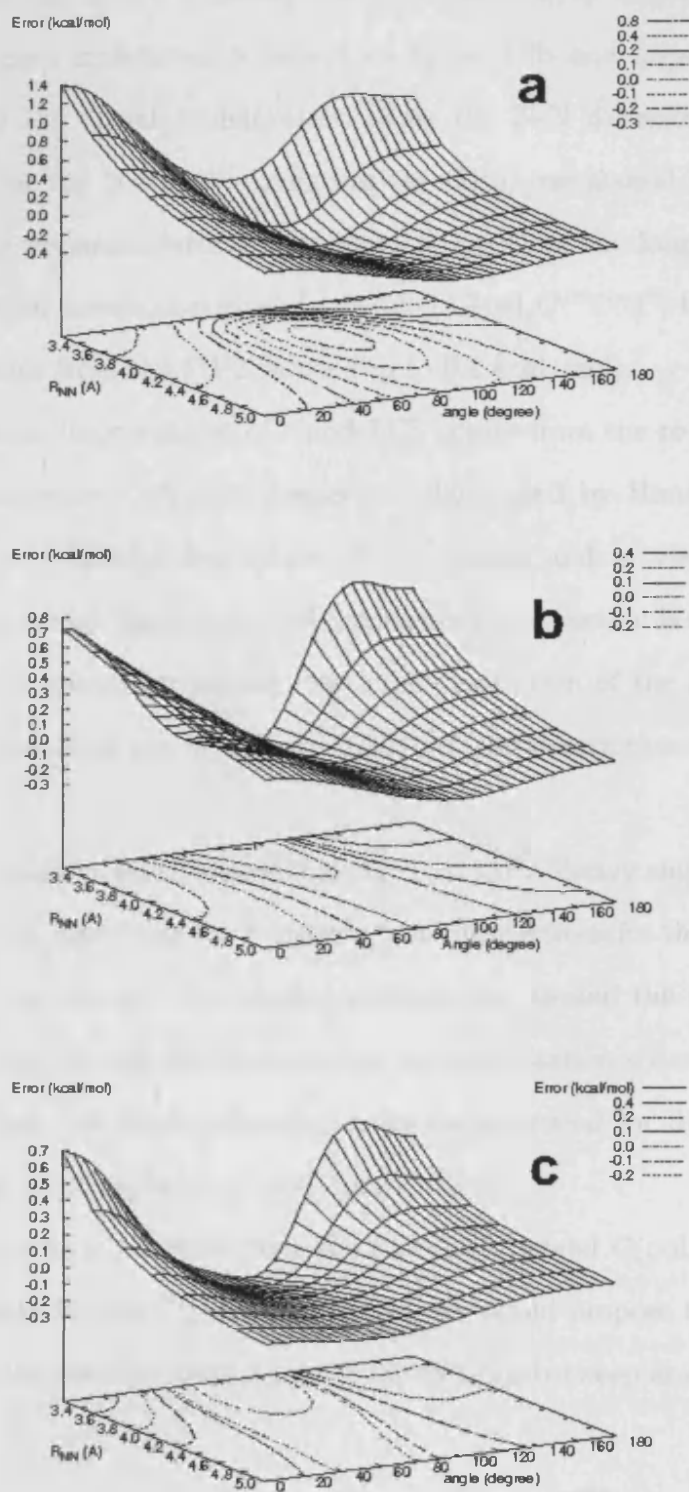


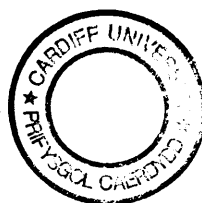
Figure 3.7: Signed energy difference between *ab initio* and model potential interaction energies. From the top, panel a shows "model C" with parameters and analytical form from reference [12], panel b shows "model C(pol, Q^{frozen})" and panel c shows "model C(pol, Q^{opt})"

This new set of parameters, basically the optimisation of Q , slightly flattens out the region of the “linear” configuration respect to figure 3.7b and improves significantly the description of the initial configuration along the N-N distance. As before, no changes are seen for the “parallel” configuration. Also, one should note that “model C(pol, Q^{opt})”, with re-parameterised Q , appears to preserve the long-range behaviour for the intermolecular interaction given by “model C(pol, Q^{frozen})”; both models show only small deviations from the MP2 values (up to 0.2 kcal/mol).

The most obvious improvement of “model C” comes from the re-parameterisation of the charges and some coefficients respect to those used by Hinchliffe *et al.* [12]. However, for a more faithful description of the system and in view of the further applications of our model, the inclusion of a polarisation correction is mandatory. Both (polarisation and re-parameterisation) refine the description of the geometry around the minimum region, and improve in 0.1 kcal/mol the description of the “parallel” structure.

In addition, it is fair to acknowledge that the reportedly “heavy emphasis” dedicated by Hinchliffe *et al.* in describing the hydrogen bond interactions for the original “model C” resulted in a surprisingly even-handed performance around the minimum region, specially considering the lack BSSE correction and polarisation scheme. However, the implementation that this work proposes proves to be crucial for dimer orientations other than “linear” such as “mirror” and “parallel”.

To conclude, we have observed that the so called “model C(pol, Q^{opt})” seems to perform better than “model C(pol, Q^{frozen})”; so, we would propose the former as the potential of choice to describe intermolecular interactions between ammonia molecules.



3.3 Results

3.3.1 Geometry Reproduction of $(\text{NH}_3)_2$

Our model $C(\text{pol}, Q^{\text{opt}})$ was used on the rigid “linear” ammonia dimer in order to see how its estimations on the geometrical parameters and binding energy compared against *ab initio* values, in particular CP-MP2/aug-cc-pVTZ level of theory. As it can be seen in figure 3.8 the analytical form and *ab initio* values are in good agreement. The model potential overestimates the NHN angle of the hydrogen bond and the N–N distance. On the other hand, “model $C(\text{pol}, Q^{\text{opt}})$ ” underestimates slightly the binding energy respect to the *ab initio* value (by 0.162 kcal/mol), this is in contrast with the original “model C” which had a tendency to overbind the ammonia dimer.

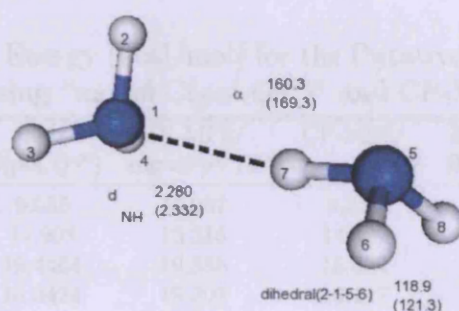


Figure 3.8: Equilibrium geometries for the ammonia dimer obtained using CP-MP2/aug-cc-pVTZ and model $C(\text{pol}, Q^{\text{opt}})$, in brackets, distances in Å.

3.3.2 Structure and Energetics of $(\text{NH}_3)_n$ ($n = 3 - 20$)

Minimum energy structures for larger ammonia clusters were optimised employing “model $C(\text{pol}, Q^{\text{opt}})$ ” as a potential. The geometry optimisation was carried out in a similar way to that suggested by Beu and Buck [14], i.e. starting from randomly positioned and oriented ammonia molecules inside a cube of side 15–20 Å. For every $(\text{NH}_3)_n$ ($n = 3-20$), several thousand structures were optimised by minimising the total energy with the Powell method [26], producing a database of local minima for each n .

Putative global minima were extracted and their structure is shown in figures 3.9 and 3.10. In the following subsection we compare the performance of “model C(pol, Q^{opt})” in reproducing the *ab initio* data presented in chapter 2 for $(\text{NH}_3)_n$ ($n = 3 - 5$). The results for the larger clusters are successively compared with other studies [14, 27] carried out employing different model potentials.

$(\text{NH}_3)_n$ ($n = 3 - 5$)

The top row of figure 3.9 shows the putative global minima for $(\text{NH}_3)_3$, $(\text{NH}_3)_4$ and $(\text{NH}_3)_5$, and their total binding energies are given in table 3.3. In agreement with our *ab initio* data, the trimer and tetramer show a cyclic structure which favours the formation of strong hydrogen bonds.

Table 3.3: Total Binding Energy (kcal/mol) for the Putative Global Minima of $(\text{NH}_3)_n$ ($n = 3 - 5$) Computed using “model C(pol, Q^{opt})” and CP-MP2/aug-cc-pVTZ

n	model C(pol, Q^{opt})	CP-MP2/ aug-cc-pVTZ	CP-MP2/ aug-cc-pVDZ	Beu and Buck [14]	model C
3	9.055	10.067	9.326	-8.258	-9.073
4	14.908	15.515	14.427	-12.628	-13.433
5(cyclic)	19.4464	19.358	18.334		
5(compact)	18.3424	19.203	18.127		
5(BB1)	18.2646	19.315	18.177	16.720	
5(pyramid)	18.1238	19.263	18.181		
5(butterfly)	17.4385	18.45	17.21		

One can see that for the trimer and tetramer structures, “model C(pol, Q^{opt})” slightly underestimates the total binding energy respect to *ab initio* MP2/aug-cc-pVTZ data. Notwithstanding, this performance is significantly better than that from the previous model potentials available, which underestimate the total binding energy for the trimer, and particularly for the tetramer, by substantially more when compared to MP2/aug-cc-pVTZ values. On the other hand, looking at table 3.3, “model C(pol, Q^{opt})” seems to provide a performance similar to that of MP2/aug-cc-pVDZ level of theory.

The original “model C” and “model C(pol, Q^{opt})” appear to be in agreement in what regards the binding energy for the cyclic trimer, not so for the tetramer; which is significantly underestimated. In fact, “model C” predicts a more compact, tetrahedral isomer as the lowest energy species instead of a ring.

Let us recall from Chapter 2 that for $(\text{NH}_3)_5$ five isomers were found to lie within 2 kcal/mol from the putative global minimum, with four of those isomers lying within 0.3 kcal/mol from the lowest one. In this challenging scenario, not only “model C(pol, Q^{opt})” has predicted the same lowest energy isomer as the MP2/aug-cc-pVTZ level of theory, but the difference in energy between these two predictions for the same structure is 0.1 kcal/mol. This is a better agreement than for the trimer and the tetramer. Considering that “model C(pol, Q^{opt})” underestimates the energy of the dimer by 0.162 kcal/mol and that this effect is likely to be additive, we suspect that the improvement in the performance is most likely due to the many-body induction term in our energy expression. In addition, “model C(pol, Q^{opt})” has produced a novel pentamer (“butterfly”) that is shown in figure 3.11.

From table 3.3, it can be seen that pentamer isomers “compact”, “BB1”, “pyramid” and “butterfly” lie at least 1 kcal/mol over the “cyclic” pentamer. This is at slight variance with the MP2 calculations. A possible explanation can be found in figures 3.7a, 3.7b and 3.7c where it can be seen that “model C(pol, Q^{opt})” lies above the MP2 surface for angles differing from $\approx 80^\circ$, i.e. the linear H-bond geometry. It seems then that the model introduces some energy penalty for all isomers whose hydrogen bonds deviate from the linearity. This artificial increase in the interaction energy may also explain the fact that “model C(pol, Q^{opt})” produces a cyclic pentamer that is flatter than the one obtained using CP-MP2/aug-cc-pVTZ. Overall, “model C(pol, Q^{opt})” has performed consistently, given the compressed energy landscape for $(\text{NH}_3)_5$, providing reasonable energies for the lowest isomers.

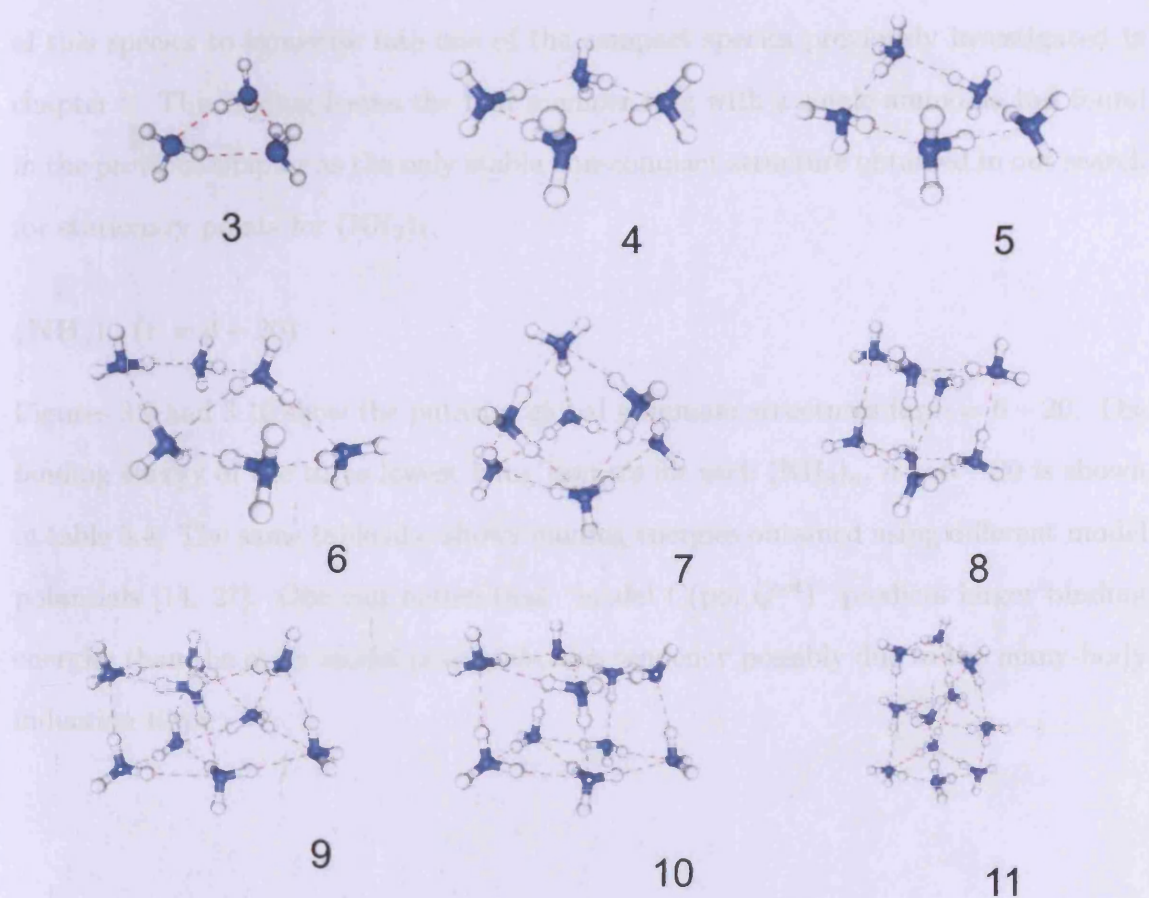


Figure 3.9: Structure of the putative global minima for $(\text{NH}_3)_n$ ($n = 3 - 11$) optimised using “model C(pol, Q^{opt})”

Apart from the pentamer species listed in table 3.3, several other isomers were located during the structural search with “model C(pol, Q^{opt})”, all of them presenting a lower number of H-bond contacts than the five lowest minima. A linear species was optimised ($\text{BE} = 14.88 \text{ kcal/mol}$), which was previously reported by Kulkarni and Pathak [34] ($\text{BE} = 18.19 \text{ kcal/mol}$ at BSSE uncorrected MP2/6-31++G(d,p) level of theory). It was also located an isomer composed of a three member ring connected to a two member chain ($\text{BE} = 15.31 \text{ kcal/mol}$). The latter occurrence may be possible inside superfluid He droplets. We tested the stability of this (“3+2”) isomer performing optimisations at the MP2/aug-cc-pVDZ level of theory, which revealed the tendency

of this species to isomerise into one of the compact species previously investigated in chapter 2. This finding leaves the four member ring with a single ammonia tail found in the previous chapter as the only stable non-compact structure obtained in our search for stationary points for $(\text{NH}_3)_5$.

$(\text{NH}_3)_n$ ($n = 6 - 20$)

Figures 3.9 and 3.10 show the putative global minimum structures for $n = 6 - 20$. The binding energy of the three lowest lying isomers for each $(\text{NH}_3)_n$, $n = 6 - 20$ is shown in table 3.4. The same table also shows binding energies obtained using different model potentials [14, 27]. One can notice that “model C(pol, Q^{opt})” predicts larger binding energies than the other model potentials, this tendency possibly due to the many-body induction term.

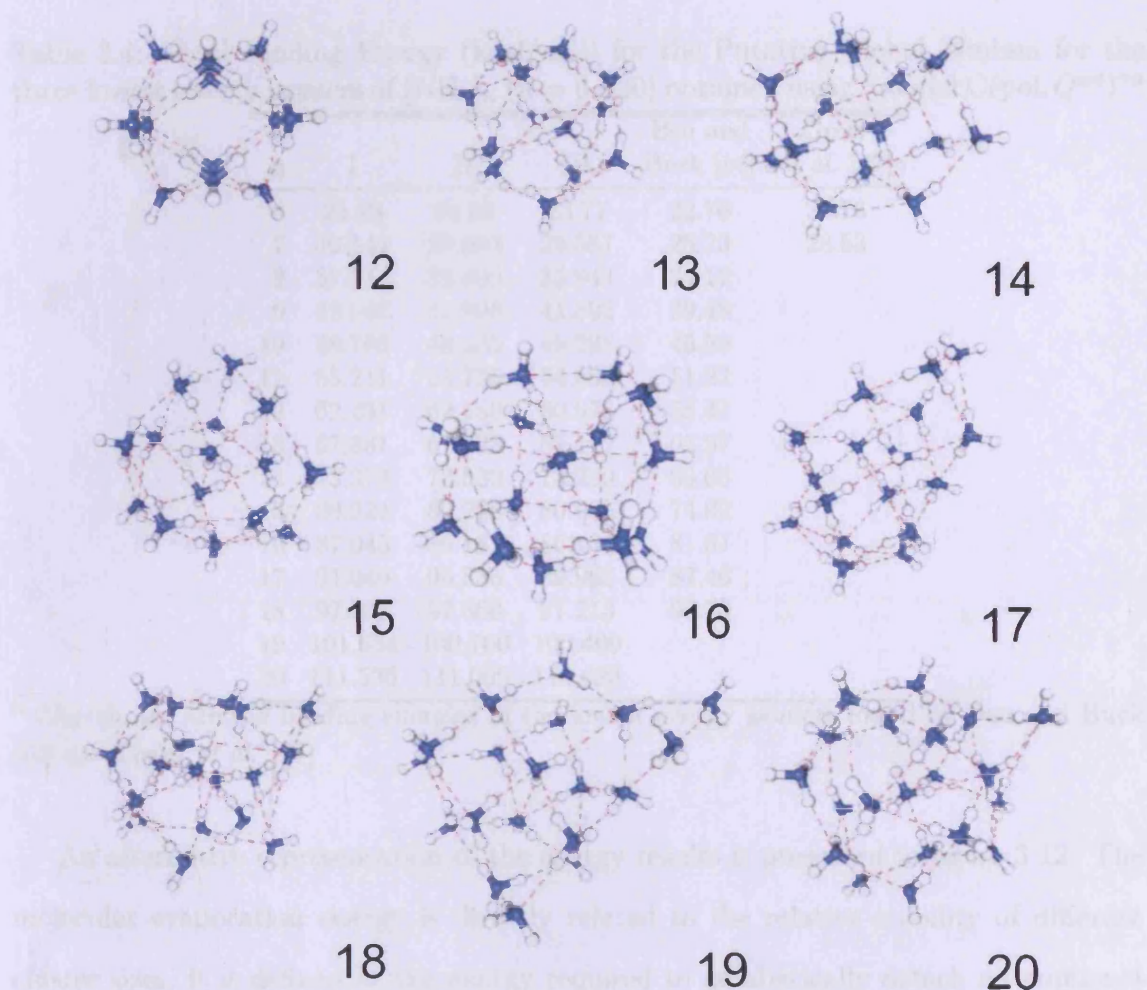


Figure 3.10: Structure of the putative global minima for $(\text{NH}_3)_n$, ($n = 12 - 20$) optimised using “model $\text{C}(\text{pol}, Q^{opt})$ ”

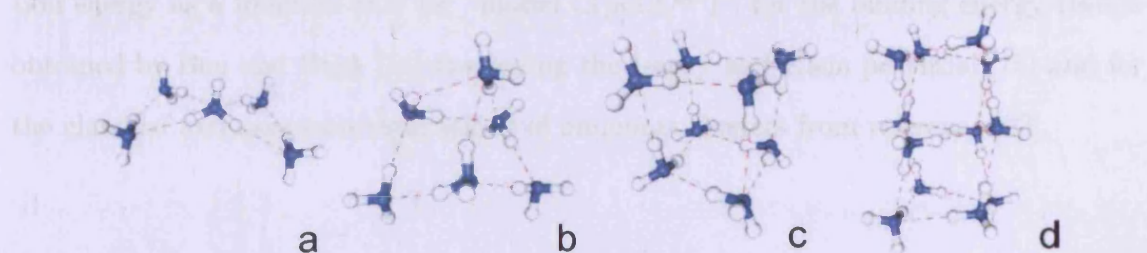


Figure 3.11: Local minimum structures obtained using “model $\text{C}(\text{pol}, Q^{opt})$ ” for some cluster size: (a) “butterfly” isomer for $(\text{NH}_3)_5$; (b) second energy isomer for $(\text{NH}_3)_6$; (c) second energy isomer for $(\text{NH}_3)_8$; (d) second energy isomer for $(\text{NH}_3)_{12}$

Table 3.4: Total Binding Energy (kcal/mol) for the Putative Global Minima for the three lowest energy isomers of $(\text{NH}_3)_n$ ($n = 6-20$) obtained using “model C(pol, Q^{opt})”^a

n	I	II	III	Beu and Buck [14]	Greer <i>et al.</i> [27]
6	24.29	24.03	23.77	22.70	22.73
7	30.142	29.993	29.587	28.23	28.53
8	37.311	36.609	35.943	34.12	
9	42.042	41.993	41.892	39.48	
10	48.786	48.485	48.238	45.59	
11	55.211	54.726	54.668	51.22	
12	62.231	62.180	60.978	58.41	
13	67.881	67.323	67.112	62.97	
14	73.373	73.330	73.259	69.06	
15	80.924	80.228	80.055	74.92	
16	87.045	86.181	86.134	81.51	
17	91.040	90.333	89.968	87.46	
18	97.958	97.666	97.213	93.73	
19	101.634	100.700	100.409		
20	111.536	111.009	110.023		

^a Also shown are the binding energies of the lowest energy isomers found by Beu and Buck [14] and Greer *et al.* [27]

An alternative representation of the energy results is presented in figure 3.12. The molecular evaporation energy is directly related to the relative stability of different cluster sizes, it is defined as the energy required to adiabatically detach an ammonia molecule from a given cluster ($E_{vap}(n) = E_n - E_{n-1}$). Figure 3.12 shows the evaporation energy as a function of n for “model C(pol, Q^{opt})”, for the binding energy results obtained by Beu and Buck [14] employing the Impey and Klein potential [15] and for the classical and quantum simulations of ammonia clusters from reference [33].

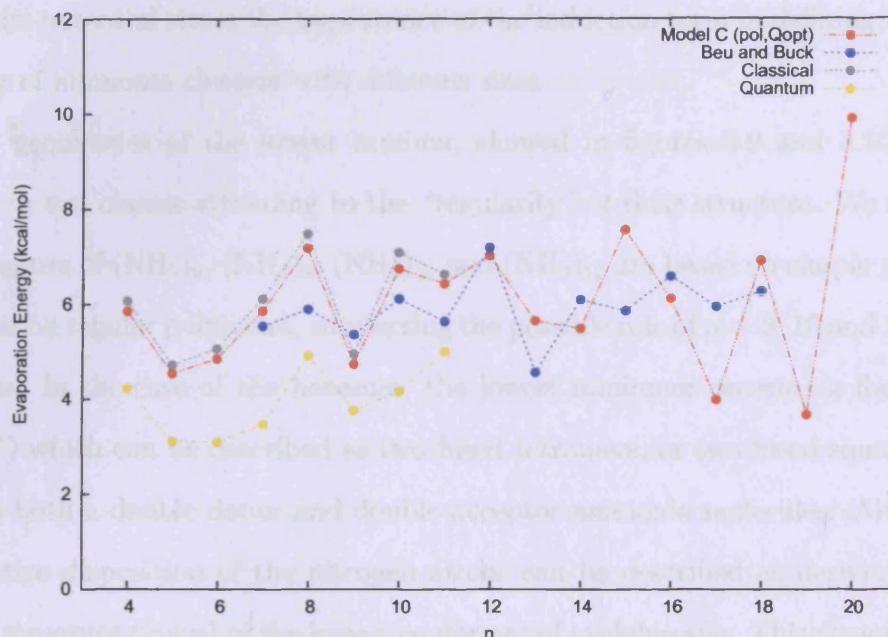


Figure 3.12: Evaporation energy ($E_{vap}(n) = E_n - E_{n-1}$, kcal/mol) for $(\text{NH}_3)_n$ computed using the total energy of putative global minima. Data obtained using “model C(pol, Q^{opt})”; also showing the results provided in references [14, 33]

One can see that “model C(pol, Q^{opt})” presents a rougher behaviour for E_{vap} than the one obtained using the pairwise model potential employed in reference [14]. This rough behaviour is also reproduced by the path integral simulations, albeit the introduction of quantum effects reduces significantly the energy needed to dissociate a monomer from the parent species, as well as smoothing the roughed behaviour showed by the minimum energy results [33].

It is interesting to note the large evaporation energy that “model C(pol, Q^{opt})” predicts for $n = 8, 10, 12, 15$ and 20 . This tendency possibly suggest that these structures have high stability, hence pointing at them as potential magic numbers. The former are usually associated with the completion of a shell with a particular symmetry, which normally optimises the balance between surface tensions and repulsive interactions [33]. As a whole, the different behaviours shown by the evaporation energy as a function of

the model potential stress the importance of the induction term in defining the relative stability of ammonia clusters with different sizes.

The geometries of the lowest minima, showed in figures 3.9 and 3.10, could be divided in two classes attending to the “regularity” of their structure. We notice that the structure of $(\text{NH}_3)_6$, $(\text{NH}_3)_8$, $(\text{NH}_3)_{10}$ and $(\text{NH}_3)_{12}$ are based on simple geometrical shapes or on regular polyhedra, supporting the possible role of $n = 8, 10$ and 12 as magic numbers. In the case of the hexamer, the lowest minimum presents a flat structure (“book”) which can be described as two fused tetramers, or two fused squares. It also features both a double donor and double acceptor ammonia molecules. Alternatively, the relative disposition of the nitrogen atoms can be described as deriving from the “chair” structure typical of the lowest conformer of cyclohexane. This structure for the hexamer is at variance with the results of previous investigations using nonpolarisable models [14, 27], which suggest a more compact 3D geometry as global minimum. A 3D structure is, however, obtained for the second lowest isomer (figure 3.11), lying only 0.26 kcal/mol above the putative global minimum. This small energy difference may prove necessary to use electronic structure calculations to assign conclusively the global minimum structure.

Regarding the $(\text{NH}_3)_8$, both the global minimum and the second lowest isomer (figures 3.8 and 3.11, respectively) were found to present structures based on a distorted cubic shape that are built starting from two different isomers of the tetramer. In particular, the tetramers in the global minimum show an alternate disposition of the free H atoms with respect to the ring plane (UDUD, where U and D indicate the direction of the free NH bond for an ammonia molecule perpendicular to the plane as pointing up or down, respectively). In contrast, the second lowest isomer has the two tetrameric moieties showing a UUDD orientation of the free NH bonds. In addition, the lowest isomer found has a higher symmetry (D_{2d}) than the second one, which presents

a binary axis only. The difference in the relative arrangement of H bonds, is reflected in an energy gap of 0.702 kcal/mol between the two species.

The second and third lowest isomers of $(\text{NH}_3)_8$ are separated by an substantial energy gap of 0.666 kcal/mol, a finding that could suggest the possibility that the low temperature thermodynamics of the octamer is likely to be dominated by the global minimum, and that it should be expected to present signatures for a phase transition in the specific heat as found in the case of $(\text{H}_2\text{O})_8$ [35]. In addition, reference [33] found that the quantum evaporation energy suggests the possibility of an enhanced kinetic stability (i.e. a longer lifetime) for the octamer, and in the classical heat capacity the octamer has the most prominent melting feature.

A somewhat similar situation is also found for the decamer, $(\text{NH}_3)_{10}$, with sizable energy gaps between the lowest three or four isomers. The lowest energy isomer for the decamer can be seen as the global minimum for the octamer with the addition of two extra molecules on the same cube face. Being connected with themselves, these two molecules also accept and donate hydrogen bonds with molecules on the face, forming two three-member rings and leaving a binary axis as the only element of symmetry for the structure.

Regarding the dodecamer, $(\text{NH}_3)_{12}$, Beu and Buck [14] predict an icosahedral geometry for the global minimum, separated from the second lowest isomer by 1.8 kcal/mol. Differently from this result, our optimisation generated two isomers with completely different geometries and extremely close in energy (0.051 kcal/mol). The lowest of the two isomers has the same icosahedral structure and evaporation energy found in reference [14], while the second one can be described as the fusion of two cubes on a face (figure 3.11). It seems that the explicit description of the electronic induction in our model does not play an important role in the relative energetics for the global minimum of $(\text{NH}_3)_{12}$, which may be due to the high symmetry of this species. There is a large

gap between the two lowest isomers and the third one (1.202 kcal/mol), signalling that signatures for a structural transformation may be found in the specific heat of this cluster. Also, for the dodecamer, high level *ab initio* calculations would be needed to provide an accurate prediction of the relative energetics for the two low lying species.

In the case of the clusters presenting a less regular disposition of the N atoms, the species containing an even number of ammonia molecules seem to present a more spherical structure than aggregates composed of an odd number of ammonia molecules. The latter opens the possibility of a non zero dipole moment of the cluster. This seems likely, given the usually low internal temperature of the clusters and the substantial energy gaps between low lying isomers. Hence, even and odd numbered clusters could be separated by means of a non-uniform electric field. The exception to this rule would be $(\text{NH}_3)_{13}$, whose geometry is closely related to the shape of the dodecamer, as it may be obtained by “squashing” the thirteenth ammonia molecule onto the edge of $(\text{NH}_3)_{12}$. This finding differs from the prediction of the pairwise model potential[14].

3.4 Conclusions

The implementation of a new model potential describing the interaction between ammonia molecules has been presented and discussed in this chapter. Its analytical form is partially based on a previous suggestion by Hinchliffe *et al.* [12]. Additionally, the model presents an explicit many-body description of the induction energy at the level of dipole polarisability, a feature that was not previously available in other semiempirical forms. The term describing the effect of induction has been implemented using the non-iterative “charge-on-spring” scheme proposed by van Gunsteren and co-workers [22], assuming an isotropic polarisability for NH_3 . The free parameters of the new model have been obtained by minimising the least square error with a set of CP-MP2/aug-

cc-pVTZ interaction energies computed over configurations relevant for the low energy dynamics of the ammonia dimer. As a consequence of this optimisation, two improved models have been obtained, both describing the interaction between two ammonia molecules with a higher accuracy than the original parameterisation of the analytical form.

Employing the most accurate model, namely “model C(pol, Q^{opt})”, a search for the global minimum structure of the NH_3 ($n = 3 - 20$) was carried out. Energy results for $n = 3 - 5$ were used to test the transferability of the model PES against *ab initio* data, suggesting that this potential has provided a substantial improvement in accuracy. A new low energy isomer was found for $(\text{NH}_3)_5$; for larger clusters, our model potential predicts larger binding energies than suggested by previous investigations employing pairwise potentials. Our data also indicate a rougher behaviour of the evaporation energy as a function of the number of ammonia molecules in the cluster, a feature suggesting the presence of magic numbers for $n = 8, 10, 12, 15$ and 20 .

Bibliography

- [1] Odutola, J. A.; Dyke, T. R.; Howard, B. J.; Muentner, J. S. *J. Chem. Phys.*, **1979**, *70*, 4884.
- [2] Nelson, D. D., Jr.; Fraser, G. T.; Klemperer, W. *J. Chem. Phys.*, **1985**, *83*, 6201.
- [3] Nelson, D. D., Jr.; Klemperer, W.; Fraser, G. T.; Lovas, F. J.; Suenram, R. D. *J. Chem. Phys.*, **1987**, *87*, 6364.
- [4] Süzer, S.; Andrews, L. *J. Chem. Phys.*, **1987**, *87*, 5131.
- [5] Snels, M.; Fantoni, R.; Sanders, R.; Meerts, W. L. *Chem. Phys.*, **1987**, *115*, 79.
- [6] Cybulsky, S. M. *Chem. Phys. Lett.*, **1994**, *228*, 451.
- [7] Lee, J. S.; Park, S. Y. *J. Chem. Phys.*, **2000**, *112*, 230.
- [8] Stårling, J.; Schütz, M.; Lindh, R.; Karlstrom, G.; Widmark, P-O. *Mol. Phys.*, **2002**, *100*, 3389.
- [9] Janeiro-Barral, P. E.; Mella, M. *J. Phys. Chem. A*, **2006**, *110*, 11244.
- [10] Olthof, E.H.; van der Avoird, A.; Wormer, P.E.S. *J. Chem. Phys.*, **1994**, *101*, 8430.
- [11] Duquette, G.; Ellis, T.H.; Scoles, G.; Watts, R.O.; Klein, M.L. *J. Chem. Phys.*, **1978**, *68*, 2544.

- [12] Hinchliffe, A.; Bounds, D. G.; Klein, M. L.; McDonald, I. R.; Righini, R. *J. Chem. Phys.*, **1981**, *74*, 1211.
- [13] Sagarik, K.P.; Ahlrich, R.; Brode, S. *Mol. Phys.*, **1986**, *57*, 1247.
- [14] Beu, T.; Buck, U. *J. Chem. Phys.*, **2001**, *114*, 7848.
- [15] Impey, R.W.; Klein, M.L. *Chem. Phys. Lett.*, **1984**, *104*, 579.
- [16] McDonald, I.R.; Klein, M.L. *J. Chem. Phys.*, **1976**, *64*, 4790.
- [17] Klein, M. L.; McDonald, I.R.; Righini, R. *J. Chem. Phys.*, **1979**, *71*, 3673.
- [18] Marchi, M.; Sprik, M.; Klein, M. L. *J. Chem. Phys.*, **1988**, *89*, 4918.
- [19] Szcześniak, M. M.; Kendal, R. A.; Chalaśiński, G. *J. Chem. Phys.*, **1970**, *95*, 401.
- [20] Dykstra, C. E.; Andrews, L. *J. Chem. Phys.*, **1990**, *92*, 6043.
- [21] Righini, R.; Klein, M. L. *J. Chem. Phys.*, **1978**, *68*, 5553.
- [22] Yu, H., Hansson, T; van Gunsteren, W. F. *J. Chem. Phys.*, **2003**, *118*, 221.
- [23] Palmo K.; Krim, S. *Chem. Phys. Lett.*, **2004**, *395*, 133.
- [24] Schaftenaar, G.; Noordik, J.H. "Molden: a pre- and post-processing program for molecular and electronic structures", *J. Comput.-Aided Mol. Design*, **2000**, *14*, 123-134.
- [25] Flükiger, P.; Lüthi, H. P.; Portmann, S.; Weber, J. MOLEKEL 4.3; Swiss National Supercomputing Centre: Manno (Switzerland).
- [26] Vetterling, W.T.; Press, W.H.; Teukolsky, S.A.; Flannery, B.P. *Numerical Recipes*; Cambridge University Press: Cambridge, U.K., **2001**; pp. 406.

- [27] Greer, J.C.; Ahlrichs, R.; Hertel, I.V. *Chem. Phys. Lett*, **1989**, *133*, 191.
- [28] Boys, S.F.; Bernardi, F. *Mol. Phys.*, **1970**, *19*, 553.
- [29] M. J. Frisch, G. W. Trucks, H. B. Schlegel, G. E. Scuseria, M. A. Robb, J. R. Cheeseman, V. G. Zakrzewski, J. A. Montgomery, Jr., R. E. Stratmann, J. C. Burant, S. Dapprich, J. M. Millam, A. D. Daniels, K. N. Kudin, M. C. Strain, O. Farkas, J. Tomasi, V. Barone, M. Cossi, R. Cammi, B. Mennucci, C. Pomelli, C. Adamo, S. Clifford, J. Ochterski, G. A. Petersson, P. Y. Ayala, Q. Cui, K. Morokuma, P. Salvador, J. J. Dannenberg, D. K. Malick, A. D. Rabuck, K. Raghavachari, J. B. Foresman, J. Cioslowski, J. V. Ortiz, A. G. Baboul, B. B. Stefanov, G. Liu, A. Liashenko, P. Piskorz, I. Komaromi, R. Gomperts, R. L. Martin, D. J. Fox, T. Keith, M. A. Al-Laham, C. Y. Peng, A. Nanayakkara, M. Challacombe, P. M. W. Gill, B. Johnson, W. Chen, M. W. Wong, J. L. Andres, C. Gonzalez, M. Head-Gordon, E. S. Replogle, and J. A. Pople. Gaussian 98, Revision A.11.1, Gaussian, Inc., Pittsburgh, PA, **2001**.
- [30] M. J. Frisch and G. W. Trucks and H. B. Schlegel and G. E. Scuseria and M. A. Robb and J. R. Cheeseman and Montgomery, Jr., J. A. and T. Vreven and K. N. Kudin and J. C. Burant and J. M. Millam and S. S. Iyengar and J. Tomasi and V. Barone and B. Mennucci and M. Cossi and G. Scalmani and N. Rega and G. A. Petersson and H. Nakatsuji and M. Hada and M. Ehara and K. Toyota and R. Fukuda and J. Hasegawa and M. Ishida and T. Nakajima and Y. Honda and O. Kitao and H. Nakai and M. Klene and X. Li and J. E. Knox and H. P. Hratchian and J. B. Cross and V. Bakken and C. Adamo and J. Jaramillo and R. Gomperts and R. E. Stratmann and O. Yazyev and A. J. Austin and R. Cammi and C. Pomelli and J. W. Ochterski and P. Y. Ayala and K. Morokuma and G. A. Voth and P. Salvador and J. J. Dannenberg and V. G. Zakrzewski and S. Dapprich

and A. D. Daniels and M. C. Strain and O. Farkas and D. K. Malick and A. D. Rabuck and K. Raghavachari and J. B. Foresman and J. V. Ortiz and Q. Cui and A. G. Baboul and S. Clifford and J. Cioslowski and B. B. Stefanov and G. Liu and A. Liashenko and P. Piskorz and I. Komaromi and R. L. Martin and D. J. Fox and T. Keith and M. A. Al-Laham and C. Y. Peng and A. Nanayakkara and M. Challacombe and P. M. W. Gill and B. Johnson and W. Chen and M. W. Wong and C. Gonzalez and J. A. Pople. Gaussian 03, Revision B.05, Gaussian, Inc., Pittsburgh, PA, **2003**.

- [31] Benedict, W.S.; Gailar, N.; Plyler, E.K. *Can. J. Phys.*, **1957**, *35*, 1235.
- [32] Marquardt, R; Quack, M.; Thanopoulos, I.; Luckhaus, D. *J. Chem. Phys.*, **2003**, *119*, 10724.
- [33] Lubombo, C.; Curotto, E.; Janeiro-Barral, P.E.; Mella, M. *J. Chem. Phys.*, **2009**, *131*, 034312.
- [34] Kulkarni, S. A.; Pathak, R. K., *Chem. Phys. Lett.*, **2001**, *336*, 278.
- [35] Tharrington, A.N.; Jordan, K.D. *J. Phys. Chem. A*, **2003**, *107*, 7380.
- [36] Benedict, W. S.; Gailar, N.; Plyler, E. K. *Can. J. Phys.*, **1957**, *35*, 1235.
- [37] Zeiss, G. D.; Meath, W. J. *Mol. Phys.*, **1977**, *33*, 1155.

3.5 Appendix 1: Routine calling potential

Routine reading data shown in Appendix 3, and calling the subroutine shown in Appendix 2. While one of the ammonia molecules remains fixed, the second one is displaced 600 steps of 0.05 size each.

```
program pepitas_in_action
implicit none
character at_s(1:8)
real*8 xx(1:8),yy(1:8),zz(1:8),pot
integer i

open(2,file='data.xyz')
do i=1,8
    read(2,*), at_s(i), xx(i), yy(i), zz(i)
enddo
close(2)

call subpepitas (at_s,xx,yy,zz,pot)

write(*,*) 'Potential '
write(*,*) pot

stop
end
```

3.6 Appendix 2: Potential

Subroutine calculating the total sum of the interaction forces.

```

subroutine subpepitass (at_s,xx,yy,zz,pot)
*   // xyz input coordinates must be in Angstrom
*   // they are ordered so that one has the first
*   // ammonia molecule (N,H,H,H)
*   // then followed by the second one (again (N,H,H,H))
*   // pot is output in kcal/mol
implicit none
character at_s(1:8)
real*8 xx(1:8),yy(1:8),zz(1:8),r_nh(1:3),r_hh(1:9),
.      atdist_nn,atdist_n2h(1:3),atdist_n1h(1:3),
.      dist_hh(1:9),
.      qdist_n2h(1:3),qdist_n1h(1:3),qdist_nn,
.      delta,Coulomb_n2h(1:3),seis,ocho,diez,dos,
.      qh,qn,Coulomb_nn,coul,Coulomb_n1h(1:3),
.      Coulomb_hh(1:9),
.      V_nn,V_hh(1:9),V_n1h(1:3),V_n2h(1:3),Vdisp_nn,
.      damp,f,bra,
.      SumaCoulomb_n2h,SumaCoulomb_n1h,SumaCoulomb_hh,
.      SumaV_n1h,
.      SumaV_n2h,SumaV_hh,totalsuma,am1(1:3),
.      am2(1:3),am3(1:3),
.      vecq1x,vecq1y,vecq1z,modvecq1,vecn1x,
.      vecn1y,vecn1z,am4(1:3),am5(1:3),am6(1:3),

```

```
.      vecq2x , vecq2y , vecq2z , modvecq2 , vecn2x , vecn2y ,
.      vecn2z , pot
```

```
integer g,h,i,j,l,m,n,p,q,u,w
```

```
parameter (coul=1.11265d-10*1d-10)!J^-1*C^2*angstroms^-1
```

```
parameter (qh=0.462*(1.602d-19)) !C
```

```
parameter (qn=-3*0.462*(1.602d-19))!C
```

```
parameter (delta=0.156d0) !angstroms
```

```
parameter (damp=4.7d0) !angstrom
```

C VECTOR TO DEFINE CHARGE DISPLACEMENT OF N1

```
g=0
```

```
do i=2,4
```

```
  g=g+1
```

```
  am1(g)=(xx(i)-xx(1))
```

```
  am2(g)=(yy(i)-yy(1))
```

```
  am3(g)=(zz(i)-zz(1))
```

```
enddo
```

```

vecq1x=am1(3)+am1(2)+am1(1)
vecq1y=am2(3)+am2(2)+am2(1)
vecq1z=am3(3)+am3(2)+am3(1)

modvecq1=sqrt((vecq1x**2)+(vecq1y**2)+(vecq1z**2))

vecn1x=((vecq1x/modvecq1)*delta)+xx(1)
vecn1y=((vecq1y/modvecq1)*delta)+yy(1)
vecn1z=((vecq1z/modvecq1)*delta)+zz(1)

```

C VECTOR TO DEFINE CHARGE DISPLACEMENT OF N2

```

h=0

do i=6,8
  h=h+1
  am4(h)=(xx(i)-xx(5))
  am5(h)=(yy(i)-yy(5))
  am6(h)=(zz(i)-zz(5))
enddo

vecq2x=am4(3)+am4(2)+am4(1)
vecq2y=am5(3)+am5(2)+am5(1)
vecq2z=am6(3)+am6(2)+am6(1)

modvecq2=sqrt((vecq2x**2)+(vecq2y**2)+(vecq2z**2))

```

```
vecn2x=((vecq2x/modvecq2)*delta)+xx(5)
```

```
vecn2y=((vecq2y/modvecq2)*delta)+yy(5)
```

```
vecn2z=((vecq2z/modvecq2)*delta)+zz(5)
```

C CALCULATE N-N DISTANCE

```
dos=((((xx(5)-xx(1))**2)+((yy(5)-yy(1))**2)
```

```
.      +((zz(5)-zz(1))**2))
```

```
atdist_nn=sqrt(dos)
```

```
qdist_nn=sqrt(((vecn2x-vecn1x)**2)
```

```
.      +((vecn2y-vecn1y)**2)
```

```
.      +((vecn2z-vecn1z)**2))
```

C CALCULATE N-N COULOMB POTENTIAL (J)

```
Coulomb_nn=qn**2/(coul*(qdist_nn))
```

C CALCULATE N-N POTENTIAL (kcal/mol, angstroms)

```
V_nn=13615.d0*exp(-2.7d0*atdist_nn)
```

C CALCULATE N-N DISPERSION

C POWERS OF R

```
seis=(dos)*(dos)*(dos)
```

```
ocho=(seis)*(dos)
```

```
diez=(ocho)*(dos)
```

C BRACKET DIVISIONS

```
bra=(1230.d0/seis+6500.d0/ocho+42100.d0/diez)
```

C CHOICE OF F(R) DEPENDING ON N-N DISTANCE RESPECT TO

C DAMPING DISTANCE

f=1

if (atdist_nn.lt.damp) then

f=exp(-(((atdist_nn-damp)/atdist_nn)**2))

endif

C EXPRESSION FOR DISPERSION (in kcal/mol)

Vdisp_nn=-f*bra

C N2 TO H's FROM MOLECULE1: DISTANCE, COULOMB

C AND H-H POTENTIALS, SUM

n=0

do i=2,4

n=n+1

atdist_n2h(n)=sqrt(((xx(5)-xx(i))**2)

+((yy(5)-yy(i))**2)

+((zz(5)-zz(i))**2))

qdist_n2h(n)=sqrt(((vecn2x-xx(i))**2)

+((vecn2y-yy(i))**2)

+((vecn2z-zz(i))**2))

enddo

q=0

SumaCoulomb_n2h=0


```

SumaV_n2h=0
do n=1,3
  q=q+1
  Coulomb_n2h(q)=qn*qh/(coul*((qdist_n2h(n))))!joule
  SumaCoulomb_n2h=SumaCoulomb_n2h
  +Coulomb_n2h(q)
  V_n2h(q)=0.4d0*exp(-4.6d0*(atdist_n2h(n)-2.5d0))
  -0.8d0*exp(-2.3d0*(atdist_n2h(n)-2.5d0))
  SumaV_n2h=SumaV_n2h+V_n2h(q)          !in kcal/mol
enddo

```

C N1 TO H's FROM MOLECULE2: DISTANCE, COULOMB
 C AND H-H POTENTIALS, SUM

```

m=0

do i=6,8
  m=m+1
  atdist_n1h(m)=sqrt(((xx(1)-xx(i))**2)
  +((yy(1)-yy(i))**2)
  +((zz(1)-zz(i))**2))
  qdist_n1h(m)=sqrt(((vecn1x-xx(i))**2)
  +((vecn1y-yy(i))**2)
  +((vecn1z-zz(i))**2))
enddo

```

```
w=0
SumaCoulomb_n1h=0
SumaV_n1h=0
do m=1,3
  w=w+1
  Coulomb_n1h(w)=qn*qh/(coul*(qdist_n1h(m))) !joule
  SumaCoulomb_n1h=SumaCoulomb_n1h+Coulomb_n1h(w)
  V_n1h(w)=0.4d0*exp(-4.6d0*(atdist_n1h(m)-2.5d0))
             -0.8d0*exp(-2.3d0*(atdist_n1h(m)-2.5d0))
  SumaV_n1h=SumaV_n1h+V_n1h(w) !in kcal/mol
enddo
```

C H-H: DISTANCE, COULOMB AND H-H POTENTIALS, SUM

```
l=0
do i=2,4
  do j=6,8
    l=l+1
    dist_hh(l)=sqrt(((xx(j)-xx(i))**2)
                    +((yy(j)-yy(i))**2)
                    +((zz(j)-zz(i))**2))
  enddo
enddo

u=0
```

```
SumaCoulomb_hh=0
SumaV_hh=0
do l=1,9
  u=u+1
  Coulomb_hh(u)=qh**2/(coul*(dist_hh(l)))
  SumaCoulomb_hh=SumaCoulomb_hh+ Coulomb_hh(u)!joule
  V_hh(u)=700d0*exp(-3.7d0*dist_hh(l))
  SumaV_hh=SumaV_hh+V_hh(u)  !in kcal/mol
enddo

pot=V_nn+Vdisp_nn
.      +(SumaCoulomb_n2h
.      +SumaCoulomb_hh
.      +SumaCoulomb_n1h)*6.0225d20*4.186d0
.      +SumaV_n2h
.      +SumaV_n1h
.      +SumaV_hh

return
end
```

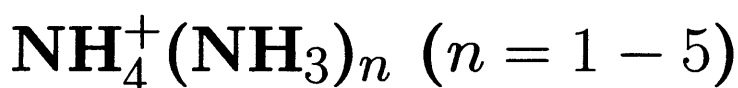
3.7 Appendix 3: Data file

Example of data file read by routine in Appendix 1.

```
N  0.  0.  0.114454
H  0.  0.93744 -0.26706
H  0.811846 -0.46872 -0.26706
H -0.811846 -0.46872 -0.26706
N  0.  0.  3.364454
H  0.  0.93744  2.98294
H  0.811846 -0.46872  2.98294
H -0.811846 -0.46872  2.98294
```

Chapter 4

Protonated ammonia clusters:



4.1 Introduction

Studying protonated ammonia clusters can be approached from different perspectives. On one hand, they are representatives of “ion-solvent” type of interaction, which is relevant to the understanding of atmospherical reactions, nucleation processes and solvation chemistry [1–3, 29]. On the other hand, these clusters are molecular aggregates with an extra proton susceptible of mobility along the cluster’s hydrogen bond network. Ammonia proton wires are thus relevant in organic chemistry, biology and have also been investigated theoretically [4–9].

There are a number of papers investigating the electronic energies of $\text{NH}_4^+(\text{NH}_3)_n$ clusters [10–15], but we feel that an *ab initio* benchmark data for protonated ammonia clusters are still missing. This is because some of the reported data has been superseded, and in those cases where a post Hartree-Fock method is used, it is matched with a Pople’s family basis set. In contrast, this work uses Dunning’s family basis sets. Re-

cently, Fouqueau and Meuwly [15] investigated the energetics, structures and dynamics of protonated ammonia clusters using DFT and semiempirical DFT methods. These are known to underestimate dispersion interactions [15] and, occasionally, to overestimate multipole moments. Although dispersion is not a dominant contribution to the stability of charged systems, we feel that at least MP2 level of theory is needed because, based in our experience with ammonia clusters, is well within computational reach at least for small clusters ($n \leq 5$), and would provide a more accurate description of the clusters at hand. In addition, the basis sets used in reference [15] for exploring the clusters were 6-31+G** and 6-31G** for which a substantial BSSE would be expected; however, no correction procedure was used.

Since the first detection of protonated ammonia clusters ($\text{NH}_4^+(\text{NH}_3)_n$, ($n > 4$)) in the gas phase by Dawson and Ticker in 1964 [16], a number of experimental studies on the ammoniation of NH_4^+ have been published [22–32]. As far as we know, the different methods used to experimentally investigate the thermodynamics of the ion-solvent molecule interactions in the reaction:



have been, namely, mass spectrometry [22–28], flowing afterglow technique [29, 30] and photoionisation [31, 32]. The results provided by mass spectrometry and flowing afterglow are in good accordance, albeit disagreeing in the value of the energy for NH_4^+NH_3 . On the other hand, the photoionisation experiments substantially underestimate the absolute values of solvation energies. The reason for this could be due to the fact that the appearance potential ¹ of ammonium solvation is determined from vibrationally

¹“Appearance Energy (appearance potential), refers to ionisation of a molecule or atom by electron collision or photon absorption. In mass spectrometry it has often been reported as the voltage which corresponds to the minimum energy of the electrons in the ionising beam necessary for the production of a given fragment ion. In photoionisation it is the minimum energy of the quantum of light which produces ionisation of the absorbing molecule” [36]

excited parent clusters generated from neutral ammonia; which could lead to a threshold potential corresponding to an upper vibrational ionic state and not to the ground state of the ion, thus leading to lower absolute values of the solvation energy [31].

It is possible to draw common trends in the published experimental data. First, attending to the enthalpy values one can see a monotonic decrease from $\Delta H_{1,2}$ to $\Delta H_{2,3}$ and $\Delta H_{3,4}$. Second, as mentioned, the $\Delta H_{0,1}$ is much higher than the consecutive solvation steps, and this value is also the major source of disagreement (up to 7.7 kcal/mol) between the different measurements using mass spectrometric methods. To compare energetic mass spectrometric and flow afterglow data one has to look at the measurement of free energy, (i.e. $\Delta G_{0,1}$) where also differences can be encountered, again ≈ 7 kcal/mol. It has been pointed out that this may be due to the dimerisation reaction being too quick and exothermic for the gas bath molecules to stabilise it [31]. It was also proposed that the high enthalpy formation for NH_4^+NH_3 dimer, compared to larger clusters, was due to the proton being equally shared by the two ammonias (N_2H_7^+ species). However, one has to note that these experiments hold no information on the structures of the clusters [28]. Finally, there is a sudden decrease in $\Delta H_{4,5}$ which is invariably attributed to the completion of the first solvation shell of the ammonium ion. In this regard, Meot-ner and Speller [28] went further and attempted to establish a general quantitative thermochemical criteria for the filling of a solvent shell. Also, in this work, it was proposed that in systems such as $\text{H}_3\text{O}^+(\text{H}_2\text{O})_n$ and $\text{NH}_4^+(\text{NH}_3)_n$, in which the formation of outer solvation shells is not sterically blocked, second and higher shells could be formed before the first one is completed; also, that a completed first solvation shell could coexist in equilibrium with isomers with partially completed inner and outer shells. In fact, *ab initio* investigations from our work and references [15] and [14] have invariably found several different isomers for a given cluster size matching this criteria.

We can advance that protonated ammonia clusters arrange themselves in two general configurations, namely, “globular” and “linear”. In the former, the NH_4^+ cation is placed at the core of the structure and surrounded by the solvating ammonia molecules. In the latter, the monomers arrange themselves in a linear chain, the cation always being placed in the inner positions of the chain.

The work from references [14, 15, 18–21, 34, 35] is concerned with the investigation of the structure of protonated ammonia clusters. They explored the infrared spectra of a varied range of frequencies, attempting to correlate spectral features with structural characteristics of the clusters.

Experimentally, different approaches to infrared spectroscopy were used; namely, radiolysis [18], vibrational predissociation [19, 34] and photodissociation [21, 35]. Theoretically, *ab initio* [14, 19, 20], DFT [14, 21] and molecular dynamic simulations [15] are the methods chosen to estimate the vibrational modes and infrared spectra of several protonated ammonia clusters.

There is qualitative agreement in the IR spectra data between theory and experiments. Two main spectral features are found, those related to the vibrations of the ammonium cation and those related to the solvating ammonia molecules [34]. There is also consensus on the tetrahedral arrangement of the $\text{NH}_4^+(\text{NH}_3)_4$. Quantitatively, the calculated harmonic vibrations are consistently higher than the experimental values, this work being no exception.

This chapter presents the MP2 study of the structure, intermolecular binding energies and harmonic frequencies of $\text{NH}_4^+(\text{NH}_3)_n$ ($n = 1 - 5$).

4.2 Methodology

The computational procedure is similar to that previously followed in the study of ammonia clusters. The electronic structure calculations on $\text{NH}_4^+(\text{NH}_3)_n$ ($n = 1-5$) were performed using the Gaussian 98 [41] and 03 [42] *ab initio* packages using the Hartree-Fock (HF) and second-order Møller-Plesset perturbation theory (MP2) with frozen core, employing Dunning's family basis sets aug-cc-pVXZ ($X=D,T$). Counterpoise (CP) Basis Set Superposition Error (BSSE) has been accounted for by means of a vertical correction on the optimised isomeric structures, and as further relaxation on the CP-corrected Potential Energy Surface (PES). All the images in this work and all inter and intramolecular parameters have been obtained with MOLEKEL [43].

To name the isomers, we adopted the very convenient nomenclature used by Fouqueau and Meuwly [15]. By means of this notation, the connectivity of a cluster is described by a four digit label ($n_1n_2n_3n_4$), each digit referring to one of the four hydrogen atoms from the ammonium cation and their level of complexation by solvating ammonia molecules. Thus, three hydrogen atoms from NH_4^+ being solvated by one ammonia molecule each, will be nominated as isomer 1110; and three ammonia molecules solvating two hydrogen atoms from NH_4^+ will give rise to isomer 2100.

4.3 Results

4.3.1 Structural Results and Binding Energies

$\text{NH}_4^+(\text{NH}_3)$

For the ammonium-ammonia dimer we have obtained two isomers presented in Figure 4.1. The structural difference between them lies in the relative position of the ammonia molecule, being eclipsed or staggered with respect to NH_4^+ . Both species are practically

isoenergetic, the sign and magnitude of their energy difference depending on the level of the calculations, being ≈ 0.03 kcal/mol at the MP2/aug-cc-pVTZ level of theory, in which the structures have been optimised on the CP-corrected PES.

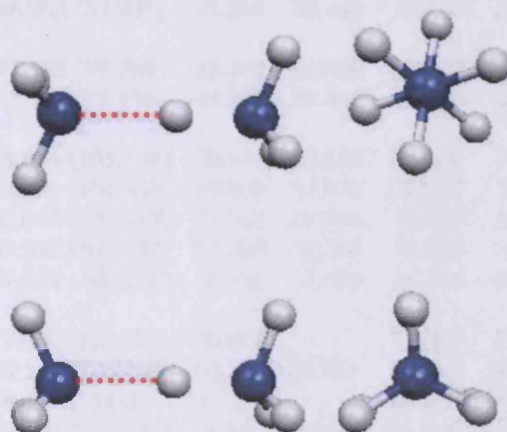


Figure 4.1: Isomer 1000 stag (top) 1000 ecli (bottom)

Table 4.1: Binding Energies for the clusters $\text{NH}_4^+(\text{NH}_3)_n$ $n = 2 - 5$ in kcal/mol.

isomer	aug-cc-pVDZ			aug-cc-pVTZ		
$\text{NH}_4^+(\text{NH}_3)$	BE ^a	BE ^{CPb}	Opt ^{CPc}	BE	BE ^{CP}	Opt ^{CP}
1000 ecli	26.974 (54.335)	25.188	25.216	26.687	25.983	25.996
1000 stag	26.953 (54.231)	25.213	25.243	26.715	26.010	26.023
$\text{NH}_4^+(\text{NH}_3)_2$						
1100 ecli	47.122 (78.208)	42.742	42.808 [†]	46.410 [†]	44.524 [†]	44.535 [†]
1100 stag	47.116 (78.198)	44.007	44.047	46.409	45.275	45.284
$\text{NH}_4^+(\text{NH}_3)_3$						
1110 ecli	63.678 (101.586)	58.879	57.972	62.194*	59.835	60.097
1110 stag	63.678 (101.545)	57.909	57.971	62.215*	59.856	-
2100 ecli	57.077 (101.137)	52.242	52.315	56.902	54.466	54.488
2100 stag	57.966 (101.132)	52.220	52.316	56.882	54.448	54.472
2100 ecliecli	57.986 (101.166)	52.231	52.306	56.884	54.450	-
$\text{NH}_4^+(\text{NH}_3)_3$						
1111	77.666 (124.753)	70.514	-	75.567*	72.746	-
2110	73.247 (124.687)	66.185	66.277	71.287*	68.466	-
2200	68.114 (124.305)	61.277	-	66.276*	63.522	63.862
3100	65.860 (124.132)	58.833	58.943	64.036*	61.156	-
3100ring	66.659 (125.004)	59.106	-	64.591*	61.567	-
$\text{NH}_4^+(\text{NH}_3)_4$						
2111ring	86.635 (148.281)	77.811	-	83.919*	80.487	-
2111	86.151 (147.831)	77.766	-	83.531*	80.284	-
2210	82.286 (147.827)	74.130	-	79.841*	76.665	-
3110	80.589 (147.763)	72.315	-	78.166*	74.905	-
3200	76.664 (147.389)	67.581	-	73.361*	70.149	-
4100	72.442 (147.119)	64.194	-	70.167*	66.836	-

^a binding energy, in brackets zero point harmonic corrections at the MP2/aug-cc-pVDZ level of theory ^b single point BSSE Counterpoise corrected binding energy, ^c optimised BSSE Counterpoise corrected binding energy, * single point calculations using the geometry of MP2/aug-cc-pVDZ optimisation. - unavailable values [†]isomerisation to 1100 stag

$\text{NH}_4^+(\text{NH}_3)_2$

We initially obtained two isomers, shown in Figure 4.2, the difference between them being the staggered or eclipsed orientation of one of the two ammonia molecules with respect to the ammonium ion, as before. However, the outcome of the CP corrected optimisation at the MP2/aug-cc-pVDZ level of theory (indicated in table 4.1 as [†]) resulted in the isomerisation of 1100 eclipsed into 1100 staggered.

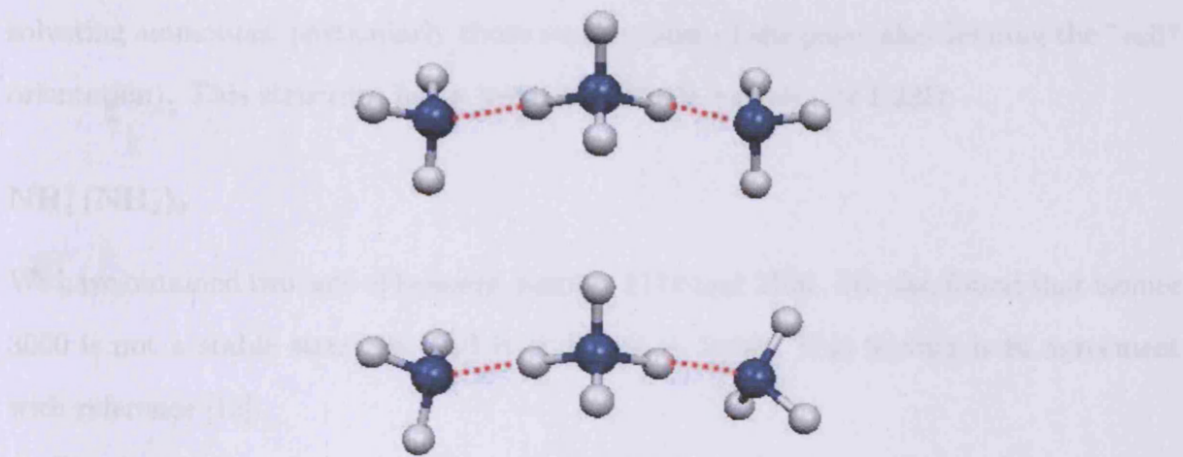


Figure 4.2: Isomer 1100 stag (top) and 1100 ecli (bottom)

The relative energy difference between the two 1100 staggered configurations taken at the CP-corrected optimisation MP2/aug-cc-pVTZ level is 0.75 kcal/mol, which is quite significant. To try and find a reason for this we had a closer look to the structural arrangement of both clusters. We found that the intermolecular and intramolecular angles, as well as N-H distances in the ammonia molecules and the non-donating hydrogens of the ammonium show no significant deviation from each other. However, we noticed slight differences in the measurements of two geometrical parameters, namely, the N-H distance of the donating hydrogens in the NH_4^+ , and hence in the N-H...N distance; and in the dihedral angle formed between the donating hydrogens from NH_4^+ and the eclipsed and the staggered hydrogens of the NH_3 molecules. The isomer first isolated as staggered (i.e. the most stable one at the highest level of theory) shows a distance of 1.066 Å for both of the solvating N-H bonds of the ammonium cation, N-H...N distances are 1.671 Å and the dihedral angle measured for the aforementioned hydrogen arrangement is 0°. In addition, it has a dipole moment of 1.66 D. In contrast, the isomer that was originally eclipsed shows more imbalanced measurements to both sides of the cation, the hydrogen atoms are off plane by -2.5° (plane defined by the bonding hydrogen atoms of the cation and one hydrogen atom of each of the

solvating ammonias, particularly those on the plane of the page, also defining the "ecli" orientation). This structure has a predicted dipole moment of 1.22D.

$\text{NH}_4^+(\text{NH}_3)_3$

We have obtained two sets of isomers, namely 1110 and 2100. We also found that isomer 3000 is not a stable structure and it collapses to 2100. This finding is in agreement with reference [15].

For the 1110 arrangement (Figure 4.3) all NH_3 molecules are in the first solvation shell. Within this arrangement two different isomers arise, staggered and eclipsed, attending to the orientation of one of the solvating molecules with respect to the cation.

Isomer 2100 (Figure 4.4) is the smallest arrangement in which an NH_3 occupies the second solvation shell of the ammonium cation. From the 2100 arrangement we isolated three isomers, 2100 stag, 2100 ecli, and 2100 ecliecli.

One can think about the first two structures as originated from 1100 stag, seen in the previous subsection, with an additional NH_3 placed in the second solvation shell. The orientation of this incoming ammonia with respect to the cation determines if 2100 is stag or ecli. The third isomer, 2100 ecliecli, shows an eclipsed ammonia with respect to NH_4^+ in the second solvation shell, and in the first solvation shell (on the right hand side in the third isomer of figure 4.4). The NH_3 that acts as a "linker" is always staggered with respect to the ammonium cation.

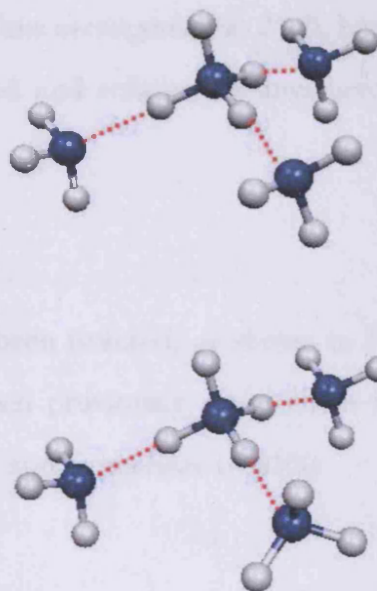


Figure 4.3: Isomer 1110 stag (top) and 1110 ecli (bottom)

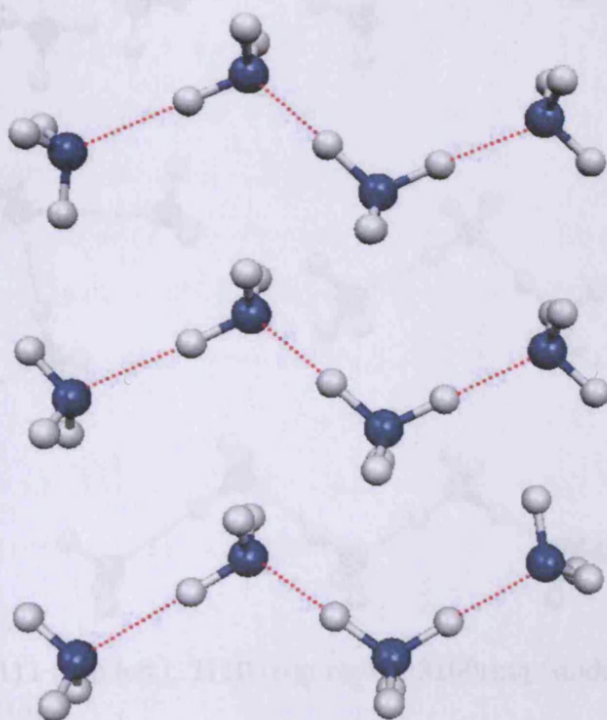


Figure 4.4: Isomer 2100 stag (top), 2100 ecli (middle) and 2100 eclicli (bottom).

We found that all levels of theory support the more compact arrangements, 1110, as

a global minima. The chain-like arrangements, 2100, lying roughly 5.6 kcal/mol above. For a given isomer, staggered and eclipsed arrangements are shown to be practically degenerate in Table 4.1.

$\text{NH}_4^+(\text{NH}_3)_4$

Five different isomers have been isolated, as shown in Figure 4.5. As far as we know, Isomer 3100ring has not been previously reported in literature, also we found that structure 4000 is not stable, and isomerises to 3100.

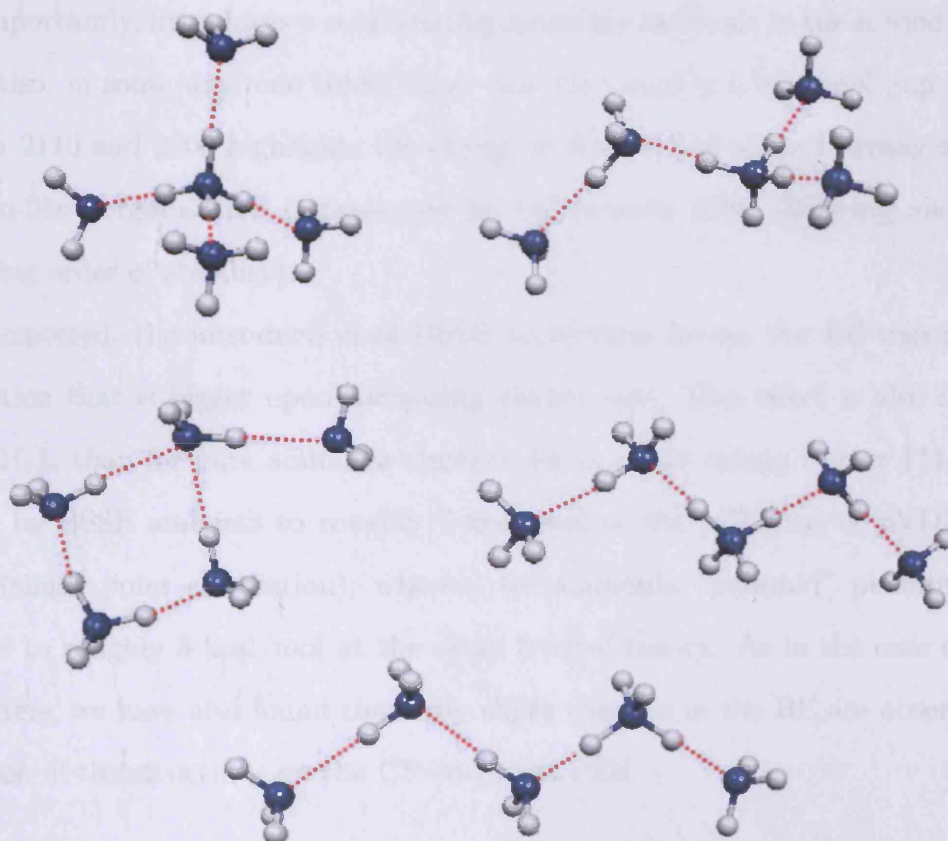


Figure 4.5: Isomer 1111 (top left), 2110 (top right), 3100ring (middle left), 2200 (middle right) and 3100 (bottom).

At the highest level of theory in this work, isomer 1111, which has all ammonium hydrogens coordinated to ammonia molecules, is the most stable species, followed by

isomer 2110 (roughly 4.3 kcal/mol above). In order of decreasing stability we found next 2200 (≈ 5 kcal/mol) higher than 2110, 3110ring (≈ 2 kcal/mol) higher than 2200, and finally 3110 (≈ 0.5 kcal/mol).

In isomer 1111, the first solvation shell of the ammonium molecule is completed by the coordination of the four available hydrogen atoms in the cation with ammonia molecules. This isomer also represents the most discernible “globular arrangement”, as dubbed in reference [15], a description that also applies to 2110. The main structural difference between them is that the latter breaks the symmetry of the 1111 isomer, but more importantly, introduces a coordinating ammonia molecule in the second solvation shell. Also, in some way, one could think that the roughly 5 kcal/mol gap in energy between 2110 and 2200 highlights the deviation from a ball-shaped arrangement into a “chain-like” organisation (represented by the isomers 2200, 3100ring and 3100 in decreasing order of stability).

As expected, the introduction of BSSE corrections lowers the BE energy values, a reduction that is bigger upon increasing cluster size. This effect is also higher for $\text{NH}_4^+(\text{NH}_3)_n$ than for pure ammonia clusters, for example taking isomer 1111 (a pentamer), its BSSE amounts to roughly 7 kcal/mol at the MP2/aug-cc-pVDZ level of theory (single point calculation), whereas for ammonia “pyramid” pentamer BSSE amounts to roughly 5 kcal/mol at the same level of theory. As in the case of ammonia clusters, we have also found that only slight changes in the BE are observed after relaxation of the structures on the CP-corrected PES.

$\text{NH}_4^+(\text{NH}_3)_5$

Six isomers have been isolated for this cluster size and are presented in Figure 4.6. To our knowledge, two of these isomers are novel structures (2111ring and 4100).

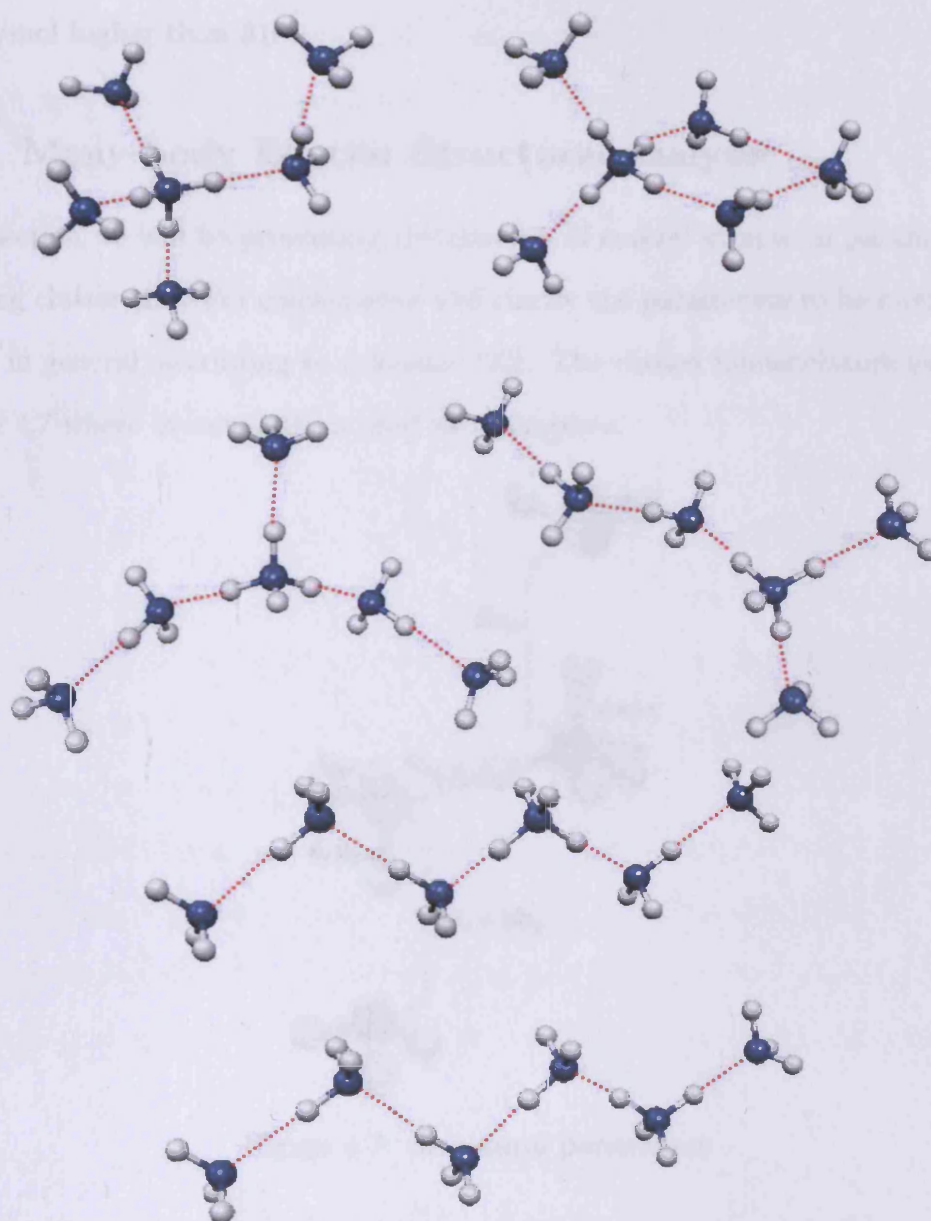


Figure 4.6: Isomer 2111 (top left), 2111ring (top right), 2210 (second row left), 3110 (second row right), 3200 (third row), 4100 (bottom)

Isomers 2111 are the most stable species, followed by 2210 which are lying roughly 3.5 kcal/mol above. As seen before, globular arrangements, i.e. clusters in which the hydrogen atoms of the ammonium cation are bonding one ammonia molecule each, have higher binding energies than chain-like isomers. Accordingly, 3200 lies roughly

4.9 kcal/mol higher than 3100.

4.3.2 Many-body Effects: Structural analysis

In this section we will be presenting the changes of several structural parameters with increasing cluster size. For convenience and clarity the parameters to be monitored are defined, in general, according to reference [20]. The chosen nomenclature can be seen in figure 4.7 where isomer 2100 is used as a template.

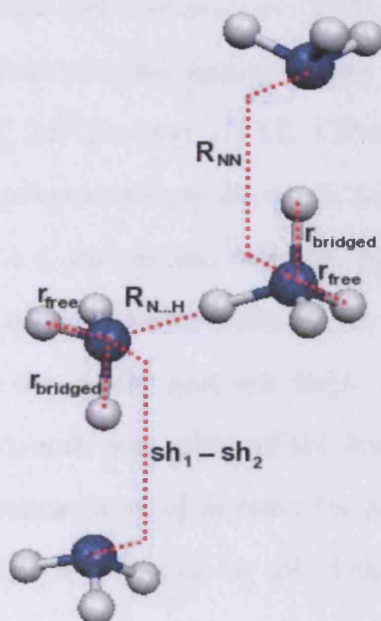


Figure 4.7: Structural parameters

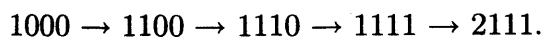
In figure 4.7 R_{NN} is the distance between two Nitrogen atoms, specifically from the nitrogen atom in NH_4^+ to the nitrogen atom in a first shell solvating NH_3 . When R_{NN} is measured between the Nitrogen atoms of ammonia molecules, this parameter is considered to be the distance between two solvation shells, namely $\text{sh}_1\text{--sh}_2$. $R_{N\cdots H}$ is the hydrogen bond distance, measured for every hydrogen bonding atom. r_{bridged} is the N–H bond distance that is part of the cluster bonding pattern, a parameter measured for both NH_4^+ and NH_3 . r_{free} is the N–H bond distance that is not part of the cluster

hydrogen bonding pattern, and as before, is measured both for NH_4^+ and NH_3 .

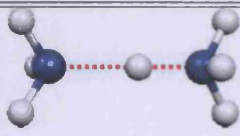
Before describing the structural features of our clusters as mentioned, we are going to look at how some of the geometrical data compares across the different levels of optimisation. This is a step we think useful because we found that upon increasing cluster size our computational resources were challenged, and as a result, the optimisation of the aggregates could not be carried out in identical fashion for all cluster sizes. To analyse if there are any significant changes in the structures across the level of optimisation we have chosen to explore three different species (1000 stag, 1100 stag, 2100 ecli) for which we have available all four possible optimisations (i.e. MP2/aug-cc-pVDZ, CP-corrected MP2/aug-cc-pVDZ, MP2/aug-cc-pVTZ, CP-corrected MP2/aug-cc-pVTZ). The results of the measured parameters are shown in tables 4.2, 4.3 and 4.4.

From tables 4.2, 4.3 and 4.4, we can see that the parameters of interest fluctuate depending on the basis set used and the inclusion or absence of BSSE correction. However, the differences are consistent and not large, allowing us to think that we could extract robust general trends regardless of the level of optimisation. Hence, we have chosen to describe the parameters of interest for all structures at the MP2/aug-cc-pVDZ level of theory, which is available for all of the structures presented in this work.

In addition, in order to draw clearer trends, we have found it useful to group the structures we isolated in “families”, attending to a possible rationale for cluster formation. In our opinion, the most immediate approach to the formation of protonated ammonia clusters is the stepwise addition of free ammonia molecules to each of the four hydrogens of an ammonium core, until it is saturated. Thus, we have the sequence:



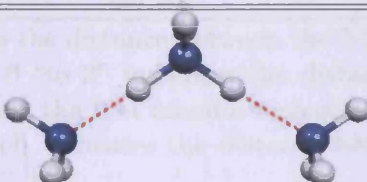
We also notice that three is the minimum number of NH_3 that can be distributed around the ammonium cation before different structural isomers can be obtained; by

Table 4.2: Inter and intramolecular lengths (Å) for optimised protonated ammonia cluster 1000 stag^a


$\text{NH}_4^+(\text{NH}_3)_3$ Isomer 1000 stag				
Level of Theory	R_{NN}^b	r_{free}^c	$r_{bridged}^d$	$R_{N...H}^e$
MP2/aug-cc-pVDZ	2.716	1.024	1.116	1.600
CP-MP2/aug-cc-pVDZ	2.743	1.024	1.108	1.635
MP2/aug-cc-pVTZ	2.697	1.018	1.118	1.579
CP-MP2/aug-cc-pVTZ	2.743	1.024	1.107	1.638

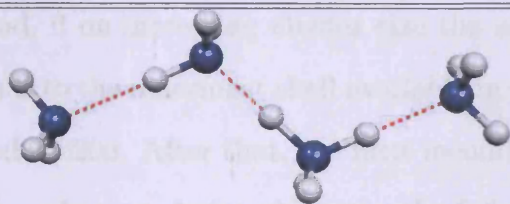
^a optimised geometric parameters obtained at the MP2/aug-cc-pVXZ $X=D,T$ level of theory, CP-MP2 indicates Counterpoise corrected optimisation. ^b R_{NN} , distance between the nitrogen atoms from NH_4^+ and complexing NH_3 molecule. ^c r_{free} , NH_4^+ N-H bond length not included in hydrogen bonding pattern with NH_3 . ^d $r_{bridged}$, NH_4^+ N-H bond length coordinating NH_3 through hydrogen bond. ^e $r_{N...H}$, hydrogen bond distance.

Table 4.3: Inter and intramolecular lengths (Å) for optimised protonated ammonia cluster 1100 stag



$\text{NH}_4^+(\text{NH}_3)_3$ Isomer 1100 stag				
Level of Theory	R_{NN}	r_{free}	$r_{bridged}$	$R_{N...H}$
MP2/aug-cc-pVDZ	2.828	1.023	1.070	1.759
CP-MP2/aug-cc-pVDZ	2.853	1.023	1.068	1.785
MP2/aug-cc-pVTZ	2.816	1.017	1.066	1.750
CP-MP2/aug-cc-pVTZ	2.827	1.017	1.066	1.761

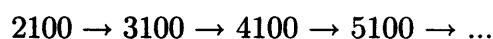
Table 4.4: Inter and intramolecular lengths (Å) for optimised protonated ammonia cluster 2100 ecli



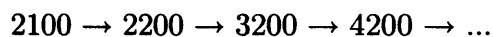
$\text{NH}_4^+(\text{NH}_3)_3$ Isomer 2100 ecli				
Level of Theory	R_{NN}	r_{free}	$r_{bridged}$	$R_{N...H}$
MP2/aug-cc-pVDZ	2.863 (to 1) ^f	1.022	1.062	1.801
	2.744 (to 2) ^g	1.022	1.097	1.647
	$\text{sh}_1\text{-sh}_2^h$	3.087	1.022	1.036
CP-MP2/aug-cc-pVDZ	2.863 (to 1)	1.023	1.069	1.739
	2.775 (to 2)	1.023	1.090	1.685
	$\text{sh}_1\text{-sh}_2$	3.134	1.023	1.035
MP2/aug-cc-pVTZ	2.852 (to 1)	1.016	1.057	1.795
	2.727 (to 2)	1.016	1.096	1.630
	$\text{sh}_1\text{-sh}_2$	3.065	1.015	1.020
CP-MP2/aug-cc-pVTZ	2.850 (to 1)	1.016	1.060	1.790
	2.746 (to 2)	1.016	1.090	1.656
	$\text{sh}_1\text{-sh}_2$	3.088	1.015	1.029

^f “to 1” indicates the distance between the NH_4^+ nitrogen atom and the nitrogen atom from the single NH_3 . ^g “to 2” indicates the distance between the NH_4^+ nitrogen atom and the nitrogen atom from the first ammonia molecule of the solvating two membered chain. ^h “ $\text{sh}_1\text{-sh}_2$ ”, “sh” for shell, indicates the distance between the nitrogen atoms of the solvating two membered chain.

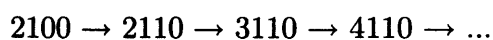
this meaning “globular”- or “linear”-like arrangements (i.e. taking $\text{NH}_4^+(\text{NH}_3)_3$ we obtain 1110 and 2100). So, the structure of isomer 2100 allows us to use it as a root for growing clusters featuring alternative spatial arrangements. In doing this, three different “building” approaches can be considered. First, if on increasing cluster size, one chooses to expand the second solvation shell, then third and so on, the following sequence will be obtained:



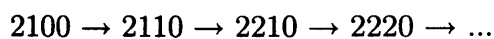
Second, if on increasing cluster size the additional ammonia molecule is placed so that bonds to the innermost shell available in the 2100 isomer, the immediate structure generated is 2200. After that, the next incoming NH_3 molecules will be used to expand one of the solvation chains obtaining the following sequence:



The third one involves adding an ammonia molecule to one of the two remaining free hydrogen atoms of the cation core, generating 2110. After this, one can either follow the first “building” procedure explained above (increasing the length of the longest ammonia chain), obtaining:



or, one can choose to increase the length of the smallest solvating chain in sequence, obtaining:



Following this rationale, we have grouped all of the isomers we have isolated in five different families and we have tried to draw trends attending to the changes in the geometrical parameters defined in figure 4.7.

Cluster family 1000 \rightarrow 1100 \rightarrow 1110 \rightarrow 1111 \rightarrow 2111

As far as we know, this is the only cluster series for which literature data are available for comparison [11, 12, 20] with the whole family. The geometrical parameters obtained in this work, as well as the trends we see in our data, are in good agreement with previously published results.

As it can be seen in table 4.5, R_{NN} , the distance between the nitrogen atom of the core cation and the nitrogen atom of the coordinating ammonia molecule(s) increases upon increasing cluster size. This is also true for $R_{N...H}$, namely the hydrogen bond distance, measured between the coordinating hydrogen from the core cation and the nitrogen or the accepting ammonia molecule. The increase is of the same magnitude for both parameters and decreases monotonically upon increasing cluster size. This trend is seen until the saturation of the first solvation shell. However, when a second solvation shell is created (isomer 2111), R_{NN} and $R_{N...H}$ to the three single coordinating NH_3 are longer (2.982 Å, 1.941 Å) than when measured to the ammonia that binds to the small two membered chain (2.890 Å, 1.836 Å).

Looking at the small two membered ammonia chain from isomer 2111, in particular at the “sh₁-sh₂” distance, which represents the separation between two ammonia nitrogen atoms coordinated in consecutive solvation shells, one can see that sh₁-sh₂ has an estimated value of 3.164 Å which is longer than the distance between the nitrogen atom in NH_4^+ and the first ammonia molecule of the two membered chain. In other words, this trend could suggest that the separation of the second solvation shell with respect to the first one is longer (3.164 Å) than that of the first solvation shell to the core (2.982 or 2.890 Å). This, together with the fact that upon increasing cluster size the average binding energy decreases, could support the idea of a preferential elimination of the ammonia molecule located in the second solvation shell during an evaporation

cluster break up for the 2111 isomer.

In this work we have measured the N–H distance of an ammonium cation at the MP2/aug-cc-pVDZ level of theory to be 1.027 Å. When coordinating to one NH_3 the N–H length (r_{bridged}) changes to 1.116 Å. After this first elongation, the NH_4^+ complexing N–H bond (r_{bridged}) reduces its length upon increasing solvation. The shortening is maximum for the cluster series when going from 1000 stag (1.112 Å) to 1100 ecli (1.066 Å). On the other hand, r_{free} , remains practically unchanged throughout. In isomer 2111, the N–H bond directed to the three single NH_3 molecules, r_{bridged} , is decreased slightly (1.042 Å) with respect to that of 1111 (1.044 Å). Contrarily, r_{bridged} , linked to the second solvation shell (“to 2” in table 4.5) is longer (1.054 Å) than that directed to the free ammonia molecules (1.042 Å). Actually, as it will be seen later for isomers of the same size (e.g. 2200-3100), the longer the solvating “chain” of ammonia molecules the greater the elongation of the ammonium N–H bond, r_{bridged} .

Cluster family 2100 → 3100 → 4100

Isomer 3100ring will not be included in the following comments on the general trends as it is structurally quite different from the other members of this group and will be dealt with separately.

In table 4.6, we can see that the distance between ammonium and the single ammonia nitrogen atoms increases upon increasing cluster size. So basically, for single solvating ammonia (“to 1” in table 4.6) same trends as before apply for R_{NN} and $R_{N...H}$. Equally, this decrease (referred to the fact that R_{NN} is shorter for a chain than for single NH_3) in R_{NN} and $R_{N...H}$ is also seen for the sequence “to 2”, “to 3”, “to 4”, that indicates the distance between the core cation and the NH_3 that acts like a link for longer solvation chains. As a natural consequence, r_{bridged} increases with cluster size.

Table 4.5: Intermolecular and intramolecular parameters (Å) for cluster family 1000 \rightarrow 1100 \rightarrow 1110 \rightarrow 1111 \rightarrow 2111

isomer	This work ^a				Literature			
	R_{NN}^b	r_{free}^c	$r_{bridged}^d$	$R_{N...H}^e$	R_{NN}^b	r_{free}^c	$r_{bridged}^d$	$R_{N...H}^e$
1000 stag	2.716	1.024	1.116	1.600	2.706 ^f	1.020 ^f	1.112 ^f	1.593 ^f
					2.732 ^g	1.008 ^g	1.085 ^g	1.647 ^g
					2.791 ^h	1.009 ^h	1.064 ^h	1.727 ^h
1100 stag	2.828	1.023	1.070	1.759	2.833 ^f	1.018 ^f	1.064 ^f	1.769 ^f
					2.828 ^g	1.006 ^g	1.051 ^g	1.777 ^g
					2.881 ^h	1.007 ^h	1.041 ^h	1.840 ^h
1110 stag	2.903	1.021	1.054	1.849	2.914 ^f	1.017 ^f	1.047 ^f	1.866 ^f
					2.902 ^g	1.005 ^g	1.036 ^g	1.860 ^g
					2.834 ^h	1.013 ^h	1.054 ^h	1.780 ^h
1111	2.963	–	1.044	1.919	2.976 ^f	–	1.039 ^f	1.938 ^f
					2.967 ^g	–	1.027 ^g	1.940 ^g
					2.862 ^h	–	1.039 ^h	1.823 ^h
2111	2.982 (to 1,1,1) ⁱ	–	1.042	1.941	2.991 ^f	–	1.036 ^f	1.955 ^f
	2.890 (to 2) ⁱ	–	1.054	1.836	2.904 ^f	–	1.047 ^f	1.857 ^f
sh ₁ -sh ₂ ^j	3.164	1.022	1.031	2.134	3.179 ^f		1.024 ^f	2.155 ^f 2.09 ^h

^a Data from this work obtained by optimising cluster structures at MP2/aug-cc-pVDZ level of theory. ^b R_{NN} , distance between the nitrogen atom of NH_4^+ and the nitrogen atom of the complexing NH_3 molecule(s). ^c r_{free} , NH_4^+ non-coordinating N–H bond length. ^d $r_{bridged}$, NH_4^+ N–H bond length involved in coordination through hydrogen bond. ^e $r_{N...H}$, hydrogen bond distance. ^f Ref. [20], MP2/6-31+G**. ^g Ref. [12], RHF/4-31G+3S. ^h Ref. [11], SCF/6-31G** for $n=1, 2$; SCF/3-21G for $n=3, 4, 5$. ⁱ (to X) X=1, 2; distance of the nitrogen atom in NH_4^+ to the nitrogen atom of the ammonia molecules coordinating the first solvation shell, either being a single molecule (“to 1”) or a chain of two members (“to 2”). ^j sh₁-sh₂, “sh” indicates shell, distance between the nitrogen atoms of the solvating two membered chain. Here r_{free} refers to the N–H length of bonds not involved in hydrogen bonds; and $r_{bridged}$, is the N–H length that bridges the solvation shells.

Table 4.6: Intermolecular and intramolecular parameters (Å) for cluster family 2100 → 3100 → 4100

isomer	This work				Literature ^j			
	R_{NN}	r_{free}	$r_{bridged}$	$R_{N...H}$	R_{NN}	r_{free}	$r_{bridged}$	$R_{N...H}$
2100 ecli	2.863 (to 1)	1.022	1.062	1.801	2.915 (to 1)	–	1.037	1.878
	2.744 (to 2)		1.097	1.647	2.827 (to 2)	–	1.054	1.773
sh ₁ -sh ₂	3.087	1.022	1.036	2.051	3.176	–	1.014	2.162
3100	2.876 (to 1)	1.022	1.058	1.818				
	2.714 (to 3)		1.110	1.604				
sh ₁ -sh ₂	3.005	1.021	1.042	1.963				
sh ₂ -sh ₃	3.181	1.021	1.030	2.151				
4100	2.885 (to 1)	1.022	1.057	1.829				
	2.699 (to 4)		1.118	1.582				
sh ₁ -sh ₂	2.979	1.022	1.044	1.936				
sh ₂ -sh ₃	3.109	1.021	1.034	2.076				
sh ₃ -sh ₄	3.218	1.021	1.028	2.190				

^j reference [13]

As first seen in 2111, for a given cluster, the R_{NN} distance is larger if the coordination is to a single ammonia than if is to a chain (i.e. for 3100 see 2.863 Å (to 1) versus 2.744 Å (to 2)). This is to say that, the longer the ammoniated “chain” linked to the core ammonium cation, the shorter the distance between the core and the ammonia located in the first solvation shell. The same is true for the hydrogen bond distance, and the opposite for $r_{bridged}$.

Looking at the separation between solvation shells (i.e. “sh₁-sh₂” in table 4.6) measured between the nitrogen atoms of NH_3 molecules, one can see that from the first to the second solvation shell there is a decrease upon increasing the ammonia chain (i.e. cluster size). In the same fashion, the distance between the second and the third solvation shells (i.e. “sh₂-sh₃”) also decreases upon increasing the ammonia chain.

Within the same ammonia chain, the distance between shells is increased as one moves away from the core (for example for 4100 “sh₁-sh₂”, “sh₂-sh₃”, “sh₃-sh₄” we have 2.979 Å, 3.109 Å and 3.218 Å, respectively). In addition, also looking at isomer 4100, it is interesting to note that the sh₁-sh₂ becomes 2.979 Å, which is closer in magnitude

Table 4.7: Intermolecular and intramolecular parameters (Å) for cluster 3100ring

	R_{NN}	r_{free}	$r_{bridged}$	$R_{N...H}$
	2.774 (to 1)	1.021	1.075	1.718
sh ₁ -sh ₂	3.262	1.021	1.028	2.234
	2.769 (to 1)		1.077	1.709
sh ₁ -sh ₂	3.247	1.021	1.029	2.220
sh ₂ -sh ₃	3.168	1.023	1.032	2.136

to the R_{NN} between the single ammonia and the NH_4^+ (2.885 Å) than it is to the R_{NN} between the “linker” NH_3 and the cation (2.699 Å).

To conclude, it would seem that when a new solvation shell is created through the elongation of the “ammonia chain” there will be a contraction of the spacing of the lower solvation shells with respect to the newly created. However, the incoming ammonia molecule responsible for the elongation of the chain will be placed at a distance higher than any other shell. This may be due to the polarisation effect of the ion decreasing with increasing chain size.

In isomer 3100ring, there are two ammonia molecules in the first solvation shell donating a hydrogen bond to a third double acceptor NH_3 that also constitutes the second solvation shell. In turn, this ammonia coordinates a fourth one through a donating H-bond. The measurements can be seen in table 4.7. It should also be noticed that differently from all the other isomers we presented so far, the H-bonds stemming from the cation deviate from linearity by roughly 8°.

We can see from table 4.7 that R_{NN} for both ammonia molecules in the first solvation shell are very similar. One would be tempted to assume that the three-membered chain stems from the NH_3 at the shortest distance from the cation (2.769 Å), also because the \hat{NHN} angle between NH_4^+ and NH_3 is marginally more linear (by 0.5°) when compared to the other one. One should remember that if higher level optimisations were available for this structures both ammonia molecules from the first shell might become

Table 4.8: Intermolecular and intramolecular parameters (Å) for cluster family 2100 → 2200 → 3200

isomer	This work				Literature ^j			
	R_{NN}	r_{free}	$r_{bridged}$	$R_{N...H}$	R_{NN}	r_{free}	$r_{bridged}$	$R_{N...H}$
2100 ecli	2.863 (to 1) ^f	1.022	1.062	1.801				
	2.744 (to 2) ^f		1.097	1.647				
sh ₁ -sh ₂	3.087	1.022	1.036	2.051				
2200	2.778	1.022	1.083	1.696	2.709	–	1.098	1.611
sh ₁ -sh ₂	3.107	1.022	1.034	2.073	2.997	–	1.029	1.968
3200	2.793 (to 2)	1.022	1.077	1.716				
sh ₁ -sh ₂	3.116		1.034	2.082				
	2.751 (to 3)		1.092	1.659				
sh ₁ -sh ₂	3.029		1.039	1.990				
sh ₂ -sh ₃	3.191		1.030	2.161				

^j reference [13]

equivalent. Either way, assigning the chain to any of the two ammonia molecules, the general trends we have seen so far apply for the measured parameters. The only novelty is the fact that the sh₂-sh₃ distance (3.168 Å) is decreased with respect to the sh₁-sh₂ (3.262, 3.247 Å), most likely due to the fact that the outermost NH₃ is a double H-bond acceptor.

Cluster family 2100 → 2200 → 3200

The same trends we have seen so far apply to this family of clusters as it can be seen from table 4.8. The only two noteworthy comments are, on one hand, that for isomer 2200 we find two structurally equivalent two-membered chains solvating a core cation judging by the same measured values for the parameters of interest. On the other hand, the R_{NN} to the two-membered chain for isomer 3200 (2.793 Å, “to 2”) is increased with respect to that of 2200 (2.778 Å, “to 2”), as a result of the expansion of one ammonia chain to three members. In the latter, a contraction of the first solvation shell is seen, as before.

Table 4.9: Intermolecular and intramolecular parameters (Å) for cluster family 2100 \rightarrow 2110 \rightarrow 3110

Isomer	This work				Literature ^j			
	R_{NN}	r_{free}	$r_{bridged}$	$R_{N...H}$	R_{NN}	r_{free}	$r_{bridged}$	$R_{N...H}$
2100 ecl	2.863 (to 1)	1.022	1.062	1.801				
	2.744 (to 2)		1.097	1.647				
sh ₁ -sh ₂	3.087	1.022	1.036	2.051				
2110	2.926 (to 1,1)	1.021	1.050	1.877	3.868 (to 1)	–	1.047	1.821
	2.823 (to 2)		1.069	1.755	2.760 (to 2)	–	1.077	1.684
sh ₁ -sh ₂	3.130	1.022	1.033	2.097	3.040	–	1.025	2.015
3110	2.935 (to 1,1)	1.021	1.048	1.887				
	2.798 (to 3)		1.074	1.724				
sh ₁ -sh ₂	3.629	1.021	1.037	2.019				
sh ₂ -sh ₃	3.197	1.021	1.030	2.168				

^j reference [13]Table 4.10: Intermolecular and intramolecular parameters (Å) for cluster family 2100 \rightarrow 2110 \rightarrow 2210

Isomer	This work ^a			
	R_{NN}	r_{free}	$r_{bridged}$	$R_{N...H}$
2100 ecl	2.863 (to 1) ^f	1.022	1.060	1.801
	2.744 (to 2) ^f		1.097	1.647
sh ₁ -sh ₂ ^g	3.087	1.022	1.036	2.051
2110	2.926 (to 1,1) ^f	1.021	1.050	1.877
	2.823 (to 2) ^f		1.069	1.755
sh ₁ -sh ₂ ^g	3.130	1.022	1.033	2.097
2210	2.947 (to 1) ^f	1.021	1.046	1.901
	2.847 (to 2,2) ^f		1.063	1.784
sh ₁ -sh ₂ ^g	3.144	1.022	1.032	2.112

Cluster family 2100 \rightarrow 2110 \rightarrow 3110

As it can be seen in table 4.9 same trends apply to this cluster family.

Cluster family 2100 \rightarrow 2110 \rightarrow 2210

Also for this family same trends apply as it can be seen in table 4.10. Let us remark the structurally equivalent two-membered ammonia chains in the case of isomer 2210, in a similar way as we saw for 2200. Also, to point out how the “sh₁-sh₂” distance increases for the same degree of NH_4^+ saturation, when going from 2110 (3.130 Å) to 2210 (3.144 Å).

4.3.3 Harmonic Frequencies

Ab initio harmonic frequencies were calculated for $\text{NH}_4^+(\text{NH}_3)_n$ ($n = 2 - 5$) on the fully optimised structures at the MP2/aug-cc-pVDZ level of theory. As for ammonia clusters, these were analysed in order to extract information on the frequency shift of the N-H stretching modes in an attempt to associate a particular geometrical feature to a range of frequencies. The results of our frequency calculations for the N-H stretches are shown in figures 4.8-4.18.

Out of the 20 minimum energy isomers we have isolated as possible minimum energy structures, only 4 featured a complete set of real frequencies (1000 ecl, 1100 ecl, 1100 stag and 3100ring). Conversely, the 15 remaining structures have a varying number of imaginary frequencies: one in the case of 1000 stag, 2100 ecliecl, 2100 ecl, 2110 and 3200; two for 2100 stag, 1111, 2200, 2111ring and 4100; three for 1110 ecl, 1110 stag, 3100, 2210 and 3110; finally, 2111 had four imaginary frequencies. In principle, this finding indicates that we have not found the true minimum structures. However, all our clusters are converged to values that are well within the threshold criteria for optimisation. In addition, they are in agreement with some structures reported in the literature, a fact that makes us confident that the spatial arrangement of the monomers correspond to reasonable structures. The most likely explanation to this finding is that, because optimisations were carried out using standard optimisation criteria, the clusters have geometrical parameter values different to those at the bottom of their PES well, thus the rise of unexpected imaginary frequencies. Also, in figures 4.9, 4.10, 4.11 and 4.12 it can be seen that those isomers whose only difference is the staggered or eclipsed orientation of a solvating ammonia molecule with respect to the core ammonium cation have practically the same frequency spectra (i.e. 1000 ecl and 1000 stag; 1100 ecl and 1100 stag; 1110 ecl and 1110 stag; 2100 ecl, 2100 stag and 2100 ecliecl).

The experimental spectra obtained in references [18, 34] for the $\text{NH}_4^+(\text{NH}_3)_n$ ag-

gregates is interpreted by considering the clusters as a “loose assemblage” [18] of “essentially isolated molecules” [34]. This means that the N–H stretches are considered shifted from the monomer (NH_3 and NH_4^+) wavenumbers by virtue of the perturbative effect of the interactions. With this in mind, it does not come as a surprise that two main spectra features arise, those related to the vibrations of NH_4^+ cation and those assigned to the vibrations of the solvating ammonia molecules.

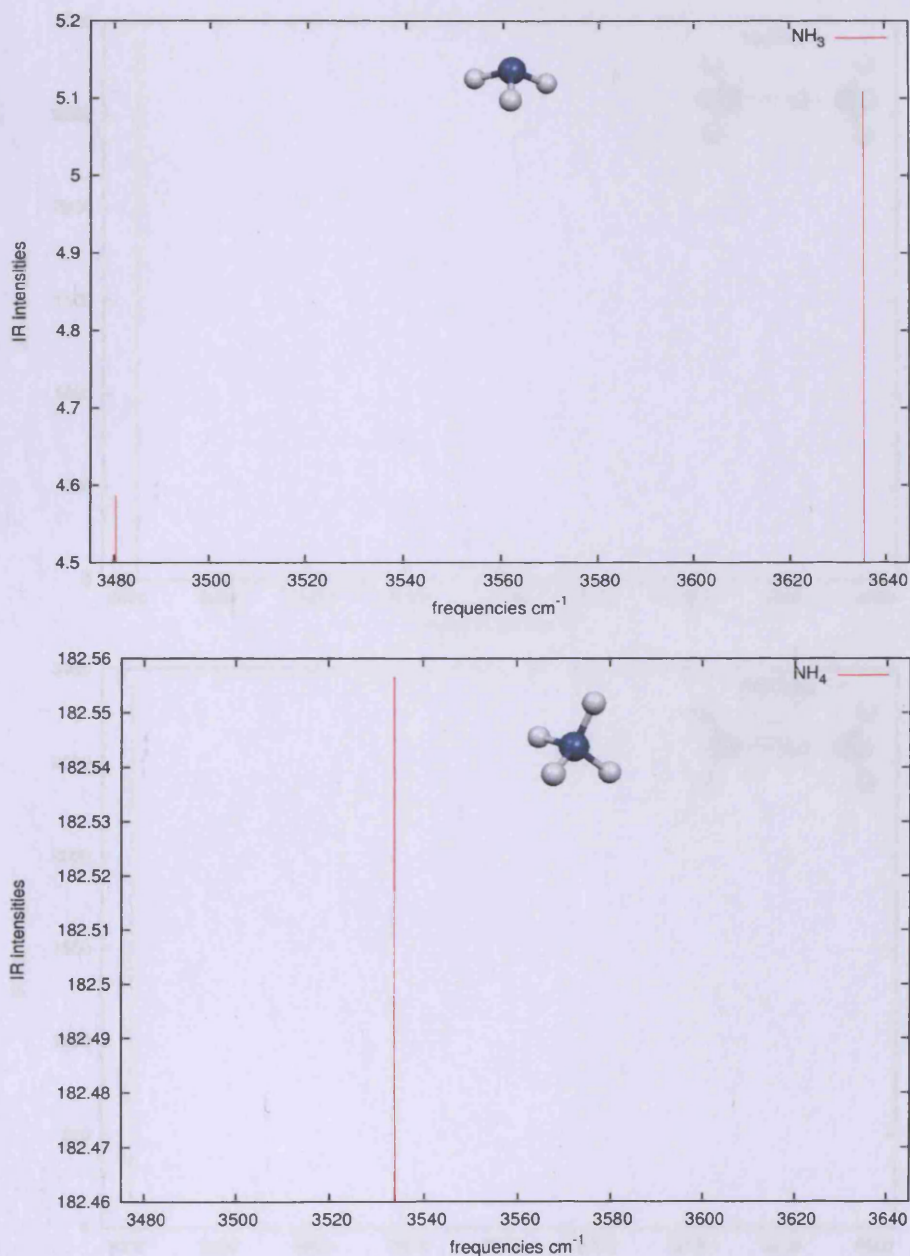


Figure 4.8: Vibrational spectra of NH_3 (top) and NH_4^+ calculated for optimised structures at MP2/aug-cc-pVDZ level of theory

NH_3 characteristic peaks are calculated at $\approx 3480 \text{ cm}^{-1}$ for symmetric N-H stretches, and $\approx 3635 \text{ cm}^{-1}$ for antisymmetric N-H stretches. NH_4^+ shows a characteristic peak at $\approx 3533 \text{ cm}^{-1}$ due to N-H antisymmetric stretches. A symmetric frequency is calculated at $\approx 3378 \text{ cm}^{-1}$ but is IR inactive due to symmetry.

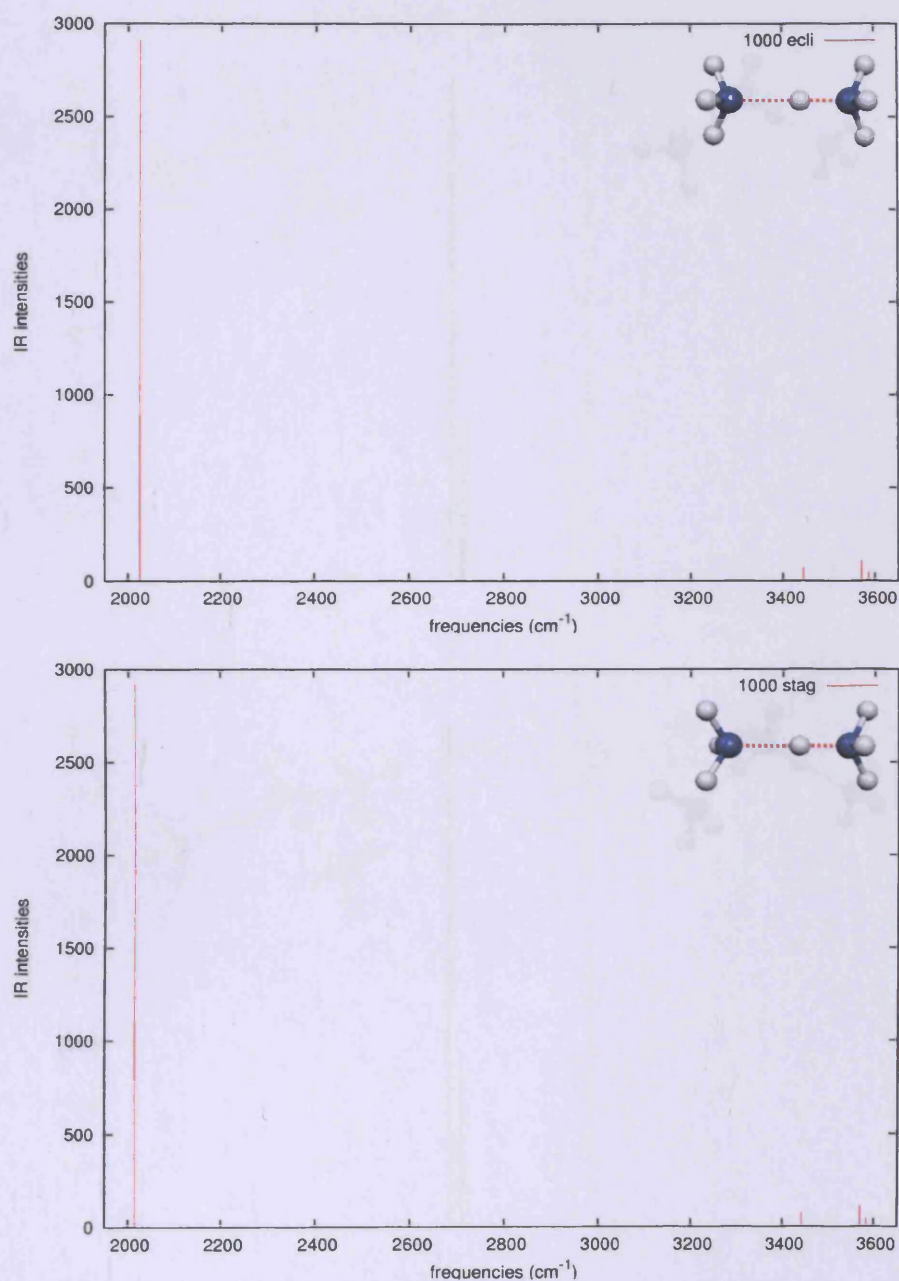


Figure 4.9: Vibrational spectra of NH_4^+NH_3 calculated for optimised structures at MP2/aug-cc-pVDZ level of theory

The characteristic peak of both spectra correspond to the N-H stretch of the proton transfer reaction coordinate with umbrella motion of the monomers at $\approx 2020 \text{ cm}^{-1}$.

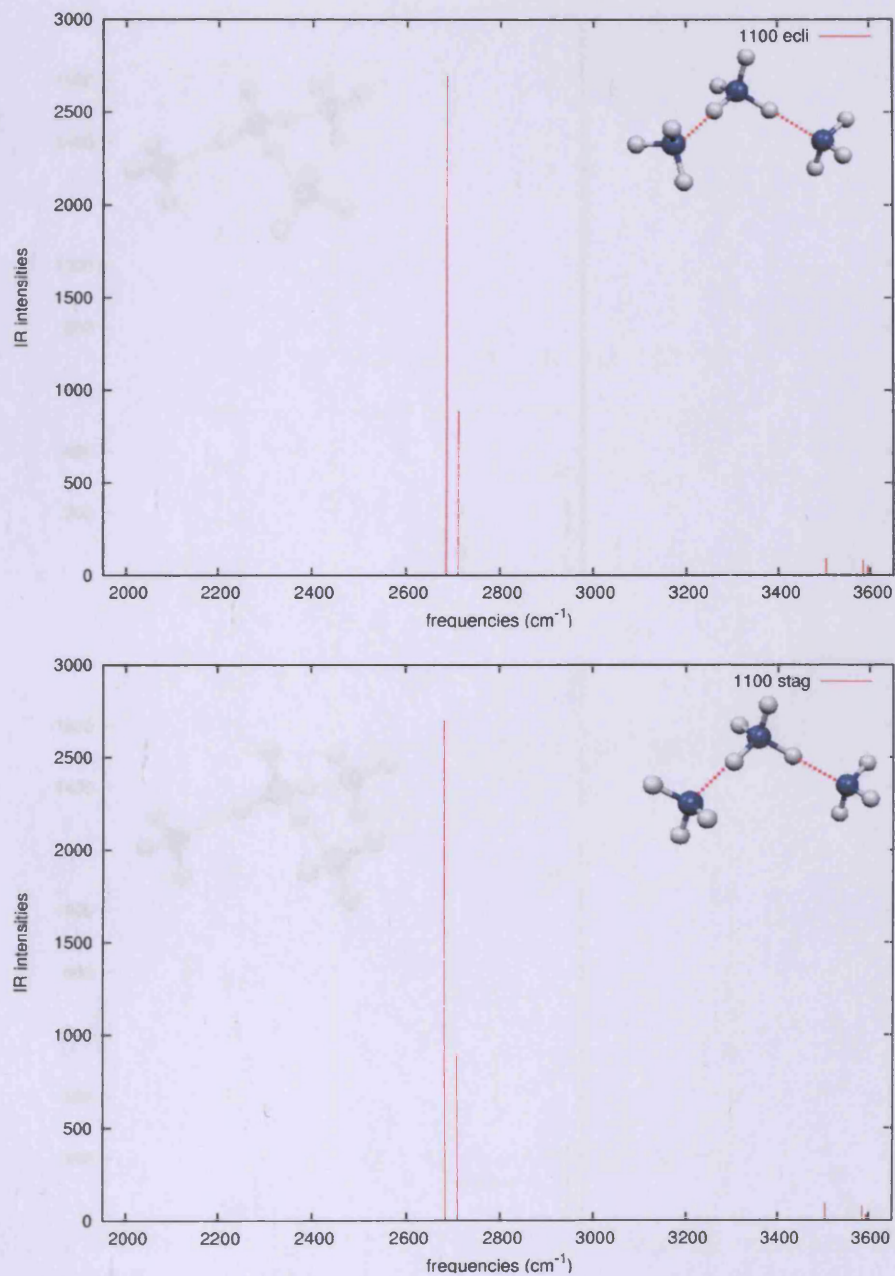


Figure 4.10: Vibrational spectra of $\text{NH}_4^+(\text{NH}_3)_2$ calculated for optimised structures at MP2/aug-cc-pVDZ level of theory

The characteristic peaks in both spectra correspond to the hydrogen bonded anti and symmetric N–H stretch of the cation at $\approx 2684 \text{ cm}^{-1}$ and $\approx 2710 \text{ cm}^{-1}$, respectively.

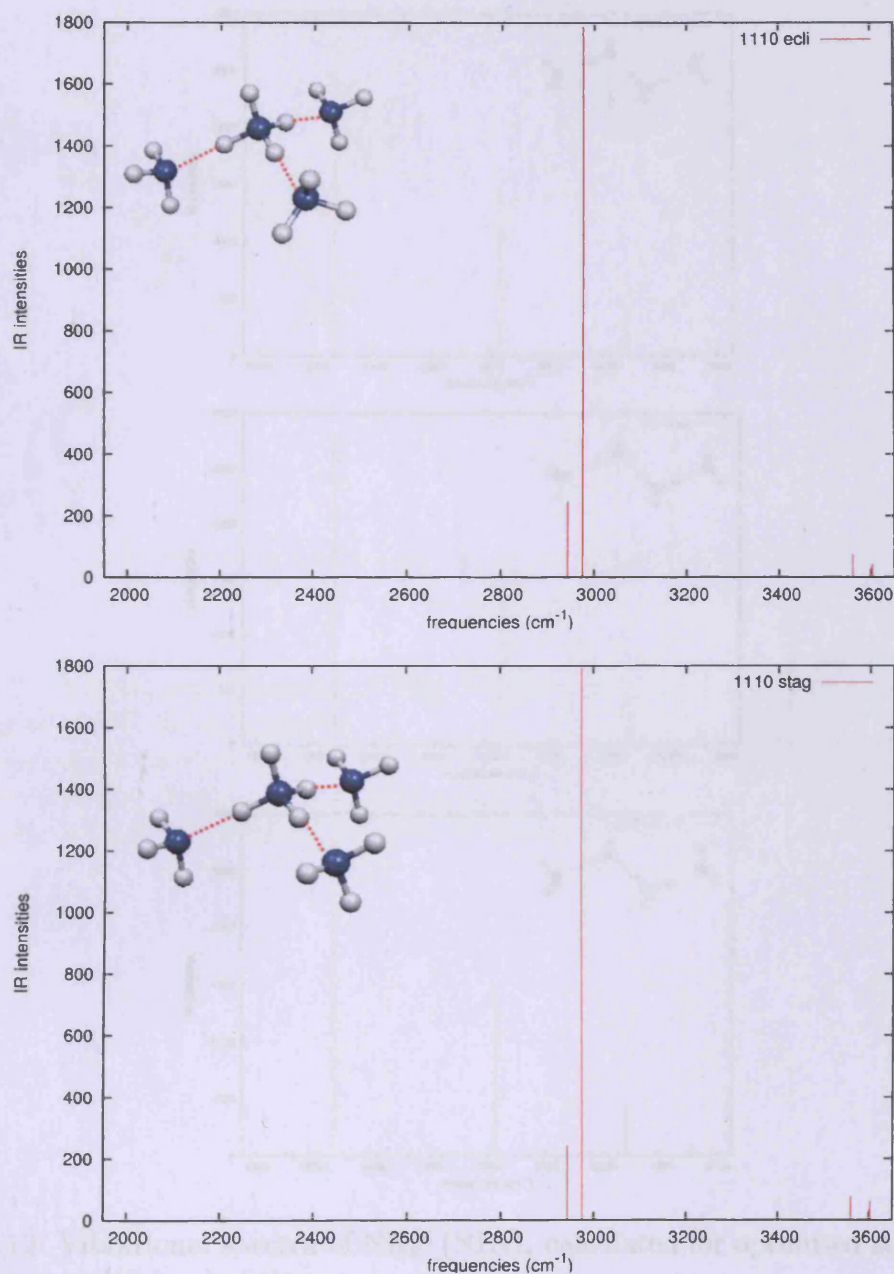


Figure 4.11: Vibrational spectra of $\text{NH}_4^+(\text{NH}_3)_3$ calculated for optimised structures at MP2/aug-cc-pVDZ level of theory

The first characteristic peak in both spectra correspond to the symmetric stretch of all N-H bonds in the core cation at $\approx 2943 \text{ cm}^{-1}$. The antisymmetric stretch of all N-H bonds in the cations correspond to a double peak seen at $\approx 2974 \text{ cm}^{-1}$ and $\approx 2975 \text{ cm}^{-1}$.

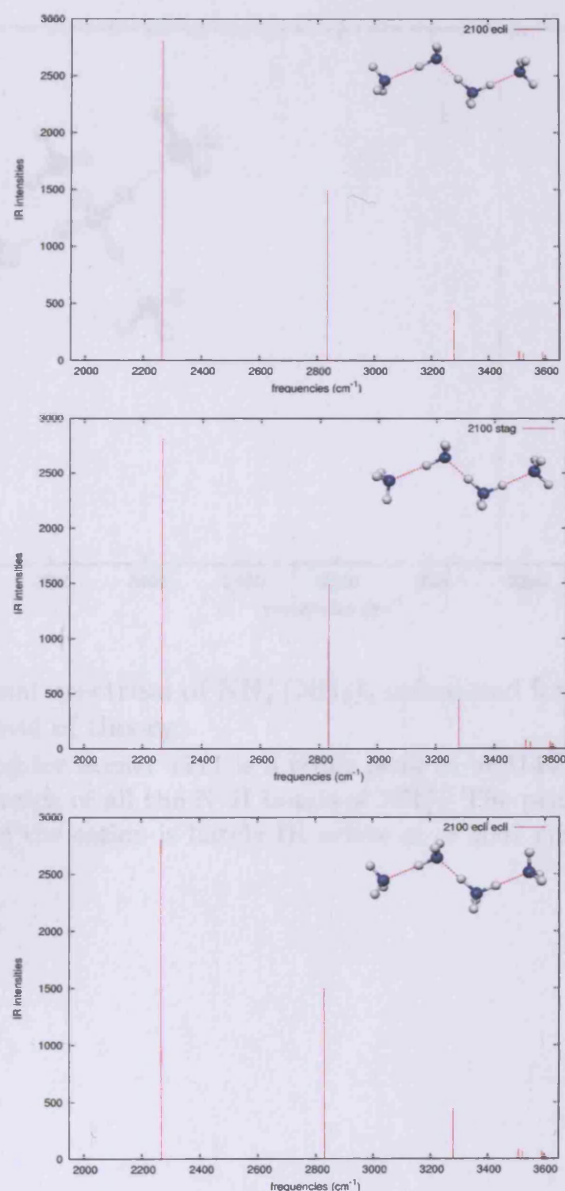


Figure 4.12: Vibrational spectra of $\text{NH}_4^+(\text{NH}_3)_4$ calculated for optimised structures at MP2/aug-cc-pVDZ level of theory

The characteristic peak that corresponds to the N-H stretch of the NH_4^+ towards the $(\text{NH}_3)_2$ chain is found at $\approx 2264 \text{ cm}^{-1}$ for 2100 ecl, $\approx 2265 \text{ cm}^{-1}$ for 2100 stag and $\approx 2260 \text{ cm}^{-1}$ for 2100 ecl ecl. The N-H stretch from the NH_4^+ to the single NH_3 is found at $\approx 2835 \text{ cm}^{-1}$ for 2100 ecl, $\approx 2832 \text{ cm}^{-1}$ for 2100 stag, $\approx 2830 \text{ cm}^{-1}$ for 2100 ecl ecl. The N-H stretch between $\text{NH}_3\text{-NH}_3$ is found at $\approx 3280 \text{ cm}^{-1}$ for 2100 ecl, and $\approx 3279 \text{ cm}^{-1}$ for 2100 stag and 2100 ecl ecl.

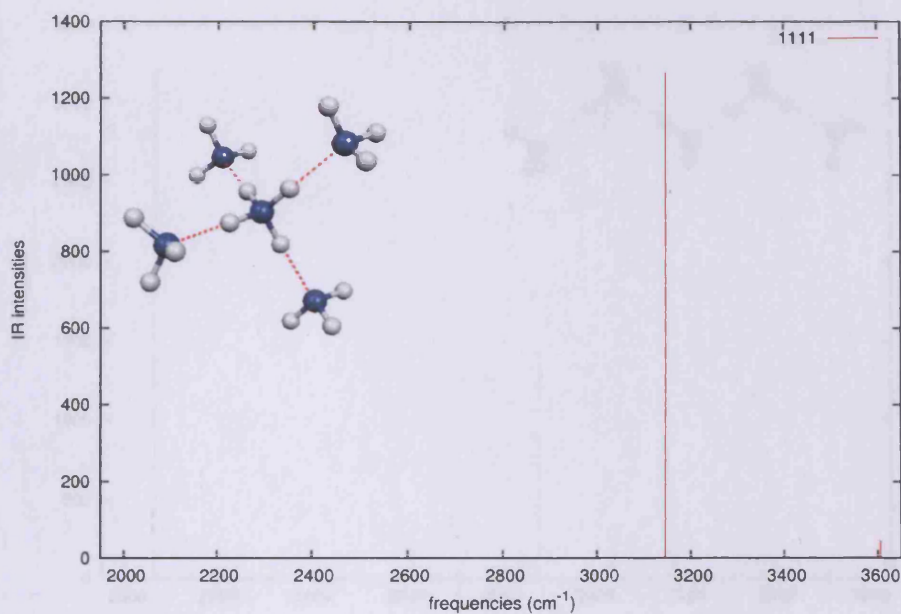


Figure 4.13: Vibrational spectrum of $\text{NH}_4^+(\text{NH}_3)_4$ calculated for optimised structure at MP2/aug-cc-pVDZ level of theory

The characteristic band for isomer 1111 is a triple peak at $\approx 3144 \text{ cm}^{-1}$, corresponding to the antisymmetric stretch of all the N-H bonds of NH_4^+ . The peak corresponding to the symmetric stretches of the cation is barely IR active at $\approx 3067 \text{ cm}^{-1}$ due to symmetry.

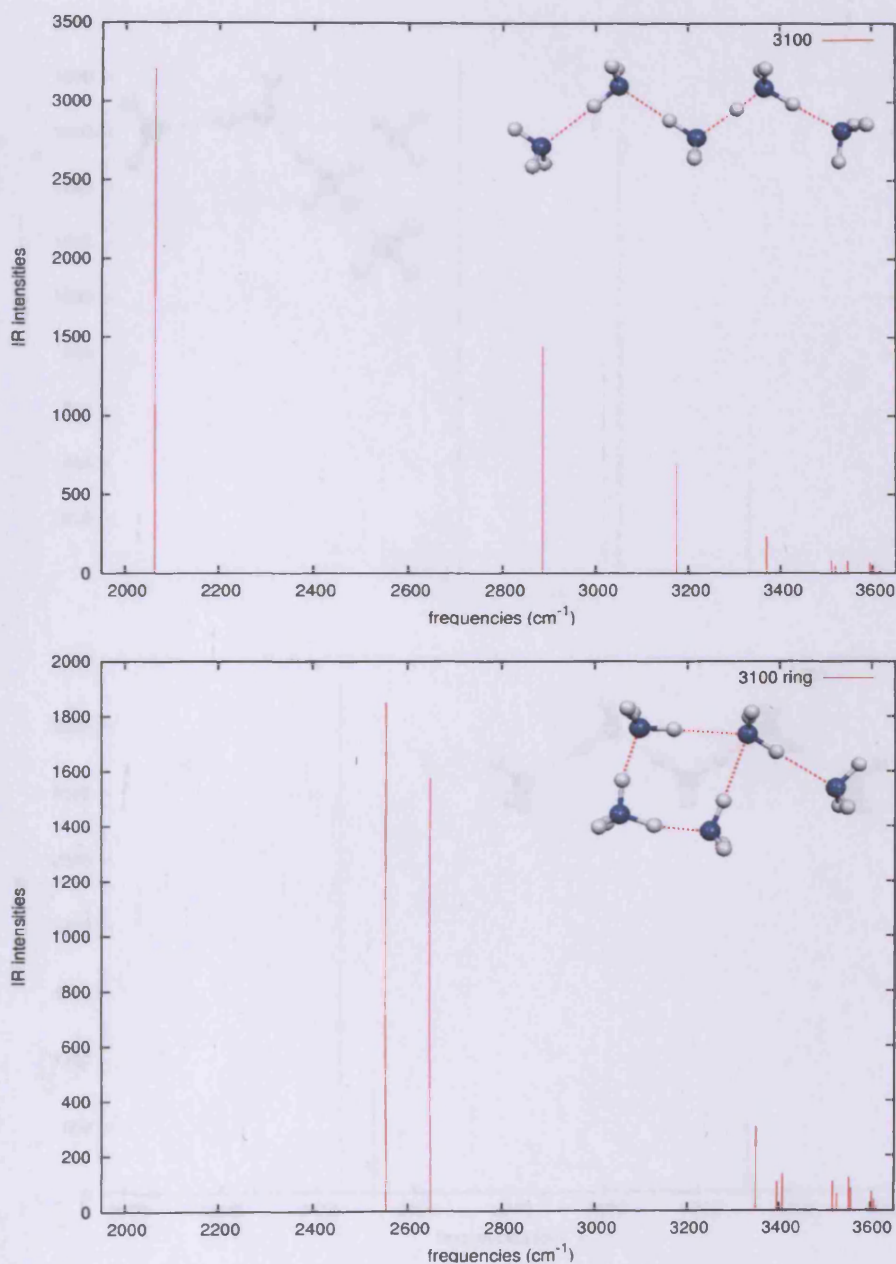


Figure 4.14: Vibrational spectra of $\text{NH}_4^+(\text{NH}_3)_4$ calculated for optimised structures at MP2/aug-cc-pVDZ level of theory

Isomer 3100 (top) has a characteristic peak at $\approx 2064 \text{ cm}^{-1}$ that corresponds to the bending and N–H stretch of the NH_4^+ complexing the three membered ammoniated chain. The stretch of the N–H bond that binds the free ammonia molecule of the isomer is found at $\approx 2886 \text{ cm}^{-1}$. The wavenumber associated with the hydrogen bond between first and second, and second and third solvation shells are found at $\approx 3173 \text{ cm}^{-1}$ and $\approx 3369 \text{ cm}^{-1}$, respectively. Characteristic peaks of 3100ring are found at $\approx 2555 \text{ cm}^{-1}$ and $\approx 2648 \text{ cm}^{-1}$

for the anti and symmetric N–H stretching modes of NH_4^+ . A peak at $\approx 3349 \text{ cm}^{-1}$ corresponds to a collective vibration of all hydrogen bonds between the ammonia solvating shells.

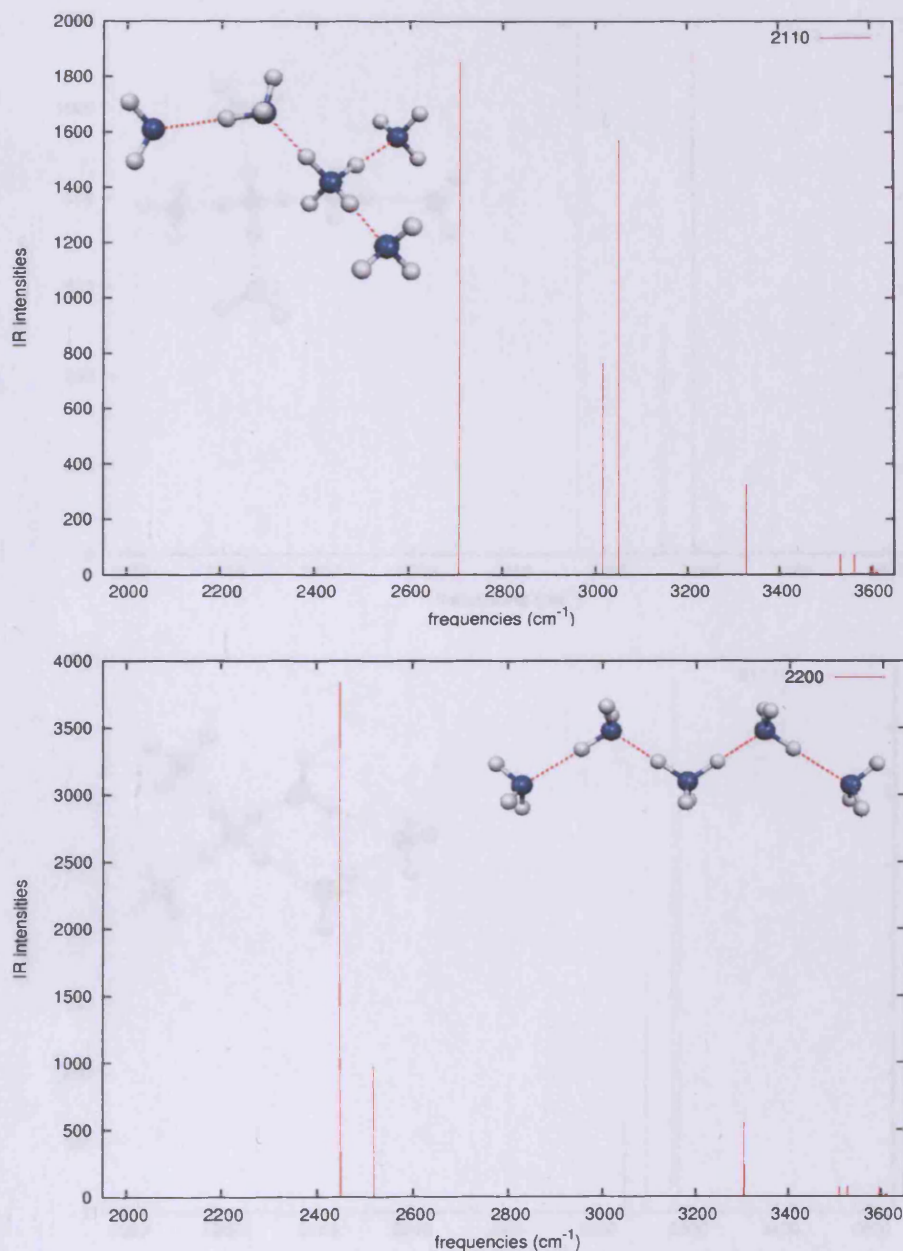


Figure 4.15: Vibrational spectra of $\text{NH}_4^+(\text{NH}_3)_4$ calculated for optimised structures at MP2/aug-cc-pVDZ level of theory

Isomer 2110 (top) has four characteristic peaks, the first located at $\approx 2706 \text{ cm}^{-1}$ corresponding to the stretch of the hydrogen bond between the cation and the two-membered ammoniated chain. At roughly 3015 cm^{-1} and 3049 cm^{-1} are located the peaks corresponding to symmetric and antisymmetric N-H stretches binding the free ammonia molecules. The hydrogen bond between first and second solvation shell vibrates at $\approx 3328 \text{ cm}^{-1}$. Isomer 2200 has a peak at $\approx 2448 \text{ cm}^{-1}$ and another one at $\approx 2518 \text{ cm}^{-1}$, both corresponding to the respectively anti and symmetric vibrations of the hydrogen bond between the core cation and the both the two membered ammoniated chains. At $\approx 3304 \text{ cm}^{-1}$ is a double peak corresponding to the vibration between first and second solvation shells.

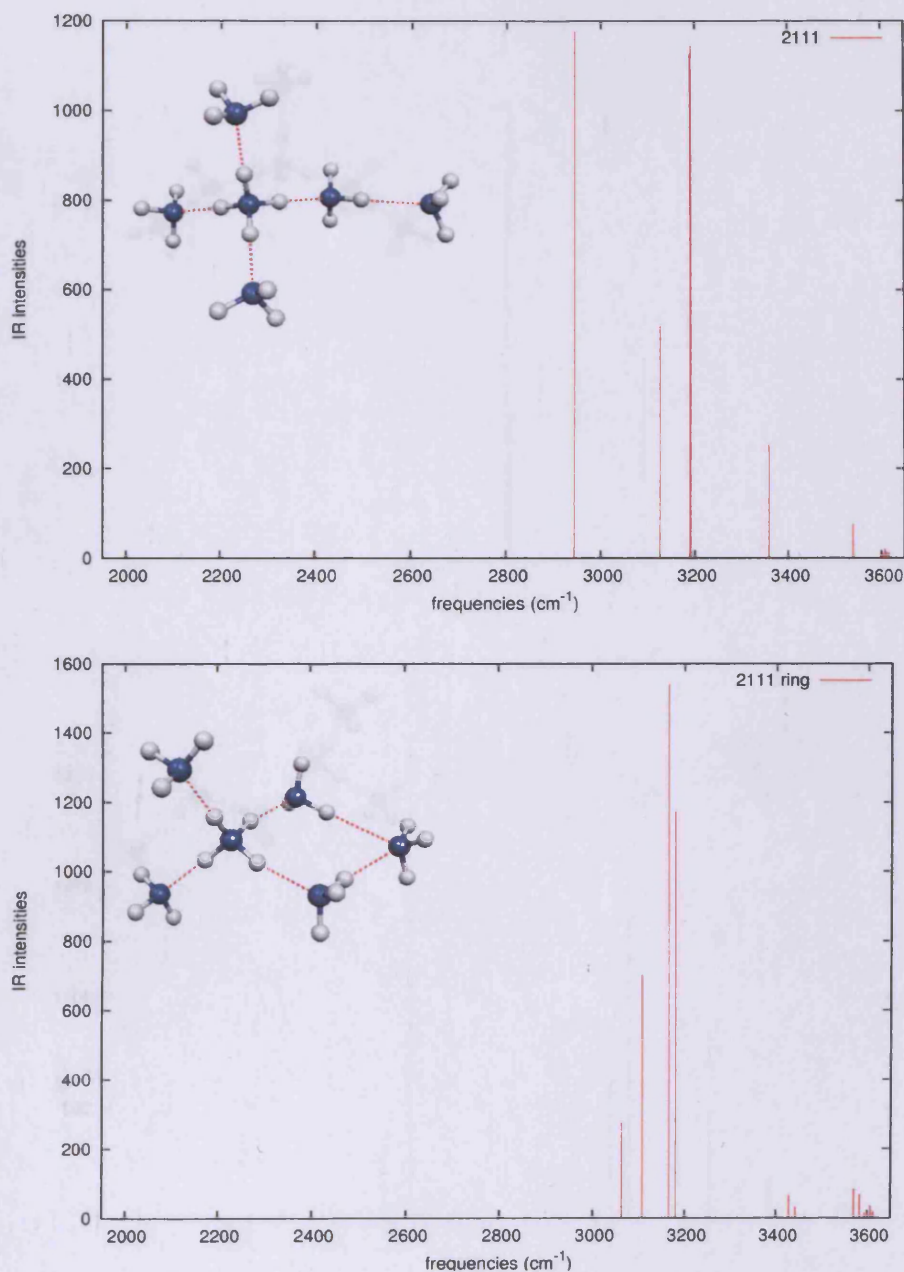


Figure 4.16: Vibrational spectra of $\text{NH}_4^+(\text{NH}_3)_5$ calculated for optimised structures at MP2/aug-cc-pVDZ level of theory

Isomer 2111 (top) has a first peak at $\approx 2943 \text{ cm}^{-1}$, corresponding to the symmetric stretch of all N–H bonds in NH_4^+ . Antisymmetric modes are found for all N–H bonds at $\approx 3125 \text{ cm}^{-1}$, and at $\approx 3190 \text{ cm}^{-1}$ for N–H bonds coordinating free NH_3 molecules only. At $\approx 3539 \text{ cm}^{-1}$ there is one asymmetric N–H stretch mode from the first shell molecule to the second shell one. Isomer 2111ring has peaks at $\approx 3063 \text{ cm}^{-1}$ and $\approx 3107 \text{ cm}^{-1}$ that corresponds, respectively, to the symmetric and antisymmetric stretches of all the cation N–H bonds.

Roughly at 3170 cm^{-1} we see a double peak that corresponds to the N–H stretches that bind to the free ammonia molecules only. The stretch between solvation shells is double and calculated at $\approx 3430 \text{ cm}^{-1}$.

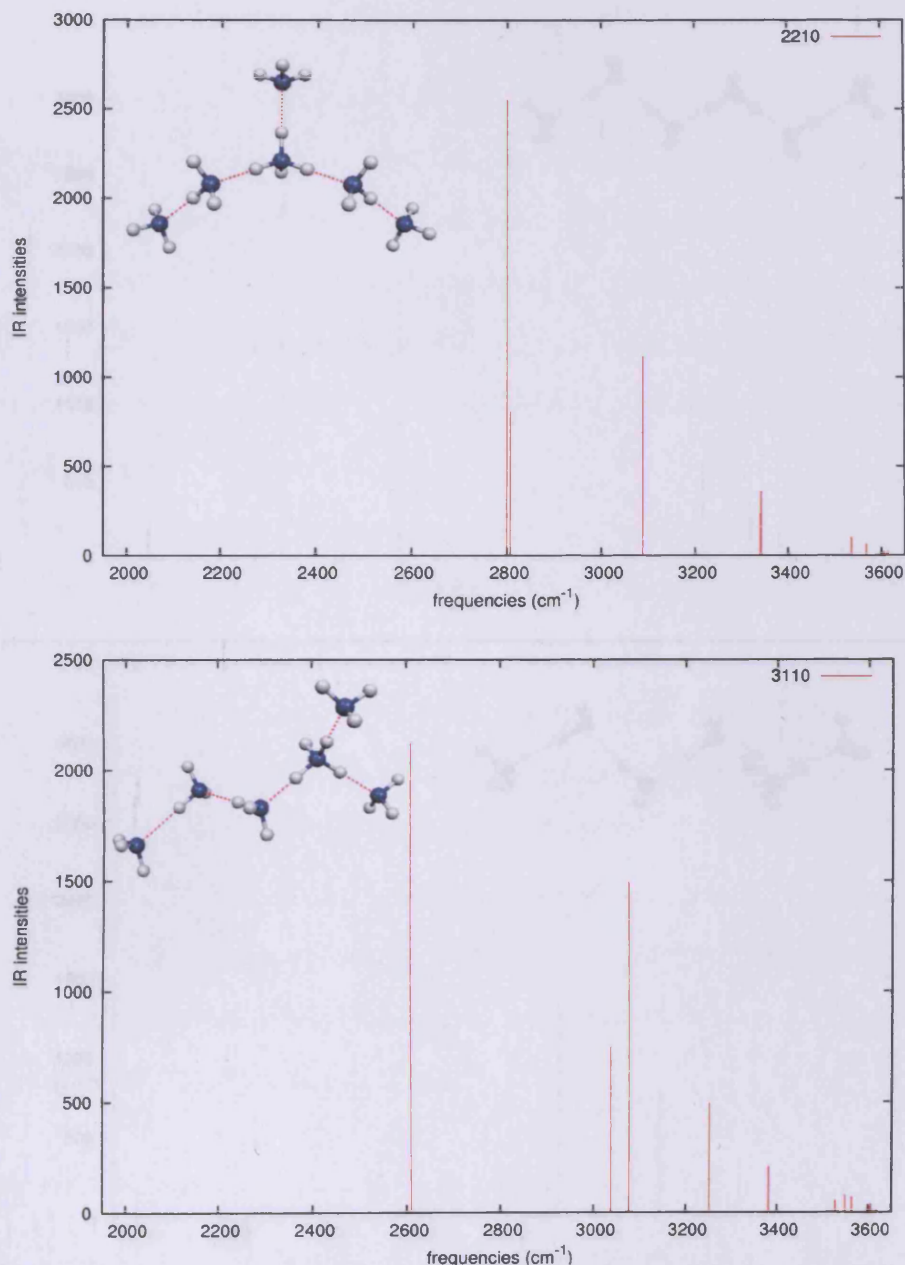


Figure 4.17: Vibrational spectra of $\text{NH}_4^+(\text{NH}_3)_5$ calculated for optimised structures at MP2/aug-cc-pVDZ level of theory

Isomer 2210 (top) features characteristic peaks at $\approx 2799 \text{ cm}^{-1}$ and $\approx 2806 \text{ cm}^{-1}$, corresponding to the anti and symmetric vibration of the hydrogen bond between the cation and both the two membered ammonia chains. The N-H stretch from the cation to the free NH_3 vibrates at $\approx 3087 \text{ cm}^{-1}$. Hydrogen bond between solvation shells is a double peak at $\approx 3341 \text{ cm}^{-1}$. Isomer 3110 has a peak at $\approx 2610 \text{ cm}^{-1}$ corresponding to the N-H stretch of the cation towards the three-membered ammonia chain. Two peaks at $\approx 3038 \text{ cm}^{-1}$ and $\approx 3077 \text{ cm}^{-1}$ correspond to the vibration of the hydrogen bond between the cation and the free ammonia molecules. Vibration of the bonds between first and second, and second and third solvation shells are found at $\approx 3251 \text{ cm}^{-1}$ and $\approx 3381 \text{ cm}^{-1}$ respectively.

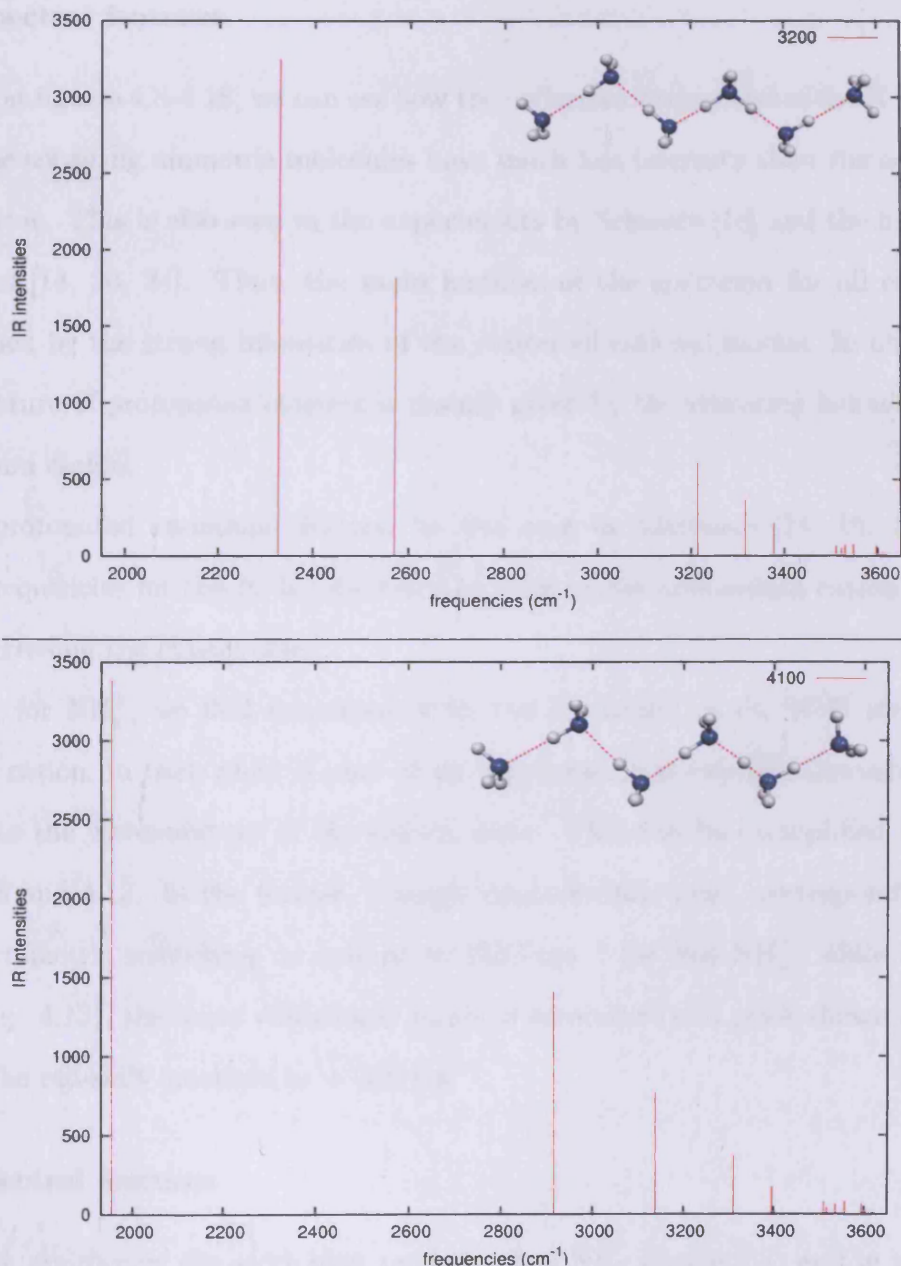


Figure 4.18: Vibrational spectra of $\text{NH}_4^+(\text{NH}_3)_5$ calculated for optimised structures at MP2/aug-cc-pVDZ level of theory

Isomer 3200 (top) has two peaks corresponding to the hydrogen bonds from the cation to the three and two-membered ammoniated chains at, respectively, $\approx 2328 \text{ cm}^{-1}$ and $\approx 2570 \text{ cm}^{-1}$. The hydrogen bonds from the first to the second solvation shell vibrate at $\approx 3214 \text{ cm}^{-1}$ in the three-membered ammonia chain, and $\approx 3377 \text{ cm}^{-1}$ in the two-membered ammoniated chain. Another characteristic peak is found at $\approx 3469 \text{ cm}^{-1}$ corresponding to the hydrogen bond between second and third solvating shells. Isomer 4100 has peaks at $\approx 1953 \text{ cm}^{-1}$ and $\approx 2915 \text{ cm}^{-1}$ corresponding to the N–H stretches from the cation to the four-membered ammonia chain and free ammonia, respectively. Peaks at $\approx 3138 \text{ cm}^{-1}$, $\approx 3311 \text{ cm}^{-1}$ and $\approx 3396 \text{ cm}^{-1}$ correspond to the hydrogen bond between the first and second, second and third, and third and fourth solvation shells respectively.

NH_4^+ spectral features

Looking at figures 4.8-4.18, we can see how the collective frequencies of the N–H stretching of the solvating ammonia molecules have much less intensity than the core ammonium cation. This is also seen in the experiments by Schwarz [18] and the figures from references [14, 20, 34]. Thus, the main features of the spectrum for all clusters are determined by the strong intensities of the cation vibrational modes. In other words, the signature of protonated clusters is mainly given by the vibrating behaviour of the ammonium cation.

For protonated ammonia clusters, as also seen in references [14, 15, 18, 20, 34] higher frequencies for the N–H vibrational modes of the ammonium cation are found upon increasing the cluster size.

Also, for NH_4^+ , we find consensus with the literature on the N–H stretching of the core cation, in that when is part of an aggregate, is noticeably downshifted with respect to the wavenumbers of the cation alone. This can be exemplified looking at Figs. 4.8 and 4.13. In the former, a single characteristic peak, corresponding to the N–H asymmetric stretching, is seen at $\approx 3533 \text{ cm}^{-1}$ for free NH_4^+ ; while for isomer 1111 (Fig. 4.13), the same vibrational mode is estimated as a peak shown at $\approx 3067 \text{ cm}^{-1}$. The red-shift amounts to $\approx 466 \text{ cm}^{-1}$.

NH_3 spectral features

As before, comparing the stretching mode for free NH_3 (figure 4.8) and in the cluster 1111 (figure 4.13) we also find it to be red-shifted ($\approx 31 \text{ cm}^{-1}$), albeit significantly less than NH_4^+ . A similar finding is also reported from the experiments in reference [34], where the red-shift of the monomers NH_4^+ and NH_3 in isomer 1111 is attributed to the fact that for species with one solvation shell the N–H bonds involved in hydrogen bonding are those of NH_4^+ . However, ammonia molecules do participate in hydrogen

bonding when a second or higher solvation shell is formed. Thus, it would be interesting to monitor how the N–H stretches of ammonia molecules donating hydrogen bonds shift from the free NH_3 .

Dependence of NH_3 spectral features on the solvation shell order

Let us start by considering isomer 2111 as an example (figure 4.16). It is interesting because it is the biggest “globular cluster” featuring a complete first shell and a single NH_3 in the second shell, and also because one can recognise three “types” of solvating ammonia molecules.

First, there are three free NH_3 molecules that are part of the first solvation shell, and as such, each accepting a hydrogen bond from the core cation. These are equivalent to those seen in isomer 1111, with their N–H asymmetric stretches being red-shifted from the free NH_3 monomer by the same amount (roughly 30 cm^{-1}).

Second, there is a free NH_3 molecule placed in the second solvation shell accepting a hydrogen bond from an ammonia molecule on the first solvation shell. In this case, the downshift is $\approx 20 \text{ cm}^{-1}$, lower than in the previous case, due to the fact that this molecule is further away from the core and more loosely bound, and also has no N–H bond participating in a hydrogen bond.

Finally, there is one first solvation shell NH_3 molecule acting as hydrogen bond donor and acceptor. In this case, two out of the three N–H modes are degenerate. In fact, the calculated frequency for the N–H stretches involving only free non hydrogen bonding hydrogen atoms, is downshifted with respect to those of the free ammonia by $\approx 34 \text{ cm}^{-1}$, similarly to other free N–H bonds. The frequency calculated for the N–H stretches involved in hydrogen bonding with the second shell is downshifted with respect to free ammonia by roughly 95 cm^{-1} , i.e. three times the non-bonding hydrogen atoms.

To summarise these observations, we can say that “free” ammonia N–H bonds in a cluster i.e. not involved in a hydrogen bond, vibrate roughly at the same frequencies. That is $\approx 20\text{--}30\text{ cm}^{-1}$ lower than NH_3 . However, the wavenumbers tend to slightly increase with increasing solvation shell order, indicating a decreased red-shift. “Engaged” or donating ammonia N–H bonds vibrate at lower wavenumbers than “free” ones; thus, the difference with respect to free ammonia molecules is larger.

Notice that by looking at how the asymmetric N–H stretch of a free ammonia molecule is perturbed when brought to form part of a protonated ammonia cluster in the example above (isomer 2111), we could identify three “types” of ammonia molecules located in different environments in the cluster (e.g. first or second shell) and if they were involved in a hydrogen bond. Based on this possibility, one could formulate two additional questions.

First, what happens to free NH_3 molecules in the first solvation shell when the latter is not complete (that is, when the cation is not fully complexed)? Also what happens to ammonia molecules in solvation shells higher than the second?

To answer the first question we can look at isomers 2110 and 2100. In isomer 2110, all N–H stretches vibrate at a slightly lower wavenumbers than in isomer 2111, translating into insignificantly higher red-shifts with respect to free ammonia molecules than those seen for isomer 2111 (e.g. $\approx 33\text{ cm}^{-1}$ for first shell ammonia molecules, $\approx 23\text{ cm}^{-1}$ for second shell ammonia molecule and for first shell linking to second shell NH_3 molecule, ≈ 35 and $\approx 102\text{ cm}^{-1}$ for free N–H bonds and donating hydrogen atom, respectively). For isomer 2100, the trend is similar even though N–H stretches of ammonia molecules vibrate at slightly lower wavenumbers than in isomer 2110. In fact the red-shift for ammonia molecules in isomer 2100 compared with free ammonia molecules is $\approx 28\text{ cm}^{-1}$ for second shell ammonia molecule, $\approx 38\text{ cm}^{-1}$ for the single free first shell ammonia molecule and for first shell linking to second shell NH_3 , ≈ 41

and 113 cm^{-1} for free N–H bonds and donating hydrogen atom, respectively.

As for what happens to ammonia molecules in solvation shells higher than the second, we can look at isomers 3100 and 4100. In isomer 3100 we have two donor/acceptor ammonia molecules in shells one and two respectively. The downshift with respect to free ammonia molecules experienced by the N–H donating hydrogen atom is $\approx 118\text{ cm}^{-1}$ for the first solvation shell ammonia and $\approx 91\text{ cm}^{-1}$ for the NH_3 in the second solvation shell. For isomer 4100, the red shift experienced by the N–H bond in the first shell donor/acceptor NH_3 molecule is ≈ 38 and 118 cm^{-1} .

In reference [34], only globular structures are reported. However, we have also to consider “linear” clusters such as 2100. This is the smallest isomer featuring a second solvation shell, and in it we encounter two types of ammonia molecules complexing the cation. First, a free ammonia molecule, as seen for isomer 1111, in which case the red shift is 28 cm^{-1} with respect to NH_3 in gas phase. Second, an ammonia molecule involved in a hydrogen bond with the second shell, in which case the downshift is 113 cm^{-1} with respect to the free monomer, i.e. significantly greater and comparable in magnitude to the one affecting the cation.

All in all, the evidences above, indicate that the red shift experienced by solvating ammonia molecules with respect to free ammonia could be determined by three general factors depending on the type of cluster they belong to. The first one is whether or not the ammonia molecules are involved in donating hydrogen bonds. As explained above, free solvating ammonia molecules have small shifts from the spectrum of the monomer, while ammonia molecules involved in linking solvating shells have a remarkable red shift. Second, for an ammonia chain the shift is determined by the level of saturation of the ammonium cation, thus the less saturated the cation is the bigger is the shift (e.g. considering the hydrogen bond between first and second solvation shell in the ammonia chain of isomer 4100 the shift is 342 cm^{-1} , while for isomer 2110 the shift amounts to

190 cm^{-1}). Third, for a given solvation shell the frequency shift varies depending on the length of the ammonia chain. Within a chain, the higher the order of solvation shell the smaller the shift (e.g. N–H symmetric stretch difference in wavenumbers from free NH_3 in isomer 4100 in shells 1-2 is 342 cm^{-1} , shells 2-3 is 169 cm^{-1} , shells 3-4 is 94 cm^{-1}).

The aforementioned findings have a clear link with the trends seen for the geometrical parameters, in particular with the distances between the core cation and the first ammoniated shell and with the distances between solvating shells. The trend is that the closer the ammonia molecule acting as a linker to the second solvation shell is to the core cation the greater is the red shift when compared to the free ammonia molecule spectrum. These characteristics are not evident from the spectrum figures at first sight because the collective frequencies of the N–H stretching of the solvating ammonia molecules have much less intensity than the core ammonium cation. This is true for this work, as well as for the experiments by Schwarz [18] and the figures from references [14, 20, 34]. Thus, the main features of the spectrum for all clusters are determined by the strong intensities of the cation vibrational modes. In other words, the signature of protonated clusters is given by the vibrating behaviour of the ammonium cation. However, the shifts in $(\text{NH}_3)_3$ vibrations convey the detailed information to discern the clusters' structures.

A common feature present in H-bonded clusters such as ammonia is that the N–H stretch frequencies are seen to decrease with cluster size. This does not seem to be the case for protonated ammonia clusters, as seen in this work and references [14, 15, 18, 20, 34] where higher frequencies for the N–H vibrational modes of the cation are found upon increasing the cluster size.

So far we have seen that our data are qualitatively in agreement with the literature (e.g. [14, 15, 18, 20, 34]). From a quantitative point of view they are, however,

significantly blue-shifted compared to the seminal experimental work by Schwarz [18], the experimental data obtained by Price *et. al* [34] and the theoretical work in reference [20]. We have found other theoretical data showing this tendency to blue shift with respect to the experiments, namely references [14, 19, 21].

Cluster families

As for “globular” clusters, paying attention to the solvation sequence 1000, 1100, 1110 and 1111, in which the number of ammonia molecules complexing NH_4^+ (by accepting a hydrogen bond from the cation) is monotonically increased by 1, a blue shift in the characteristic peaks of the spectra is observed upon increasing solvation. The tendency of the average frequency of antisymmetric stretches in the solvating NH_3 molecules is to increase by $\approx 12 \text{ cm}^{-1}$ going from 1000 to 1100, by $\approx 6 \text{ cm}^{-1}$ going from 1100 to 1110 and by $\approx 3 \text{ cm}^{-1}$ going from 1110 to 1111. In the same way, the average frequency of the symmetric shifts for the solvating NH_3 molecules increases by roughly 13 cm^{-1} going from 1000 to 1100, by $\approx 4 \text{ cm}^{-1}$ going from 1100 to 1110 and by $\approx 2 \text{ cm}^{-1}$ from 1110 to 1111. Upon going from 1111 to 2111 the gap in both anti and symmetric N–H stretches is roughly two and one wavenumbers, respectively. This lead us to think that, in regards to the frequency at which the ammonia molecules vibrate, a plateau is reached when the first solvation shell is completed. This would mean that probably a further increase in solvating molecules (e.g. 2211) would produce little or no change in the characteristic wavenumbers corresponding to anti and symmetric N–H stretches. Analogously, for the same cluster solvation sequence $\text{N}^+\text{-H}\dots\text{H}$ bonds get elongated by 0.16 \AA going from 1000 to 1100; by 0.09 \AA from 1100 to 1110; and by 0.07 \AA from 1110 to 1111. Thus, longer hydrogen bonds associate to higher frequencies, a feature already seen in ammonia clusters.

Isomer 2111 has a single ammonia molecule placed in the second shell. The forma-

tion of this new layer is reflected in the spectrum for this isomer with the appearance of a noticeable peak at $\approx 3539 \text{ cm}^{-1}$. This wavenumber corresponds to the N-H stretch from the hydrogen bond from shell 1 to shell 2.

Something we have noticed in the spectrum that corresponds to isomer 2111 is that it agrees with that shown by references [14, 15], but it does not with the figure shown in reference [20]. The structure from this work that fits best with the work presented by Park [20] is the isomer 2111ring.

Concerning “linear” clusters, we can see from the cluster family 2100, 3100 and 4100 a pattern in which higher frequency vibrations are associated to the antisymmetric stretches experienced by those ammonia molecules that are further apart from the ammonium cation. There is also a dependency between the frequency at which the solvating molecules vibrate and the distance to the ammonium cation, with the molecules of the second and higher solvation shells vibrating at slightly higher frequencies (in isomer 4100 $4\text{-}6 \text{ cm}^{-1}$, 5 cm^{-1} third to fourth and second to third solvation shells respectively) than first solvation shell molecules. For the latter, the same dependency applies, thus the free ammonia molecule, at a higher distance from the core cation ($\approx 0.19 \text{ \AA}$), vibrates at a higher frequency than the ammonia molecule that links to higher solvation shells. Still concerning antisymmetric stretches, it should be added that, free H atoms are found to participate only in antisymmetric stretches, vibrating at higher frequencies ($\approx 38 \text{ cm}^{-1}$ for isomer 4100) than H-bonded ones, as already seen for neutral ammonia clusters [40].

Concerning symmetric stretches, lower frequency values are associated to ammonia molecules closer to the core cation. However, one has to point out an additional underlying trend, arising when an ammonia molecule is a simultaneous hydrogen bond donor-acceptor, as it happens in the ammoniated chains. Thus, solvent molecules involved in the “ammoniated chain” are associated to lower wavenumbers, the closer

to the core cation the lower the wavenumber.

In the range of symmetric stretches, a number of normal modes, typically with the lowest wavenumbers are related to both symmetric and antisymmetric N-H stretches of the ammonium cation, the latter vibrating at the highest wavenumbers within this group. It appears that the number of these modes is determined by the saturation of the cation, e.g. four modes will describe cation stretches in isomer 1111. These wavenumbers have also associated a variable presence of bending, the highest the frequency the smallest the presence of the bending.

We found the same vibrating trends as above for isomers 2200, 3200, 2110, 2210 and 3110.

Clusters featuring a ring: 3100ring, 2111ring

In what regards the isomers presenting a ring, we have to revise the trends above, except for the one just introduced describing the N-H stretches of the ammonium cation. For the isomer 2111ring, we see that the free hydrogen atoms from the ammonia molecules in the first solvation shell that form the ring vibrate at the highest frequencies. Depending on their distance to the core cation, this would be opposite to what we have seen for the isomers displaying “ammoniated chains” given that the molecules forming the ring are closer (2.909 Å and 2.920 Å) to the ammonium than the other two ammonia molecules in the first solvation shell (2.975 Å). Vibration of the free hydrogen atoms occurs roughly 6 cm^{-1} above the first solvation shell ammonia molecules that are not included in the ring, and roughly 15 cm^{-1} above the ammonia molecule in the second solvation shell. The latter is a double hydrogen bond acceptor, and it vibrates at lower frequencies from those expected for an ammonia molecule in such position with respect to the ammonium cation.

In isomer 3100 the highest normal modes correspond to the third solvation shell

ammonia molecule, as seen for isomer 2100ring, the double acceptor ammonia molecule vibrates at lower frequencies ($\approx 14 \text{ cm}^{-1}$ in antisymmetric stretches) than the ammonia molecules from the first solvation shell.

In what regards symmetric stretches, for both ring isomers, the molecules vibrating at the highest wavenumbers are the ones not involved in the ring (ammonia molecule in the third solvation shell for isomer 3100ring, and two ammonia molecules in the first solvation shell for isomer 2100ring), which are also the ones further away from the core cation. All the molecules involved in the ring tend to vibrate collectively at the same frequencies, albeit with different strengths.

4.3.4 Comparison with experiments

In the following section, we compare the binding energies and thermochemical data estimated by this work and the same values, both experimental and theoretical, found in the literature.

Table 4.11 shows binding energies for protonated ammonia clusters for this work and those from references [10–15, 17, 38].

We can see from table 4.11 that, across literature data (columns 3 to 14), Pople's basis sets, with different degrees of flexibility, are the most popular choice for any level of theory, probably because they are computationally less demanding than Dunning's family.

Three works, apart from this one, deal with protonated ammonia clusters at the MP2 level of theory, these are references [13, 14, 17], in columns ten, five and eleven, respectively. They all have chosen double- ζ basis with diffusion functions in the heavy atoms and one d-polarisation functions for nitrogen atoms (references [13, 14], columns ten and five, respectively) and one p-polarisation functions for hydrogen atoms (reference [17], column eleven). The values provided by Deakyne [13] in col-

umn ten, are remarkably different from those by Wang *et. al.* [14], in column five. The reason for the discrepancy, both using the same level of theory, may be found in the fact that is likely that reference [13] corresponds to a single point calculation performed on a geometry optimised at HF/6-31+G*, and also to the lack of BSSE and ZPE corrections, both included in reference [14]. The need for both the aforementioned corrections is clear after the comparison between the data from the columns five and ten, as already predicted in the work by Kassab and Evleth [12]: “Accurate theoretical estimates of ion-molecule complexation energies require using [...] zero-point, thermodynamic, correlation, and basis set superposition error corrections”.

The work by Del Bene *et. al* [17], in column eleven, at the MP2 level of theory, provides a better description of the polarisation with respect to references [14] and [13] by incorporating polarisation functions in the hydrogen atoms (6-31+G**). In addition, the electronic energy is corrected, although only with the value obtained for the ZPE calculated for the HF equilibrium structures with 6-31+G*. The value from column eleven is the value that better agrees with the dimer from this work. It is probably fortuitous (values from reference [17] lack BSSE correction), perhaps due to error cancellation, and since no clusters above the dimer are reported, no conclusion on the performance of that theoretical approach can be reached with respect to the one used in this work.

The works using DFT to investigate protonated ammonia clusters are references [14, 15, 38], in columns four, three and seven, respectively. They all choose B3LYP as a functional with different double- ζ basis sets. The work by Nakai *et. al* [38], in column seven, overestimates the binding energies quite dramatically with respect to references [14] and [15]. We think that the reason for this is that the tendency of B3LYP to overestimate the binding energy may be enhanced by the choice of cc-pVDZ as a basis set. For these data no BSSE or ZPE corrections have been introduced.

Table 4.11: Binding energies for $\text{NH}_4^+(\text{NH}_3)_n$, ($n = 2 - 5$) in kcal/mol^a

Isomer	This work ^a	FM ^b	WCJL ^c		NGIOT ^d		KE ^e	D ^f		BFP ^g	HFNKY ^h		PA ⁱ
	MP2 aTZ	B3LYP 631**	B3LYP ^I 631+*	MP2 ^{II} 631+*	HF ^I D95	B3LYP ^{II} DZ	HF 431	HF ^I 631*	MP2 ^{II} 631+*	MP ^I 631+**	HF ^I 321*	HF ^{II} 631**	HF STO3G
1000	26.023(24.433)	29.223	25.99	22.83	25.30	30.92	30.6	26.2	30.5	24.35, 23.37, 23.6	32.20	26.21	42.2
1100	45.284(41.406)	45.702	43.21	39.71	45.83	55.87	53.03	47.1	54.1		56.82	46.82	74.2
1110	59.856(54.412)	59.009	56.83	53.08	62.61	76.20	71.74				77.20		97.3
2100	54.488(50.145)	53.828	51.98	47.26				64.3					
1111	72.746(65.471)	68.720	67.37	64.27	76.42	92.97	87.68	74.4					114.9
2110	68.466(61.252)	64.770	63.90	59.60									
2200	63.862(57.036)	60.493	59.59	54.31									
3100	61.156(54.502)	unstable											
3100ring	61.567(54.041)												
2111	80.284(71.509)	73.280	73.83	69.80			96.27				113.98		125.2
2111ring	80.487(71.262)												
2210	76.665(67.894)	70.160											
3110	74.905(66.198)	68.397											
3200	70.149(60.815)	64.517											
4100	66.836(58.773)	unstable											

^a This work, calculated binding energies for the most stable isomers, shown are the best values for each isomer calculated at the MP2/aug-cc-pVTZ with vertical Counterpoise correction or optimisation in the CP-corrected PES. In brackets binding energy with ZPE correction, calculated at the MP2/aug-cc-pVDZ level of theory. ^bRef.[15], B3LYP/6-31G** ; ^cRef.[14], ^I B3LYP/6-31+G*, ^{II} MP2/6-31+G* ; ^dRef.[38], ^I HF/D95, ^{II} B3LYP/cc-pVDZ ; ^eRef.[12] HF/4-31G + 3S ; ^fRef.[13] ^I MP2/6-31G*, ^{II} MP2/6-31+G**, ^{III} MP3/6-31+G** ; ^gRef.[17] MP2/6-31+G**//HF/6-31+G* + ZPE, MP2/6-31+G**//HF/6-31+G* + ZPE, MP4SDQ/6-31+G**//HF/6-31+G* + ZPE, respectively. ^hRef.[11] ^I HF/3-21G, ^{II} HF/3-21G* ; ⁱRef.[10] HF/STO 3G

References [14], in column four, and [15], in column three, show values in reasonable agreement. Wang *et. al* [14] correct for BSSE and ZPE and choose in their basis set to have diffusion functions and not to include polarisation on the hydrogen atoms (6-31+G*). Fouqueau and Meuwly [15] choose to fully polarise the basis set of choice and not adding diffusion functions (6-31G**), which leads them to use a basis set that is known to underestimate binding energies, thus potentially benefiting from a cancellation of errors when used with B3LYP. This cancellation is perhaps the reason behind the reasonable agreement between both set of data. Still, data from reference [14] in column four lie above what reported in column three [15], but still below than that presented by this work.

Overall, from all the table values and despite differences higher than 1 kcal/mol, our data compares best with that presented by Wang *et. al.* [14], in column five. When comparing our data with that of column five, we can see how the choice of basis set affects the discrepancy between the binding energies of both works. As has been already mentioned, 6-31+G* is not only smaller than aug-cc-pVTZ, but also does not provide a very good description of the polarisation, important in a system that includes a charged species. Also, compared to aug-cc-pVTZ, 6-31+G* lacks diffuse functions, something that although not conclusive (for a given cluster size this work has isolated more isomers), can perhaps be reflected in the worse agreement found in isomers featuring ammonia chains, as oppose to “globular” ones. For example, for isomer 1111 the data in column five lies ≈ 1.2 kcal/mol lower than that of this work, while isomer 2200 lies ≈ 2.7 kcal/mol lower than that of this work.

In turn, when comparing the data of this work with that of Wang *et. al* at the B3LYP level of theory (column four), we find that the discrepancy is smaller. This is most likely due, as has already been mentioned, to the tendency that B3LYP has to overestimate binding energies.

Table 4.11, can also give us an idea of how many and which of the clusters isolated by this work have been reported before in the literature. Clusters 3100, 3100ring, 4100 and 2111ring from this work appear to be novel structures. Fouqueau and Meuwly [15] report isomers 3100 and 4100 as unstable, it is suggested that this could be due to the underestimation by DFT of the small energy barrier shuttling of the proton.

To finish with the structural considerations, let us recall that although not included in table 4.11, for clusters $\text{NH}_4^+(\text{NH}_3)_n$ ($n = 1 - 3$) we have found pairs of practically isoenergetic structures, differing only in the orientation of the hydrogen atoms of the ammonia molecules with respect to the ammonium cation (e.g. “eclipsed” and “staggered”). We have not found this consideration in any of the papers we have reviewed. In fact, all literature presenting the symmetry or figures of the clusters agrees with the arrangement of the earliest pictoric model from reference [11]: “optimum orientation of the hydrogens on a NH_3 group with respect to the hydrogens of NH_4^+ or another NH_3 is staggered” [13].

Regarding the spatial arrangement of the ammonium ammonia dimer, our calculations are in agreement with the well established idea that the equilibrium structure for the ammonium ammonia dimer is $\text{NH}_4^+(\text{NH}_3)$ as reported in references. [10–15, 17, 38, 39], and not the N_2H_7^+ cation as an early theoretical study [37] first suggested. However, we understand that this is not conclusive, since the barrier for proton shuttling between the two ammonias is very low, and quantum effects could even make the proton delocalised.

All binding energies from table 4.11 have been used to compute thermochemical data, as presented in tables 4.12 and 4.13. In these tables only the isomers with the lowest total energy are included, the best binding energy data available for each isomer presented (i.e. the largest available basis set with Counterpoise corrected optimisation), alongside with the the ZPE correction at the MP2/aug-cc-pVDZ level of theory (in

brackets). It should be noticed that in table 4.11 the energetic ranking of isomers 2111 and 2111ring is inverted, upon introduction of BSSE and ZPE corrections.

Table 4.12: Binding energies (BE) and vaporisation energies (ΔE) for $\text{NH}_4^+(\text{NH}_3)_n$, ($n = 1 - 5$) in kcal/mol, comparison with experiments^a

n-1,n	BE ^a	This work	ΔE^b	ΔE^c	ΔE^d	ΔE^e	ΔE^f	ΔE^g
(0,1)	26.023 (24.433)	24.433	21.5	27.0	24.8	25.4	-	13.8
(1,2)	45.284 (41.406)	16.973	16.2	17.0	17.5	17.3	16.9	6.4
(2,3)	60.097 (54.412)	13.006	13.5	16.5	13.8	14.2	15.1	
(3,4)	72.746 (65.471)	11.509	11.7	14.5	12.5	11.8	13.5	
(4,5)	80.284 (71.509)	6.038	7.0	7.5	-	-	9.6	

^a The first column shows adiabatic and ZPE corrected (between brackets) binding energies computed in this work using Counterpoise corrected energies at the MP2/aug-cc-pVTZ and ZPE at the MP2/aug-cc-pVDZ; ΔE values for this work are computed including ZPE corrections. ^b Ref.[27], ^cRef.[24], ^dRef.[25], ^eRef.[33], ^fRef.[26], ^g[31]

On table 4.12, this work data are compared to the experimental values found in the literature for the cluster nucleation enthalpy. It can be seen that the agreement with experiments is good, qualitatively and quantitatively, particularly with the mass spectrometry experiments from references [24–27, 33]. Also, this work’s data reproduce the constant decrease in nucleation enthalpy upon increasing cluster size, as well as the characteristic “dip” in energy seen after the completion of the first solvation shell with good numerical accuracy.

On table 4.13, from the data estimated from references [14] (columns four and five) and [15] (columns three), the experimental trend is qualitatively reproduced. All the references showing data for higher clusters than the dimer reproduce a constant decrease in nucleation energy upon increasing cluster size; as well as the sudden energy drop at $\Delta_{(4,5)}$, in those references in which data for the hexamer is presented. Quantitatively, the most accurate values when compared to the experiment, apart from those from this work, are those provided by Fouqueau and Meuwly [15] and Wang *et. al* [14]. The different approaches into the investigation of protonated ammonia clusters by these two papers and how they compare to ours have already been considered. Per-

Table 4.13: Binding energies (BE) and vaporisation energies for $\text{NH}_4^+(\text{NH}_3)_n$, ($n = 1 - 5$) in kcal/mol, comparison with theory^a

n-1,n	This work ^a	FM ^b	WCJL ^c		NGIOOT ^d		KE ^e		D ^f	BFP ^g	HFKY ^h		PA ⁱ
	MP2 aTZ	B3LYP 631**	B3LYP ^I 631+*	MP2 ^{II} 631+*	HF ^I D95	B3LYP ^{II} DZ	HF 431	HF ^I 631*	MP2 ^{II} 631+**	MP ^I 631+*	HF ^I 321*	HF ^{II} 631**	HF STO3G
(0,1)	24.433	25.99	22.83	29.20	23.46	29.70	29.98	26.2	30.5	24.35, 23.37, 23.6	32.20	26.21	42.2
(1,2)	16.973	17.15	16.49	16.46	18.55	24.65	23.06	20.9	23.6		24.63	20.62	32.0
(2,3)	13.006	13.51	13.18	13.29	14.84	17.62	18.69	17.2			20.37		23.1
(3,4)	11.059	10.33	10.74	9.69	11.92	15.15	15.91	10.1					17.6
(4,5)	6.038	6.40	5.61	4.56			8.53						

^aThe first column shows adiabatic and ZPE corrected (between brackets) binding energies computed in this work using Counterpoise corrected energies at the MP2/aug-cc-pVTZ and ZPE at the MP2/aug-cc-pVDZ; vaporisation energies from this work are computed including ZPE corrections. ^bRef.[15]; ^cRef.[14]; ^dRef.[38]; ^eRef.[12]; ^fRef.[13]; ^gRef.[17]; ^hRef.[11]; ⁱRef.[38]

haps it is worth mentioning the tendency to underestimate the nucleation enthalpy ($\Delta_{(3,4)}$ and $\Delta_{(4,5)}$) in column five by reference [14].

4.4 Conclusions

In this chapter, we have presented a high level *ab initio* study on the structure and energetics of small protonated ammonia clusters $\text{NH}_4^+(\text{NH}_3)_n$ ($n = 1 - 5$). We have carried out electronic calculations at the MP2 level of theory with the aug-cc-pVXZ (X=D,T) family of basis sets, and we have accounted for BSSE with the Counterpoise procedure. Harmonic frequencies have been calculated at the MP2/aug-cc-PVDZ level of theory, to include the ZPE correction and to investigate if particular N-H modes can be associated to certain structural cluster features.

Protonated ammonia clusters arrange themselves in two general configurations, namely, “globular” and “linear”. For particular configurations of $\text{NH}_4^+(\text{NH}_3)_n$ ($n = 1 - 3$), we have found sets of practically isoenergetic isomers, differing in the staggered or eclipsed orientation of NH_3 with respect to NH_4^+ . Also, we have isolated what to our knowledge are four novel isomeric structures: 3100, 3100ring, 2111ring and 4100.

In addition, we have monitored the changes in a set of intramolecular and intermolecular parameters (figure 4.7), in order to extract general trends on structural changes associated with cluster size and level of NH_4^+ coordination. In this regard, we have found that the distance between the nitrogen atoms of the NH_4^+ and directly coordinating NH_3 (defined as R_{NN}), increases upon increasing cluster size when the coordinating ammonia is a single molecule. However, the same distance decreases when the core cation coordinates a chain $(\text{NH}_3)_n$; the longer the chain, the shorter the distance. The hydrogen bond distance, $R_{N...H}$, follows the same trends as R_{NN} . Within the same ammonia chain, the distance between solvating shells (sh-sh) is increased as one moves away from the core cation. It would seem that when a new solvation shell is created through the elongation of a $(\text{NH}_3)_n$ chain there is a contraction of the spacing of the lower shells, with the new incoming ammonia placed at a distance longer than any other shell.

Regarding the harmonic frequencies calculations, we see that two main features arise; those related to the vibrations of NH_3 and those related to the vibrations of NH_4^+ , which show much stronger intensities. In fact, the signature of protonated ammonia clusters is mainly given by the vibrating behaviour of the ammonium cation. In agreement with the literature, we have found that higher frequencies for the N-H vibrational modes of the NH_4^+ are seen upon increasing cluster size; also, the N-H stretching of the cation when part of an aggregate is noticeably downshifted with respect to the wavenumbers of the cation alone. Regarding the solvating ammonia molecules, we classified them in two “types”; the single coordinating NH_3 are only slightly shifted from the spectrum of the monomer, while the NH_3 involved in linking solvating shells show a significant red shift with respect to the monomer. Within a $(\text{NH}_3)_n$ chain we find that the molecules in the second and higher order solvation shells vibrate at slightly higher frequencies than first solvation shell molecules. Qualitatively, theoretical calculations are typically higher than the results obtained from experiment.

Finally, we have compared the vaporisation energies computed in this work with the experimental and theoretical values found in the literature (tables 4.12 and 4.13). This work thermal data, in agreement with the literature, reproduces the constant decrease in nucleation enthalpy upon increasing cluster size, as well as the characteristic “dip” in energy seen after the completion of the first solvation shell.

Bibliography

- [1] Castleman Jr., A.W. *Chem. Phys. Lett.*, **1978**, *53*, 560.
- [2] Castleman Jr., A.W.; Holland, P.M.; Lindsay, D.M.; Peterson, K.I. *J. Am. Chem. Soc.*, **1978**, *100*, 6039.
- [3] Spears, K.G. *J. Chem. Phys.*, **1972**, *57*, 5.
- [4] Bach, A.; Leutwyler, S. *J. Chem. Phys.*, **2000**, *112*, 160.
- [5] Mehata, M.S. *Chem. Phys. Lett*, **2007**, *436*, 357.
- [6] Tanner, C.; Manca, C; Leutwyler, S. *Science*, **2003**, *302*, 1736.
- [7] Manca, C; Tanner, C.; Leutwyler, S. *Int. Rev. Phys. Chem.*, **2005**, *24*, 457.
- [8] Meuwly, M.; Karplus, M. *J. Chem. Phys.*, **2002**, *116*, 2572.
- [9] Khademi, S.; O'Connell III, J.; Remis, J.; Robles-Colmenares, Y.; Miercke, L.J.W; Stroud, R.M. *Science*, **2004**, *305*, 1587.
- [10] Pullman, A.; Armbruster, A.M. *Chem. Phys. Lett*, **1975**, *36*, 558.
- [11] Hirao, K.; Fujikawa, T; Konishi, H.; Yamabe, S. *Chem. Phys. Lett.*, **1984**, *104*, 184.
- [12] Kassab, E.; Evleth, E.M. *J. Am. Chem. Soc.*, **1987**, *109*, 1653.

- [13] Deakyne, C.A. *J. Phys. Chem.*, **1986**, *90*, 6625.
- [14] Wang, B.C.; Chang, J.C.; Jiang, J.C.; Lin, S.H. *Chem. Phys.*, **2002**, *274*, 93.
- [15] Fouqueau, A.; Meuwly, M. *J. Chem. Phys.*, **2005**, *123*, 244308.
- [16] Dawson, P.H.; Tickner, A.W. *J. Chem. Phys.*, **1964**, *40*, 3745.
- [17] (a) Frisch, M. J.; Pople, J. A.; Del Bene, J. E. *J. Phys. Chem.*, **1985**, *89*, 3664.
(b) Del Bene, J. E.; Frisch, M. J.; Pople, J. A. *J. Phys. Chem.*, **1985**, *89*, 3669.
- [18] Schwarz, H. A. *J. Chem. Phys.*, **1980**, *72*, 284.
- [19] Ichihashi, M.; Yamabe, J.; Murai, K.; Nonose, S.; Hirao, K.; Kondow, T. *J. Phys. Chem.*, **1996**, *100*, 10050.
- [20] Park, J.K. *Bull. Korean Chem. Soc.*, **1999**, *20*, 1067.
- [21] (a) Tono, K.; Bito, K.; Kondoh, H.; Ohta, T.; Tsukiyama, K. *J. Chem. Phys.*, **2006**, *125*, 224305. (b) Tono, K.; Fukazawa, K.; Tada, M.; Fukushima, N.; Tsukiyama, K. *Chem. Phys. Lett.*, **2007**, *442*, 206.
- [22] Hogg, A.M.; Kebarle, P. *J. Chem. Phys.*, **1965**, *43*, 449.
- [23] Hogg, A.M.; Haynes, R.M.; Kebarle, P. *J. Am. Chem. Soc.*, **1965**, *88*, 28.
- [24] Searles, S. K.; Kebarle, P. *J. Phys. Chem.*, **1968**, *72*, 742.
- [25] Payzant, J. D.; Cunningham, A. J.; Kebarle, P. *Can. J. Chem.*, **1973**, *51*, 3242.
- [26] Long, J. W.; Franklin, J. L. *Int. J. Mass. Spectrom. Ion Phys.*, **1973**, *12*, 403.
- [27] Arshadi, M. R.; Futrell, J. H. *J. Phys. Chem.*, **1974**, *78*, 1482.
- [28] Meot-Ner, M.; Speller, C. V. *J. Phys. Chem.*, **1986**, *90*, 6616.

- [29] Fehsenfeld, F. C.; Ferguson, E. E. *J. Chem. Phys.*, **1973**, *59*, 6272.
- [30] Glosík, J.; Zakouřil, P.; Hanzal, V.; Skalský, V. *Int. J. Mass. Spectrom. Ion Phys.*, **1995**, *149*, 187.
- [31] Ceyer, S.T.; Tiedemann, P.W.; Mahan, B.H.; Lee, Y.T. *J. Chem. Phys.*, **1979**, *70*, 14.
- [32] Fuke, K.; Takasu, R.; Misaizu, F. *Chem. Phys. Lett.*, **1994**, *229*, 597.
- [33] Tang, I. N.; Castleman Jr., A. W. *J. Chem. Phys.*, **1975**, *62*, 4576.
- [34] (a) Price, J. M.; Crofton, M. W.; Lee, Y. T. *J. Chem. Phys.*, **1989**, *91*, 2749. (b) Price, J. M.; Crofton, M. W.; Lee, Y. T. *J. Phys. Chem.*, **1991**, *95*, 2182.
- [35] Nonose, S; Taguchi, T.; Chen, F.; Iwata, S.; Fuke, K. *J. Phys. Chem. A*, **2002**, *106*, 5242.
- [36] *IUPAC Compendium of Chemical Terminology*, **1997** 2nd Edition, <http://www.iupac.org/goldbook/A00421.pdf>, last accessed 2010, September 27.
- [37] Merlet, P.; Peyerimhoff, S. D.; Buenker, R.J. *J. Am. Chem. Soc.*, **1972**, *94*, 8301.
- [38] Nakai, H.; Goto, T.; Ichikawa, T.; Okada, Y.; Orii, T.; Takeuchi, K. *Chem. Phys.*, **2000**, *262*, 201.
- [39] Cybulski, S.M.; Scheiner, S. *Chem. Phys. Lett.*, **1990**, *166*, 57.
- [40] Janeiro-Barral, P. E.; Mella, M. *J. Phys. Chem. A*, **2006**, *110*, 11244.
- [41] M. J. Frisch and G. W. Trucks and H. B. Schlegel and G. E. Scuseria and M. A. Robb and J. R. Cheeseman and Montgomery, Jr., J. A. and T. Vreven and K. N. Kudin and J. C. Burant and J. M. Millam and S. S. Iyengar and J. Tomasi and

- V. Barone and B. Mennucci and M. Cossi and G. Scalmani and N. Rega and G. A. Petersson and H. Nakatsuji and M. Hada and M. Ehara and K. Toyota and R. Fukuda and J. Hasegawa and M. Ishida and T. Nakajima and Y. Honda and O. Kitao and H. Nakai and M. Klene and X. Li and J. E. Knox and H. P. Hratchian and J. B. Cross and V. Bakken and C. Adamo and J. Jaramillo and R. Gomperts and R. E. Stratmann and O. Yazyev and A. J. Austin and R. Cammi and C. Pomelli and J. W. Ochterski and P. Y. Ayala and K. Morokuma and G. A. Voth and P. Salvador and J. J. Dannenberg and V. G. Zakrzewski and S. Dapprich and A. D. Daniels and M. C. Strain and O. Farkas and D. K. Malick and A. D. Rabuck and K. Raghavachari and J. B. Foresman and J. V. Ortiz and Q. Cui and A. G. Baboul and S. Clifford and J. Cioslowski and B. B. Stefanov and G. Liu and A. Liashenko and P. Piskorz and I. Komaromi and R. L. Martin and D. J. Fox and T. Keith and M. A. Al-Laham and C. Y. Peng and A. Nanayakkara and M. Challacombe and P. M. W. Gill and B. Johnson and W. Chen and M. W. Wong and C. Gonzalez and J. A. Pople Gaussian 98, Revision 11.01, Gaussian, Inc., Wallingford, CT, **2001**.
- [42] M. J. Frisch and G. W. Trucks and H. B. Schlegel and G. E. Scuseria and M. A. Robb and J. R. Cheeseman and Montgomery, Jr., J. A. and T. Vreven and K. N. Kudin and J. C. Burant and J. M. Millam and S. S. Iyengar and J. Tomasi and V. Barone and B. Mennucci and M. Cossi and G. Scalmani and N. Rega and G. A. Petersson and H. Nakatsuji and M. Hada and M. Ehara and K. Toyota and R. Fukuda and J. Hasegawa and M. Ishida and T. Nakajima and Y. Honda and O. Kitao and H. Nakai and M. Klene and X. Li and J. E. Knox and H. P. Hratchian and J. B. Cross and V. Bakken and C. Adamo and J. Jaramillo and R. Gomperts and R. E. Stratmann and O. Yazyev and A. J. Austin and R. Cammi and C. Pomelli and J. W. Ochterski and P. Y. Ayala and K. Morokuma and G. A. Voth

and P. Salvador and J. J. Dannenberg and V. G. Zakrzewski and S. Dapprich and A. D. Daniels and M. C. Strain and O. Farkas and D. K. Malick and A. D. Rabuck and K. Raghavachari and J. B. Foresman and J. V. Ortiz and Q. Cui and A. G. Baboul and S. Clifford and J. Cioslowski and B. B. Stefanov and G. Liu and A. Liashenko and P. Piskorz and I. Komaromi and R. L. Martin and D. J. Fox and T. Keith and M. A. Al-Laham and C. Y. Peng and A. Nanayakkara and M. Challacombe and P. M. W. Gill and B. Johnson and W. Chen and M. W. Wong and C. Gonzalez and J. A. Pople Gaussian 03, Revision B.05, Gaussian, Inc., Wallingford, CT, **2003**.

- [43] Flükiger, P.; Lüthi, H. P.; Portmann, S.; Weber, J. MOLEKEL 4.3; Swiss National Supercomputing Centre: Manno (Switzerland).

Chapter 5

Conclusions and further work

5.1 Aims and achievements of this work

This work has aimed to explore the structures and interaction potential of pure, $(\text{NH}_3)_n$, and protonated, $(\text{NH}_4^+)_n$, ammonia clusters of small size ($n = 2 - 5$), using *ab initio* techniques. On pursuing this aim, we have attained an extensive and robust set of data that adds to the relatively scarce pool of ammonia studies and that compares well with both theoretical and experimental works already published on this topic.

More specifically, chapters 2 and 4 present 13 and 20 isomeric structures for pure and protonated ammonia clusters, respectively. For each cluster, we have calculated interaction energies, which were further rectified by introducing ZPE and BSSE corrections. Our energy data was additionally used to calculate clusters' vaporisation energies. Also, we have calculated the harmonic frequencies for all isomers presented and have analysed the N-H vibrations in order to relate its wavenumbers to particular structural features. In the case of pure ammonia clusters, and in view of the construction of a model potential, we have also decomposed the binding energy in its many-body contributions.

In chapter 3, we presented the development and completion of an analytical model for the potential energy surface of ammonia clusters. Our model included a polarisation description and was fitted to *ab initio* data. This potential was successfully used to describe the interaction between ammonia molecules and was applied further in the exploration of clusters of $n > 5$; resulting in the finding of isomeric structures (20 more are shown), and the estimation of their interaction energies.

5.2 Further work

We believe that the expansion of the work presented in this thesis rests in the simulation tool that is the model potential; its applications laying on the ubiquitous nature of ammonia. We present below three possible directions of progress:

First, our potential could carry on being used to study neutral ammonia clusters, to describe intermolecular interactions in Monte Carlo and molecular dynamics simulations. This work is underway in our laboratory, Mella and Curotto [1] have explored thermal and quantum effects in small and medium size ($n = 2 - 11$) neutral ammonia clusters. Using our model potential in the simulation on bigger clusters could contribute to the understanding of the structure and energetics of bulk ammonia, by, for instance, looking at processes such as nucleation and freezing. Additionally, our potential could be used in the simulation of “electron doped” ammonia clusters, which would be carrying an electron excess.

Second, the model potential presented in this thesis could be applied in the field of solvation chemistry. Our model would be the starting point for the generation of new interaction potentials between ammonia and other species such as water or ions (i.e. Al^{+3} , Be^{+2} , Ca^{+2} , OH^- , H^+). These new potentials could be exploited to obtain the energetics of the clusters; in the simulation of thermal effects on structural

details; on the relative distribution of the species constituting the aggregates; in the simulation of evaporation processes and the solvent exchange kinetics for ion-ammonia or water-ammonia clusters as well as the exchange kinetics of molecules belonging to different solvent shells. An example of this approach can be found in the Quantum Mechanics/Molecular Mechanics (QM/MM) study of silver in aqueous ammonia solution [2], where a three-body potential has been applied to describe the MM region. Other examples are the QM/MM studies on Ca^{+2} [3] and Mg^{+2} [4] both, as before, in an aqueous ammonia solution.

Thirdly, our model potential could be of use in the field of atmospheric chemistry. Pollutants get into the atmosphere as gases, solid particles and/or liquids, the latter two forming the so-called aerosols, which affect a great variety of atmospheric processes [5]. Nitrate aerosols are formed in the atmosphere, their precursors being ammonia and nitric oxides coming from natural and antropogenic sources [6]. We think our model potential could be used in molecular dynamics simulations of nitrate aerosols, perhaps along the same lines as it has been done for water [7]. This approach could provide information on the structures and reaction dynamics taking place within the aggregate and in the gas/aerosol interface.

Bibliography

- [1] Lubombo, C.; Curotto, E.; Janeiro-Barral, P. E.; Mella M. *J. Chem. Phys.*, **2009**, *131*, 0343312.
- [2] Armunanto, R.; Schwenk, C. F.; Rode, B. M. *J. Phys. Chem. A*, **2005**, *109*, 4437.
- [3] Tongraar, A.; Sagarik, K.; Rode, B. M. *Phys. Chem. Chem. Phys.*, **2002**, *4*, 628.
- [4] Tongraar, A.; Sagarik, K.; Rode, B. M. *J. Phys. Chem. B*, **2001**, *105*, 10559.
- [5] Ackermann, I. J.; Hass, H.; Memmesheimer, M.; Ziegenbein, C.; Ebel, A. *Meteorol. Atmos. Phys.*, **1995**, *57*, 101.
- [6] Bauer, S. E.; Koch, D.; Unger, N.; Metzger, S. M.; Shindell, D. T.; Streets, D. G. *Atmos. Chem. Phys*, **2007**, *7*, 5043.
- [7] Jungwirth, P.; Tobias, D. J. *J. Phys. Chem. B*, **2001**, *105*, 10468.

